Surface-Enhanced Raman Scattering from a Modified Silver Electrode

by

Aaron Craig Sanderson
B.A.Sc., University of British Columbia, 1993
M.Sc., University of Toronto, 1994

A Dissertation Submitted in Partial Fulfillment of the
Requirements for the Degree of

DOCTOR OF PHILOSOPHY

in the Department of Physics and Astronomy.

Surface-Enhanced Raman Scattering from a Modified Silver Electrode

by

Aaron Craig Sanderson
B.A.Sc., University of British Columbia, 1993
M.Sc., University of Toronto, 1994

Supervisory Committee

Dr. A. G. Brolo (Department of Chemistry)
Supervisor

Dr. J. M. Roney (Department of Physics and Astronomy)
Departmental Member

Dr. A. Watton (Department of Physics and Astronomy)
Departmental Member

Dr. C. Bohne (Department of Chemistry)
Outside Member

Dr. G. Leach (Department of Chemistry, Simon Fraser University)
External Examiner

Supervisory Committee

Dr. A. G. Brolo (Department of Chemistry)
Supervisor

Dr. J. M. Roney (Department of Physics and Astronomy)
Departmental Member

Dr. A. Watton (Department of Physics and Astronomy)
Departmental Member

Dr. C. Bohne (Department of Chemistry)
Outside Member

Dr. G. Leach (Department of Chemistry, Simon Fraser University)
External Examiner

ABSTRACT

Electrochemical and spectroelectrochemical data was obtained for a silver electrode modified with oxazine 720. A quasi-reversible redox behaviour was observed for the modified electrode. Surface adsorption density, calculated from the measured electrochemical charge transfer, is higher than would be expected for a monolayer of flat-adsorbed oxazine 720. Surface-enhanced Raman scattering (SERS) data, in conjunction with results of a density functional theory (DFT) calculation, suggest that the molecule is adsorbed with its rings perpendicular to the electrode surface, consistent with the electrochemically estimated adsorption density. SERS was recorded *in situ* at different applied potentials. The SERS intensity remains relatively stable between -200 and -500 mV (versus Ag|AgCl|Cl-sat), but decreases dramatically as the applied potential is made more negative than -500 mV. Ths is consistent with the onset of oxazine 720 reduction observed during cyclic voltammetry. The spectroelectrochemical data indicates that oxazine 720 remains adsorbed at the SERS-active sites even in its reduced form.

Similar *in situ* SERS data was collected for rhodamine 6G and pyridine. Spectra in the Stokes and anti-Stokes regions were obtained at several applied potentials using two different laser excitation energies. Normalized ratios of the anti-Stokes to Stokes intensities

were calculated for various vibrational bands of the three molecules. The measured ratios vary with changes in the excitation energy, the applied voltage and the energy of the vibrational mode being investigated. The ratios for oxazine 720 show a preferential enhancement of the Stokes scattering while the ratios for rhodamine 6G indicate an enhancement of the anti-Stokes scattering. For pyridine, the preferential enhancement changes between Stokes and anti-Stokes depending on the excitation wavelength used, the applied voltage and the vibrational band being examined. The main trends of the anti-Stokes to Stokes ratios can be satisfactorily explained using resonance models based on standard SERS theories. No evidence of a SERS-induced non-thermal population distribution among the vibrational states of the adsorbed molecules (vibrational optical pumping) was observed.

Contents

List of Figures

Acknowledgments

Has it really been this long? What started out as a 3 year stepping stone on the path of my life has become a 10+ year journey down an unintended road. Along this journey I have met various locals and had numerous travel companions, many of whom I owe a debt of gratitude to for one reason or another.

As with any adventure, the logical place to start is the beginning, so I will start by thanking Jean-Pierre Egger, who supplied some much needed guidance at the start of it all in a land far, far away. From my time in the far-away lands I would also like to thank Ross King III and Takeyasu Ito, both for their guidance and their friendship. Whether they knew it or not, they helped me along some of the darker paths in the early days of this epic journey.

I owe Chris Brown, Dominique Fortin and Brigitte Vachon, as well as numerous other graduate students in the department, a heartfelt "Thank You" for their camaraderie and assistance during the course-work leg of my journey. One could not ask for better travel companions during the red-eye portions of my voyage.

I would like to thank the Brolo-group grad students, especially Gabriele Hager and Chris Addison, who made my expedition far more exciting by allowing me take day trips into their journeys. Their support and insights were often helpful, and, at a minimum, entertaining. A special thanks goes to Anderson Smith who was an excellent summer student who helped keep things on track when they were going full steam ahead.

I am especially thankful to Luis Netter for his assistance with LabVIEW. I would also like to thank the staff of the machine, instrument and glass shops for keeping things running smoothly.

With a road as long as mine, travel companions are bound to move off in new directions. Fortunately, that leaves room for new travel companions. The journey of education should most definitely not be a a simple path for which the destination is known, but rather a voyage of exploration. I would like to thank Daniel Vanderster, Ian Gable and Steven Tieu for their interesting and insightful conversations about anything and everything.

I would like to thank my family, Craig, Leslie, Arnold, Arthur and Anne, for their

unconditional support, through the good times and the bad. No matter how long my journey took, or which backwoods route I followed, they were always there. Extra credit goes to Craig, and especially Arthur, for their proofreading of this dissertation.

I owe a special debt to Christine Lipus, who has put up with years of awkward commuting, various temperamental moods and a much longer expedition than expected. Her love and support have helped me keep going more than once.

And most importantly, I would like to thank my supervisor, Alexandre Brolo, without whom this dissertation would not have been completed. In addition to saving me from the dead end that my journey had led to, he has been infinitely patient, has supplied me with much guidance, has applied an appropriate amount of pressure, and has used his motivation and interest to shore up mine when it was waning. *Alexandre, muito obrigado por toda a ajuda.*

It is the journey, not the destination, that matters most.

The time has come...

Lewis Carroll

For my parents, Craig and Leslie.

Chapter 1

Overview and Introduction

THIS CHAPTER PROVIDES AN OVERVIEW OF THE DISSERTATION. A BRIEF SUMMARY, WHICH INCLUDES THE GENERAL TOPICS COVERED AND THE MOTIVATION BEHIND THE RESEARCH, IS GIVEN FOR EACH CHAPTER.

Surface-enhanced Raman scattering (SERS) has become a common research tool, being used for both fundamental measurements and as a method for studying the various phenomena and mechanisms involved in the SERS process itself. The research presented in this dissertation employs SERS in both of these capacities and organizes the results into five chapters: this overview, an introduction to SERS, SERS results from a laser dye adsorbed on a silver electrode, an exploration of the anti-Stokes asymmetry phenomenon and its relationship to optical pumping, and an overall summary of the results.

Chapter 2

The purpose of chapter 2 is to provide sufficient background information to understand the results presented in chapters 3 and 4. Chapter 2 starts with an introduction to Raman scattering including both a classical and perturbative quantum mechanical derivation of the phenomenon. This is followed by an introduction to SERS and its principal mechanisms, the electromagnetic (EM) and charge transfer (CT) mechanisms. Chapter 2 also describes three specialized Raman-related techniques and concludes with some examples of active areas of SERS research.

Chapter 3

Chapter 3 presents an analysis of SERS data collected from oxazine 720 adsorbed on a roughened silver electrode with various applied potentials. This spectroelectrochemical data is used to estimate the molecular orientation while also demonstrating the quasi-reversible electrochemistry of oxazine 720 and the resonant behavior of one particular vibrational band. The investigation in this chapter was motivated by three distinct needs. The collection of this data provided an opportunity to test and calibrate the equipment. The oxazine 720 spectroelectrochemical data contributes a previously unreported set of basic knowledge to the SERS community. The resonant behavior of a SERS band provides an ideal platform to study the CT enhancement mechanism.

Chapter 4

Chapter 4 describes the SERS anti-Stokes asymmetry issue and provides data that confirms its existence while simultaneously showing that it is not the result of optical pumping. A resonance model capable of explaining the data, as well as data previously published by others, is developed. The effects of laser induced heating are modeled and explored as a possible contributor to the anti-Stokes asymmetry. The research in this chapter was carried out in response to previous publications claiming that the SERS anti-Stokes asymmetry was solely the result of optical pumping. Chapter 4 concludes with a summary of recent research in the field of SERS anti-Stokes asymmetry.

Chapter 5

Chapter 5 summarizes the results of the dissertation. The conclusions from chapters 3 and 4 are recapitulated along with a brief discussion about the current and future state of SERS research.

Chapter 2

An Introduction to Surface Enhanced Raman Scattering

THIS CHAPTER BEGINS WITH A BRIEF HISTORY AND DESCRIPTION OF RAMAN SCATTERING, FOLLOWED BY A BASIC MATHEMATICAL DEVELOPMENT OF THE PROCESS. THE CONCEPT OF SURFACE-ENHANCED RAMAN SCATTERING (SERS) IS THEN INTRODUCED AND ITS MAJOR CONTRIBUTING FACTORS, THE ELECTROMAGNETIC (EM) AND CHARGE TRANSFER (CT) MECHANISMS, ARE DESCRIBED. BRIEF EXAMPLES OF SOME SPECIALIZED RAMAN-RELATED TECHNIQUES AND METHODS, INCLUDING RESONANCE RAMAN SCATTERING, AB INITIO RAMAN-MODE CALCULATIONS AND MOLECULAR ORIENTATION DETERMINATION ARE THEN GIVEN. THE CHAPTER CLOSES WITH A SUMMARY OF SOME CURRENT AREAS OF RAMAN RESEARCH.

2.1 Description and History of the Raman Effect

The inelastic scattering of light from molecules, known as Raman scattering, was first observed by Raman and Krishnan in 1928.[1] Although the phenomenon had been predicted on theoretical grounds in 1923 by Smekal,[2] it was Raman's detailed research that confirmed the effect and earned him the 1930 Nobel Prize in Physics. The importance of Raman's discovery was obvious by the speed with which papers were published on the topic: 70 publications by the end of 1928.[3]

Unlike Rayleigh scattering,[4] which changes only the direction of the incident light, Raman scattering also changes the energy of the scattered photons. In vibrational Raman scattering energy is exchanged between the vibrational modes of the interacting molecule and the scattering photon. If energy is transferred from the photon to the molecule, the process is said to be Stokes Raman scattering, whereas if energy is transferred from the molecule to the photon, the process is said to be anti-Stokes Raman scattering. The use of the terms "Stokes" and "anti-Stokes" is somewhat of an accepted misnomer since "Stokes' Law" originally applied only to fluorescence and simply stated that an emitted fluorescence photon should have less energy than the excitation photon.

A schematic representation of these Raman processes is shown in figure 2.1. It is important to note that the dashed line in the diagram represents a virtual state, not an excited electronic state. If the incident photon excites the molecule to an excited electronic state the process is known as resonant Raman scattering and is described in section 2.4.1.

As figure 2.1 shows, anti-Stokes scattering can only occur if the molecule starts in an excited vibrational state. The population of excited vibrational modes is described by the Boltzmann distribution,[3] which implies that at room temperature, Stokes Raman scattering is more probable than anti-Stokes Raman scattering. This characteristic becomes more prominent as the energy of the vibrational mode increases. Since the vibrational information is contained in both the Stokes and anti-Stokes signal, but the anti-Stokes signal suffers from an exponential fall off in intensity with energy, most Raman spectroscopy uses only the Stokes Raman signal.

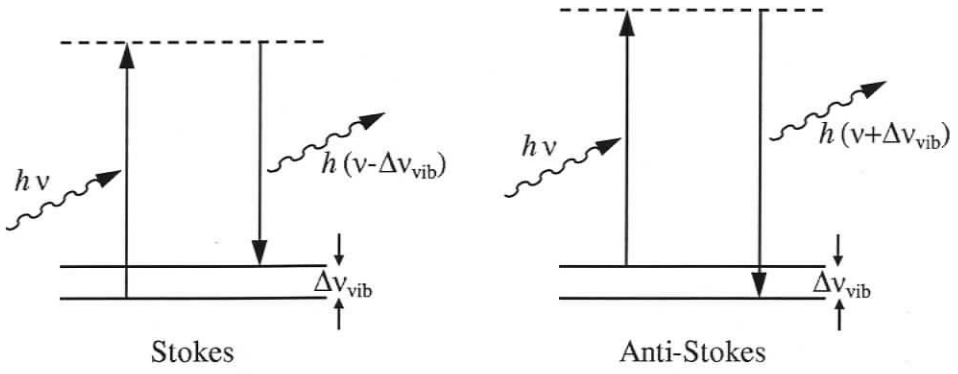

Figure 2.1: Simple energy-level diagrams for Raman scattering.

The energy of interest in Raman spectroscopy is the difference in energy between the incident and scattered photons, the Raman shift, which is normally given in units of inverse wavelength, or wavenumber. A typical Raman spectrum, with the Rayleigh scattering peak removed, is shown in figure 2.2. This spectrum clearly shows the difference in intensity between the Stokes and anti-Stokes processes as well as the relative decrease in anti-Stokes intensity as the Raman shift becomes larger. As stated above, it is common to collect only the Stokes Raman signal, in which case it is customary to plot the Stokes Raman shifts as positive rather than negative.

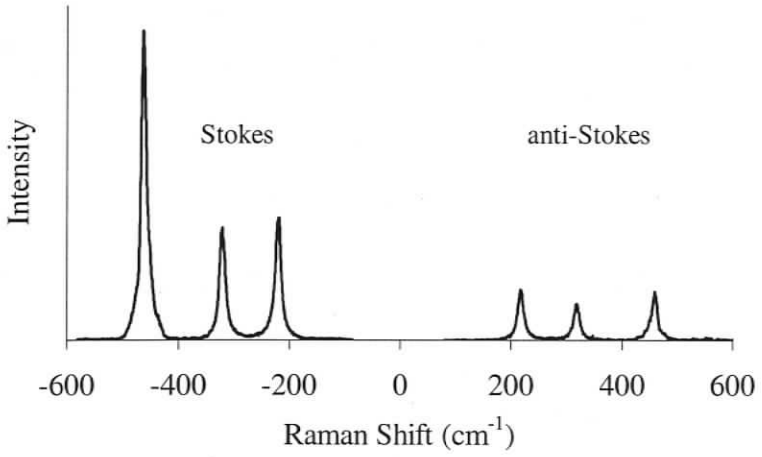

Figure 2.2: A typical Raman spectrum. (CCl_4 using 632.8 nm excitation.)

Raman's original work, using sunlight, filters and visual observation[1] was a proof

of concept, but was incapable of producing spectra. The collection of Raman spectra requires a monochromatic light source, an optical train to collect the scattered light, and a detection system to analyze the wavelength/energy of the signal. The optical train and detector must also prevent the Rayleigh scatter, which is orders of magnitude more intense than the Raman scatter, from contaminating the signal. Raman systems have evolved from filtered mercury lamps and photographic plates to diode lasers, holographic notch filters, dispersion gratings and charge-coupled devices (CCDs) allowing techniques such as Raman imaging, Raman microscopy and Fourier Transform Raman to be offered in readily available commercial products. Information about the historical development of Raman spectroscopy equipment can be found in a number of sources.[5–7]

2.2 Basic Theory

2.2.1 Simple Molecular Vibrations

In order to formulate a mathematical description of Raman scattering, a basic understanding of molecular vibrations is required.

Assuming atomic nuclei to be geometric points with mass, 3 coordinates (quantum numbers) are required to fully define their positions (states). Thus, a molecule with N nuclei will have $3N$ coordinates, or degrees of freedom. Of these $3N$ degrees of freedom, 3 represent translational motion of the molecule and a further 3 (2 in the case of a linear molecule) represent rotation of the molecule as a unit. This leaves $3N-6$ ($3N-5$) degrees of freedom representing vibrational modes. These vibrational modes, or "normal modes", form an orthogonal basis set for all possible molecular vibrations. Each "normal coordinate" is designated Q_i and has vibrational frequency ν_i. A set of mass-weighted Cartesian displacement coordinates, q_i, can be constructed through appropriate linear combinations of the normal coordinates.[5] During a normal mode vibration all the nuclei in the molecule oscillate in phase and at the same frequency.[8] Techniques to calculate the normal modes exist[9] and are discussed in section 2.4.2.

2.2.2 Classical Derivation

Classically, Raman scattering occurs when a radiating dipole moment is produced by the interaction of an incident electric field with a molecule through the polarizability:

$$\boldsymbol{P} = \alpha \boldsymbol{E} \tag{2.1}$$

where $\boldsymbol{P}$ is the dipole moment vector, $\boldsymbol{E}$ is the incident field vector and α is the polarizability tensor. For simplicity, and without loss of generality, the remainder of this derivation is carried out in one dimension.

When a molecule undergoes a normal mode vibration its nuclei, and therefore its charges, oscillate along the appropriate coordinate Q_i. This oscillation can be quantified by

$$Q_i = Q_{i0}\cos(2\pi\nu_i t + \delta_i) \tag{2.2}$$

where Q_{i0} is the equilibrium position, ν_i is the frequency of oscillation, and δ_i represents the phase difference between the incident field and the molecular vibration.

Since the polarizability of a molecule is a function of the relationship between its positive and negative charges, a molecular nuclear vibration can cause a concomitant oscillation in the polarizability of the molecule. Assuming small displacements, the changing polarizability can be expanded in a Taylor series

$$\alpha = \alpha_0 + \left(\frac{\partial\alpha}{\partial Q_i}\right)_0 Q_i + \frac{1}{2}\left(\frac{\partial^2\alpha}{\partial Q_i^2}\right)_0 Q_i^2 + \cdots \tag{2.3}$$

Limiting equation (2.3) to first order in Q_i and substituting equation (2.2) gives

$$\alpha = \alpha_0 + \left(\frac{\partial\alpha}{\partial Q_i}\right)_0 Q_{i0}\cos(2\pi\nu_i t + \delta_i) \tag{2.4}$$

A classical monochromatic plane wave of frequency ν_0, representing the excitation laser, is described by

$$E = E_0\cos(2\pi\nu_0 t) \tag{2.5}$$

Substituting equations (2.4) and (2.5) into (2.1) gives

$$P_i = \alpha_0 E_0\cos(2\pi\nu_0 t) + \left(\frac{\partial\alpha}{\partial Q_i}\right)_0 Q_{i0}E_0\cos(2\pi\nu_0 t)\cos(2\pi\nu_i t + \delta_i) \tag{2.6}$$

Using the trigonometric identity $\cos(x)\cos(y) = \frac{1}{2}[\cos(x+y)+\cos(x-y)]$, equation (2.6) becomes

$$P_i = \alpha_0 E_0 \cos(2\pi\nu_0 t) + \frac{1}{2}\left(\frac{\partial\alpha}{\partial Q_i}\right)_0 Q_{i0} E_0 \cos[2\pi(\nu_0+\nu_i)t+\delta_i] + \frac{1}{2}\left(\frac{\partial\alpha}{\partial Q_i}\right)_0 Q_{i0} E_0 \cos[2\pi(\nu_0-\nu_i)t+\delta_i] \quad (2.7)$$

In the classical model an oscillating dipole radiates at its oscillation frequency. Thus the three terms of equation (2.7) accurately predict Rayleigh scattering at ν_0, Raman anti-Stokes scattering at $\nu_0+\nu_i$ and Raman Stokes scattering at $\nu_0-\nu_i$, respectively. Also, since δ_i can take on any value between 0 and 2π there is no correlation between the phase of the incident field and the Raman scattered fields. The classical model correctly identifies normal Raman scattering as incoherent and Rayleigh scattering as coherent. Equation (2.7) also appropriately indicates a linear relationship between the incident intensity and both the Rayleigh and Raman scattering intensities. The classical model also encompasses the fundamental Raman selection rule: a normal mode vibration must induce a change in polarizability in order to be Raman active, i.e. $(\partial\alpha/\partial Q_i)_0 \neq 0$. Although not a result of the foregoing derivation, classical theory also predicts that Rayleigh and Raman scattering intensities should vary with the fourth power of the scattered frequency.[4,10,11] These results are in agreement with the quantum mechanical model and experiment.

As has been demonstrated, the classical theory of Raman (and Rayleigh) scattering accurately describes a number of characteristics of the process and is a useful model for forming a basic understanding of the effect. However, there are a few features that are not adequately explained by the model. The most significant shortcoming of the classical model is that it provides no way to link the Raman scattering tensor terms, $\frac{1}{2}Q_{i0}(\partial\alpha/\partial Q_i)_0$, to the properties of the molecular system. One clear indication of this shortcoming is the fact that the classical method suggests that the probability of a Stokes scattering event is equal to that of an anti-Stokes scattering event, which obviously ignores the requirement of a pre-existing excited state in order for anti-Stokes scattering to occur. Another obvious problem resulting from this limitation of the classical model is the fact that it provides no means to determine which Raman scattering tensor terms are iden-

tically zero (i.e. the Raman selection rules). A quantum mechanical model of Raman scattering, as described in the next section, provides a more complete description.

2.2.3 A Quantum Mechanical Model

To produce a quantum mechanical model of Raman scattering the dipole moment associated with a transition between two vibrational states, via a third virtual state, must be calculated. Such a calculation is carried out using perturbative methods in a number of texts[3,5,12,13] and the result is included here without derivation:

$$(\alpha_{\rho\sigma})_{fi} = \sum_{v \neq f,i} \left(\frac{\langle \psi_f | \hat{p}_\rho | \psi_v \rangle \langle \psi_v | \hat{p}_\sigma | \psi_i \rangle}{E_{vi} - E_0 - i\Gamma_v} + \frac{\langle \psi_f | \hat{p}_\sigma | \psi_v \rangle \langle \psi_v | \hat{p}_\rho | \psi_i \rangle}{E_{vf} + E_0 + i\Gamma_v} \right) \quad (2.8)$$

Here, $(\alpha_{\rho\sigma})_{fi}$, with ρ and σ running over the x, y, and z molecular axes, are the components of the transition polarizabilty tensor between the initial and final states; ψ_f, ψ_v and ψ_i represent the wavefunction of the final, virtual and initial states respectively; $\hat{p}$ is the electric dipole moment operator; E_{vi} is the energy between the virtual and initial states; E_{vf} is the energy between the virtual and final states; E_0 is the energy of an incident photon; and Γ_v is the half-width of the virtual state, given by its lifetime and the uncertainty principle. The derivation used for this result uses a classical incident field and treats it as a perturbation of the molecular wavefunction rather than using a full quantum mechanical description. This derivation is also limited to electric dipole interaction and assumes the initial and final states are completely stable (infinite lifetimes). If the initial and final states are the same state, equation (2.8) is still valid, but describes Rayleigh scattering.

The transition polarizability tensor, $(\alpha)_{fi}$, is used to calculate the transition electric dipole, $(\boldsymbol{P})_{fi}$, in much the same way as the classical polarizability, α, is used to calculate the classical oscillating electric dipole, $\boldsymbol{P}$, in equation (2.1), with the caveat that complex conjugates need to be included in the calculation. However, unlike the classical polarizability, the transition polarizability tensor is defined in terms of quantitative molecular properties (energy levels, lifetimes and wavefunctions), allowing the properties of the scattered radiation to, in principle, be calculated.

Another advantage of the quantum mechanical model is its ability, in certain circum-

stances, to predict whether a vibrational mode is Raman active or not. For a mode to be Raman active at least one of its transition polarizability tensor components must be non-zero. From equation (2.8) it is clear that this is essentially equivalent to

$$\sum_{v \neq f,i} \langle \psi_f | \hat{p}_\rho | \psi_v \rangle \langle \psi_v | \hat{p}_\sigma | \psi_i \rangle \neq 0 \tag{2.9}$$

for at least one combination of ρ and σ. With appropriate approximations this equation leads to important vibrational Raman selection rules.

The first step in simplifying equation (2.9) is to apply the Born-Oppenheimer approximation[14] which asserts that electrons, being much less massive than nuclei, adjust nearly instantaneously to changes in nuclear positions, allowing a time independent representation of the nuclear potential. This approximation allows the electronic, vibrational and rotational components of the wavefunctions to be treated independently. Using this approximation it can be shown that equation (2.9) will only be satisfied if at least one of the transition polarizability tensor components belongs to the same symmetry species as the normal mode in question.[5,15] Since establishing the point group of a normal mode is significantly more straightforward than determining its wavefunction this method can greatly simplify the process of finding which normal modes are Raman active. This aspect of Raman selection rules, and the accompanying group theory, is covered in detail in numerous texts.[3,5,8,16]

A second simplification is to approximate the molecular normal mode as a harmonic oscillator. For low-level molecular vibrations this is a reasonable estimate.[3,5,15] Using this additional approximation it can be shown[5,15] that equation (2.9) will only be satisfied if the initial state, $|\psi_i\rangle$, and final state, $|\psi_f\rangle$, differ by only a single quantum in a single normal mode, i.e. only fundamental modes are active. Since real molecular modes are not exactly described by the harmonic oscillator model real Raman spectra do show overtone transitions and combination transitions, but with significantly reduced intensities compared to the fundamental transitions.

This quantum mechanical model also confirms many of the conclusions of the classical model described in the previous section: scattering occurs at ν_0 (Rayleigh), $\nu_0 - \nu_i$

(Stokes Raman), and $\nu_0 + \nu_i$ (anti-Stokes Raman); Rayleigh scattering is coherent while Raman scattering is incoherent; the scattering intensity is linearly dependent on the incident intensity; and the Raman scattering intensity is linearly related to the fourth power of the scattered frequency. This is in addition to the selection rules described above and the ability to quantitatively describe the scattered radiation. This quantum mechanical perturbation model, although still limited, gives a much more complete picture of the Raman process.

2.3 The Discovery and Theory of Surface Enhancement

In 1977 Jeanmaire & Van Duyne[17] and Albrecht & Creighton[18] independently reported that pyridine adsorbed on specially prepared silver surfaces produces Raman intensities five to six orders of magnitude stronger than expected. This effect has since been shown to exist for hundreds of molecules on various metal surfaces prepared with numerous techniques[19–21] and has become an important tool in analytical chemistry and biochemistry.[22] Certain experiments have measured enhancement factors as high as 14 orders of magnitude,[23,24] allowing the detection of single molecules of analyte. Shortly after the initial discovery similar surface enhancements were observed in numerous other spectroscopic techniques, such as second harmonic generation and photochemistry,[25] and previously observed spectroscopic enhancements were now seen to have a common origin.[19] The discovery of surface-enhanced Raman scattering (SERS) generated renewed interest in Raman spectroscopy and surface spectroscopy in general.

The mechanisms responsible for the observed enhancement have garnered considerable study and a certain amount of controversy.[5,19] The two most widely accepted enhancement mechanisms are the electromagnetic (EM) mechanism, which effectively increases the local electromagnetic field, and the charge transfer (CT) mechanism, which alters the molecular polarizability via the formation of a metal-molecule complex. Of the $\sim 10^6$ enhancement typically quoted for SERS the EM mechanism is believed to be responsible for $\sim 10^{4-5}$ of this while the CT mechanism is responsible for the remaining $\sim 10^{1-2}$.

2.3.1 Electromagnetic Enhancement Mechanism

The electromagnetic (EM) enhancement mechanism is a function of the properties of the adsorption surface with the only dependence on the adsorbate typically being its distance from the surface. A study of the EM enhancement mechanism therefore centers on the characteristics of the surface. Experimentally it is known that only certain metals (Ag, Cu, Au, etc.) and certain treatments (oxidation/reduction cycling, controlled diameter colloids, cold-substrate vapour deposition, etc.) create SERS-active surfaces.[19,26] The common features of these surfaces are their suitable dielectric constant and their roughness on a sub-wavelength scale. Both of these properties play a significant role in the EM enhancement mechanism.

The EM enhancement factor

The EM enhancement mechanism works by increasing the local electromagnetic field in the neighbourhood of the analyte molecule. Since the effect is acting on EM fields it affects both the incident field and the Raman scattered field. In the approximation that the enhancement is equal at both the incident wavelength and the scattered wavelength (i.e. the enhancement effect acts equally over a range of wavelengths, or, alternatively, the Raman shift is small) the overall enhancement to Raman intensity is proportional to the fourth power of the field enhancement

$$\frac{I_{\text{SERS:EM}}}{I_{\text{normal:Raman}}} \propto \left| \frac{E_{\text{enhanced}}}{E_{\text{normal}}} \right|^4 \tag{2.10}$$

This can be made clear with a simple example. The most basic form of EM enhancement is caused by reflection. A molecule adsorbed on a reflective surface is illuminated by the directly incident field and the reflected incident field, as shown in figure 2.3. In the case of a perfect reflector this results in a doubling of the local field, i.e. $E_{\text{enhanced}} = 2E_{\text{normal}}$. The scattered Raman field is also reflected causing a second doubling. Since intensity is the square of the field we see that $I_{\text{SERS:EM}} = 16 I_{\text{normal:Raman}}$, as predicted by equation (2.10). Calculations using the properties of real metals lead to reflection enhancement factors on the order of 5 or 6.[27] It is clear from equation (2.10) that even

moderate field enhancements can produce substantial increases in Raman intensity.

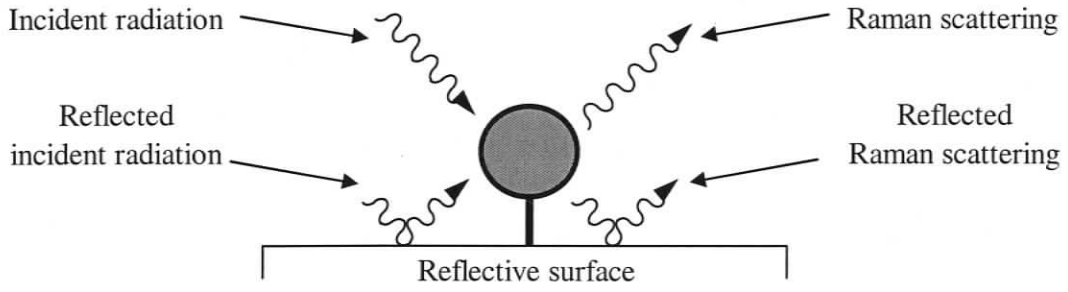

Figure 2.3: A molecule adsorbed on a reflecting surface is illuminated by the direct and reflected incident fields. The Raman scattered field is also reflected. For a perfect reflector, this leads to a quadrupling of the scattered Raman field which is a 16 fold increase in the Raman intensity. Note that an adsorbed molecule is actually orders of magnitude smaller than the wavelength.

Surface plasmons and EM enhancement

The major process behind the EM enhancement mechanism is an amplification of the localized electric field through the driven oscillation of free electrons at the surface of the metal. Such oscillations, which are confined to the surface, are known as surface plasmons. On a smooth surface the surface plasmons cannot couple to an electromagnetic field because of a momentum mismatch.[21] However, a surface that presents a spatially modulated electron surface density, such as a rough or patterned surface, is capable of coupling photons to surface plasmons and vice versa. This is one of the reasons that SERS-active surfaces need to be rough or nanostructured. If the excited surface plasmon is in resonance with the dimensions of a particular surface feature the field will be amplified at specific locations on the feature. This is shown schematically in figure 2.4.

It is important to note that the excitation of surface plasmons does not increase the total energy in the field, but simply redistributes it creating "hot spots" at specific surface structures. Since the Raman intensity varies as the field enhancement to the fourth power this redistribution can greatly increase the Raman signal. This also has the effect of heavily biasing the measurement towards the output of the analyte adsorbed at the hot spots.

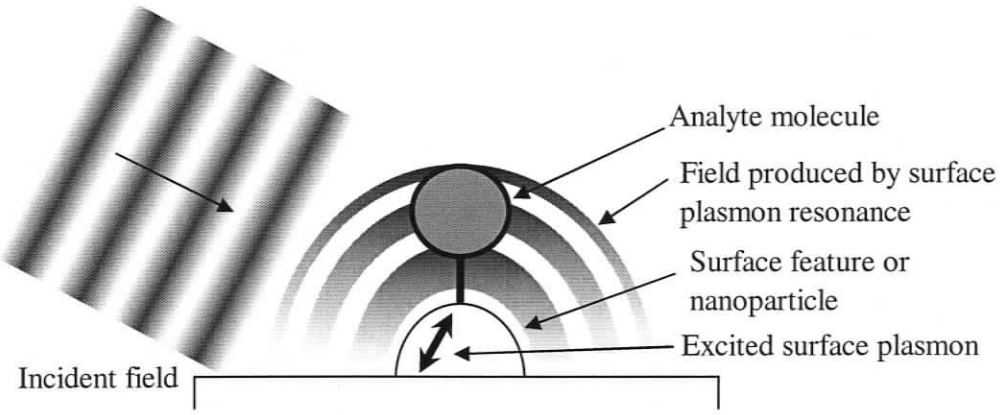

Figure 2.4: The EM field at the analyte is amplified by the field from the excited surface plasmons. This diagram is not to scale: the surface feature should be a fraction of the wavelength of the incident field and the analyte, which is a single molecule, should be much smaller than the surface feature.

EM enhancement from a non-interacting sphere

A simple method to quantitatively investigate the effect of the EM enhancement is to approximate a rough metal surface by a single sub-wavelength metal sphere. Such an approach has been used by various authors.[21,26,28,29] Slightly more complex models involving spheroids, embedded hemispheres and hemispheroids have also been investigated.[25,29,30] The results show that smaller spheres produce higher maximum enhancements, but over smaller ranges in wavelength. For instance, a 5 nm silver sphere produces a maximum enhancement of more than 10^6 but only over a very narrow range of wavelengths ($\sim$380$\pm$20 nm), whereas a 50 nm sphere produces an enhancement between 10^3 and 10^4 over most of the visible range.[28] As expected these studies also find that the maximum enhancement occurs when the adsorbed molecule is closest to the surface. The studies using spheroids and embedded hemispheres show that the EM enhancement is significantly higher than for spheres and is highest at the "sharp" points, the so called lightning rod effect.[19]

One of the more interesting results of the sphere-model studies is a relationship between the optical dielectric of the metal sphere and the electromagnetic field enhancement

factor. This relationship states[28]

$$\frac{E_{\text{sphere}}}{E_{\text{normal}}} \propto \frac{\varepsilon_1(\omega) - \varepsilon_2(\omega)}{\varepsilon_1(\omega) + 2\varepsilon_2(\omega)} \tag{2.11}$$

where $\varepsilon_1(\omega)$ is the (complex) dielectric of the metal and $\varepsilon_2(\omega)$ is the dielectric of the surrounding medium. From equation (2.11) it is clear that large enhancement factors will be achieved if $\text{Re}(\varepsilon_1(\omega)) = -2\varepsilon_2(\omega)$, and $\text{Im}(\varepsilon_1(\omega))$ is small. This explains why certain metals, like silver, gold and copper, produce significant SERS enhancement while other metals do not: the dielectric of these metals at visible wavelengths is most appropriate for producing large enhancements. This also explains why higher enhancements are achieved by matching specific metals to specific excitation wavelengths (i.e. using silver substrates for green excitation while using gold substrates for red excitation).

Where available, experimental results have compared favourably to the results of these models.

EM enhancement from interacting structures

The most advanced models allow multiple metal objects to interact with the incident field as well as with each other. Some models represent the rough surface as coupled spheres,[31] others as a superposition of gratings,[32] some as arrays of embedded half cylinders,[33] and others as fractal clusters.[34] In all cases, the general result is the same: interaction between the small-scale objects increases the EM enhancement significantly and the locations of maximum enhancement occur at the voids or points of contact between the metallic substructures.

One of the more advanced models that uses multiply-coupled colloids with size, shape and spacing as free parameters[35] was used in an optimization process to attempt to determine the absolute maximum possible EM enhancement. The study determined that the maximum possible EM enhancement is of the order of 10^{11} which is 3 orders of magnitude lower than has been measured for an overall SERS enhancement.[23] This suggests that an enhancement mechanism in addition to the EM mechanism is at work in SERS.

2.3.2 Charge Transfer Enhancement Mechanism

Although the EM enhancement model is very successful at explaining the bulk of SERS enhancement it does not adequately explain all of the observed enhancement behaviour. To address these shortcomings Otto proposed the adatom, or charge-transfer (CT), model.[36,37] The basis for this model is the creation of a complex between the analyte molecule and an atomic scale surface feature, or adatom. Within this complex, charge transfer between the adsorbate and the adatom may occur, creating a new channel of interaction with the incident electric field, effectively increasing the cross section. This interaction is shown schematically in figure 2.5. Additionally, the momentum matching requirements for photonic interaction are relaxed due to the additional degrees of freedom present in the complex. Since the CT mechanism relies on the chemical interaction between the adsorbate and the surface, it is clear that its effects are very dependent on the chemical properties of the materials involved and is therefore sometimes referred to as the chemical mechanism.

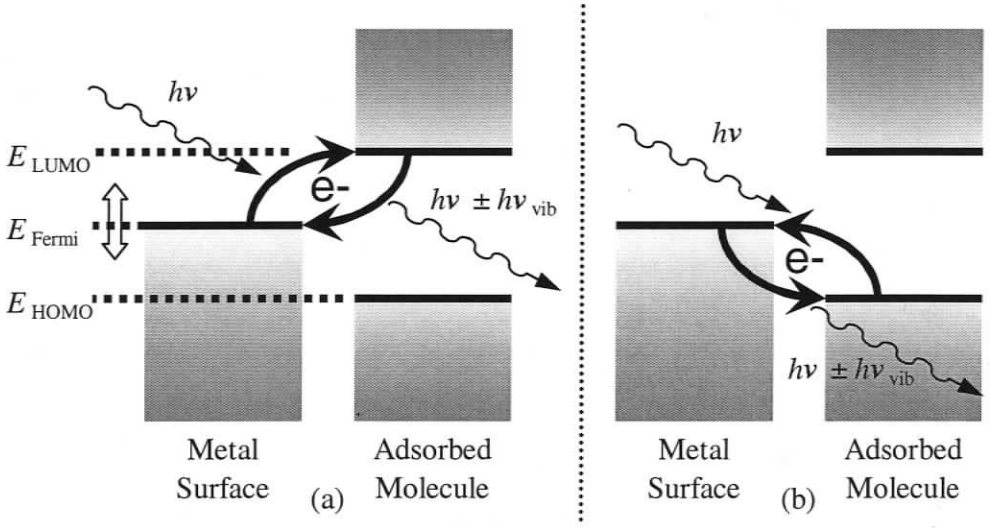

Figure 2.5: The charge-transfer mechanism allows the transfer of an electron between the adsorbate and a surface adatom and vice versa. An electron can transfer from the Fermi level of the metal to the lowest unoccupied molecular orbital (LUMO) and back (a), or from the highest occupied molecular orbital (HOMO) to the Fermi level and back (b). A potential applied to the metal will change the energy of the Fermi level.

The importance of the CT mechanism can best be demonstrated through example. Each of the following four paragraphs gives an example of a SERS observation that the EM mechanism is incapable of fully explaining followed by an account of how the CT mechanism solves the shortcoming.

As was alluded to in the previous section, certain SERS systems have produced enhancement factors in excess of what can be accounted for by the EM mechanism.[35] The enhancement produced by the CT mechanism is in addition to the enhancement produced by the EM mechanism. Thus, although it generally produces enhancements that are orders of magnitude smaller than the EM mechanism, it can adequately explain the difference between the measured enhancement and that expected from the EM mechanism alone.

It was noted early on in SERS research that different molecules with modes belonging to the same symmetry species and with similar normal Raman cross sections, such as CO and N_2, could have different SERS enhancements,[38] well in excess of what could be explained by the EM mechanism's minor adsorbate sensitivity. Such enhancements are sometimes found in conjunction with significant shifting and broadening of the Raman bands. The CT mechanism naturally explains these effects as the result of different chemical interactions between the analytes and the surface. Both the bond strength and the energy difference between the molecular orbitals and the metal's Fermi level can cause significant analyte specificity with the CT mechanism.

In some SERS experiments Raman modes within the same molecule undergo differential enhancement.[39] This is to be expected to some extent with the EM mechanism, but should simply be a function of how the dielectric of the metal changes with the scattered wavelength which is not what is found experimentally. Such a result is predicted with the CT mechanism since the interaction with the surface may be predominantly through a specific portion of the adsorbed molecule producing differential enhancement to those modes dominated by that portion of the molecule.

A common experimental method is to perform SERS with the analyte adsorbed to the electrode of an electrochemical cell. In such a configuration it is possible to apply a potential to the adsorption surface which can affect various parameters, including surface

coverage, adsorption species, etc. With the EM mechanism, variation of the applied potential is expected to alter the enhancement through higher order electromagnetic effects and changes to the properties of the adsorption, such as orientation at the surface and surface coverage. While performing such experiments, it becomes clear that the relationship between enhancement and applied potential has a dependence on the energy of the incident laser that cannot be explained by the EM mechanism alone.[40] A potential applied to a metal surface changes its Fermi energy which, as shown in figure 2.5, can create a resonance with the CT mechanism if the Fermi level is set appropriately for a given incident field. Again, the CT mechanism can successfully explain an experimental result that is beyond the EM mechanism.

In a number of specific experimental situations the EM mechanism on its own is insufficient to satisfactorily explain the results and it falls upon the CT mechanism to complete the picture. However, the CT mechanism is viewed as being for special situations and is often considered only when required. This view is somewhat justified considering that the EM mechanism provides enhancements orders of magnitude larger than the CT mechanism and is a general mechanism for localized field enhancement that affects all surface spectroscopic techniques, whereas the CT mechanism only plays a major role for specific techniques and specific adsorbates. The commonly held opinion of the relationship between the EM and CT mechanisms is concisely given by Moskovits:[19] "it seems more correct to think of the chemical effects [CT] as changing the nature and identity of the adsorbate while the em [EM] effect actually produces the enhancement."

2.4 Specialized Raman-Related Techniques

2.4.1 Resonance Raman

An additional advantage of the quantum model described in section 2.2.3 is its ability to explain resonance conditions. Equation (2.8) shows that the transition polarizability tensor is calculated by summing over all possible virtual states. Intuitively one would expect the most likely virtual state, and therefore the one that dominates the summation,

to be the virtual state with an energy level exactly E_0 above the initial level. Equation (2.8) supports this belief since the denominator of the first term is minimized when $E_0 = E_{vi}$, thus maximizing the weighting causing it to dominate the summation. When $E_0 = E_{vi}$ the denominator of the first term is equal to $-i\Gamma_v$ which is inversely proportional to the lifetime of the virtual state $|\psi_v\rangle$. If the "virtual" state when $E_0 = E_{vi}$ is an allowed excited electronic state it will have a very long lifetime, meaning $-i\Gamma_v$ will approach 0 causing the first term of Eq (2.8) to increase dramatically. Such a resonance condition is known to increase the Raman signal by 3 to 5 orders of magnitude.[5]

2.4.2 An Introduction to Molecular *Ab Initio* Calculations

Some methods for analyzing Raman data require information that would be difficult or impossible to produce experimentally. One technique for generating such data theoretically is molecular *ab initio* calculations.

Optimization of Molecular Geometry and Electronic Orbitals

The field of quantum chemistry is essentially the pursuit of solutions to the Schrödinger equation for a molecular system. For most chemical systems it is sufficient to use the nonrelativistic, time-independent Schrödinger equation. Applying the Born-Oppenheimer approximation (fixed nuclei) further simplifies the equation by eliminating the nuclear kinetic energy, reducing the nucleus-nucleus potential energy to a constant, and allowing the nuclear potential to be treated as static.

With this approximation the Schrödinger equation for a molecular system is

$$\hat{H}\psi_i = E\psi_i \tag{2.12}$$

where $\hat{H}$ is the Hamiltonian operator

$$\hat{H} = \hat{T} + \hat{V}_{\mathrm{Ne}} + \hat{V}_{\mathrm{ee}} + \hat{V}_{\mathrm{NN}} \tag{2.13}$$

and the wave function ψ is a function of the positions and spin states of the M electrons

$$\psi_i = \psi_i(\boldsymbol{r}_1, s_1, \boldsymbol{r}_2, s_2, \ldots, \boldsymbol{r}_M, s_M) \tag{2.14}$$

The four operators of the Hamiltonian are the kinetic energy of the electrons, $\hat{T}$, the potential energy due to interaction between the nuclei and the electrons, $\hat{V}_{\mathrm{Ne}}$, the potential energy due to interaction between the electrons, $\hat{V}_{\mathrm{ee}}$ and the potential energy due to interaction between the nuclei, $\hat{V}_{\mathrm{NN}}$. As mentioned above this last term is a constant for a given geometry. Unfortunately, except in the case of hydrogen-like systems, we have no closed form solution for ψ_i. The problem then becomes how to develop appropriate estimates for wavefunctions that will satisfy equation (2.12).

One option would be to develop a test wavefunction and, through an iterative procedure, refine the wavefunction until it is a satisfactory solution to equation (2.12), but this requires a method for testing the goodness of the wavefunction. Fortunately the ground state wavefunction, ψ_0, should produce a solution with the minimum energy, E_0, so by modifying the test wavefunction to try to minimize E it should be possible to determine an approximation for the ground state wavefunction. One possible problem with this method is that it is not obvious that the energy cannot be optimized to an energy lower than the ground state. Fortunately the variational principle of the Schrödinger equation[41,42] provides assurance that this will not occur:

$$\left\langle \psi_{\mathrm{test}} \middle| \hat{H} \middle| \psi_{\mathrm{test}} \right\rangle = E_{\mathrm{test}} \geq E_0 = \left\langle \psi_0 \middle| \hat{H} \middle| \psi_0 \right\rangle \tag{2.15}$$

It should be made clear that the minimization of energy technique is only useful for finding the ground state wavefunction and cannot be used to find any other state of the system.

A method for actually calculating the expectation of the Hamiltonian of the system, $\left\langle \psi \middle| \hat{H} \middle| \psi \right\rangle$, is still required. Calculating the $\hat{T}$, $\hat{V}_{\mathrm{Ne}}$ and $\hat{V}_{\mathrm{NN}}$ terms are relatively straight forward for a given geometry, but the number of integrations required for the electron-electron interaction term which is given by[41]

$$\hat{V}_{\mathrm{ee}} = \sum_{i=1}^{M-1} \sum_{j=i+1}^{M} \frac{1}{r_{ij}} \tag{2.16}$$

becomes computationally intensive with even the simplest test wavefunction. One method for reducing the computational requirements is to allow each electron to interact with the mean potential of all the other electrons combined as a single field rather than interacting

with all the other electrons in a pair-wise fashion. This method was proposed by Hartree in 1928[43] and generalized by Fock in 1930[44] and is known as the Hartree-Fock (HF) method. It is typically implemented following a process described by Roothaan.[45]

Finally, a method for constructing appropriate test wavefunctions is needed. The HF approximation allows the multi-electron wavefunctions to be estimated by a linear combination of atomic orbitals (LCAO), however a basis set from which to construct the atomic orbitals is required. One possible choice would be to construct the orbitals from the solutions to the hydrogen-like system. This was the original basis set used in the HF method but produces computationally difficult integrations and converges too slowly to be useful for all but the smallest systems. A slightly better choice was formulated by Slater in 1930[46] and are known as Slater type orbitals (STO). The STO converge more quickly and are slightly easier to integrate. In 1950 Boys suggested that STO could be approximated by combinations of Gaussian type orbitals (GTO)[47] which can be integrated analytically instead of numerically. Even though more GTO than STO are required to produce the same quality of approximation the greatly reduced computational needs of the GTO make them a far superior option. Essentially all current molecular HF calculations use Gaussian basis sets.

The wavefunction for the HF method requires 3 spatial coordinates and a spin coordinate for each of the M electrons in the system resulting in $4M$ parameters, yet the Hamiltonian operator (equation (2.13)) only acts on at most two particles at a time regardless of the size of the system. This discrepancy led to a search for a more compact way to describe the M-electron system. In 1964 Hohenberg and Kohn[48] proved that a system of any number of electrons could be completely described by a single electron density function, $\rho(\boldsymbol{r})$, and that this function would be a solution to the Schrödinger equation. This methodology is referred to as density functional theory (DFT) and transforms the required solution from a large number of independent values to a single function. In 1965 Kohn and Sham[49] developed a procedure for calculating a self-consistent electron density function for molecular systems. One shortcoming of the DFT method is the lack of a procedure for producing an appropriate initial test function. A low level HF calculation

is often used to calculate the initial guess for the DFT method. The DFT method requires less computation yet provides more accurate results than HF methods. The vast majority of today's quantum molecular chemistry uses DFT methods.

Regardless of the method used to calculate the test wavefunctions or the energy of the system, the algorithms used to calculate the optimized ground state typically use an iterative self consistent field (SCF) method. This is a process of using the solution from one iteration of the procedure as the initial guess for the start of the next iteration which continues until the changes in a given iteration are sufficiently small. Such a method is used to calculate the optimal electron distribution for a given geometry, and, through an alternating iteration of SCF calculations, the optimal nuclear geometry itself. The end result is a complete, consistent description of both the nuclear and electronic molecular ground-state configurations.

Normal Coordinates for Molecular Vibrations

Molecular vibrational modes can be solved using standard classical methods for an N body system. The optimized nuclear geometry, as calculated using the *ab initio* methods described above, represents the equilibrium state of the system. Using mass-weighted Cartesian displacement coordinates, $q_i = \sqrt{m_i}(x_i - x_{i\mathrm{eq}})$, the classical kinetic energy of a N-nuclei system is

$$T = \frac{1}{2}\sum_{i=1}^{3N}\left(\frac{\mathrm{d}q_i}{\mathrm{d}t}\right)^2 \tag{2.17}$$

and the potential energy, given as a Taylor series, is

$$V = V_{\mathrm{eq}} + \sum_{i=1}^{3N}\left(\frac{\partial V}{\partial q_i}\right)_{\mathrm{eq}} q_i + \frac{1}{2}\sum_{i=1}^{3N}\sum_{j=1}^{3N}\left(\frac{\partial^2 V}{\partial q_i \partial q_j}\right)_{\mathrm{eq}} q_i q_j + \frac{1}{6}\sum_{i=1}^{3N}\sum_{j=1}^{3N}\sum_{k=1}^{3N}\left(\frac{\partial^3 V}{\partial q_i \partial q_j \partial q_k}\right)_{\mathrm{eq}} q_i q_j q_k + \cdots \tag{2.18}$$

Since the equilibrium point is, by definition, a minimum in the potential energy function, the second term of the Taylor series is equal to zero. Limiting the expansion to the quadratic order, which is an appropriate approximation for small oscillations, gives

$$V = V_{\mathrm{eq}} + \frac{1}{2}\sum_{i=1}^{3N}\sum_{j=1}^{3N}\left(\frac{\partial^2 V}{\partial q_i \partial q_j}\right)_{\mathrm{eq}} q_i q_j \tag{2.19}$$

The Lagrange equation in mass-weighted Cartesian displacement coordinates is

$$\frac{\mathrm{d}}{\mathrm{d}t}\left(\frac{\partial T}{\partial \dot{q}_k}\right)+\frac{\partial V}{\partial q_k}=0 \qquad k=1,2,\ldots,3N \tag{2.20}$$

Substituting equation 2.17 and equation 2.19 into equation 2.20 gives

$$\frac{\mathrm{d}^2 q_k}{\mathrm{d}t^2}+\frac{1}{2}\frac{\partial}{\partial q_k}\sum_{i=1}^{3N}\sum_{j=1}^{3N}\left(\frac{\partial^2 V}{\partial q_i \partial q_j}\right)_{\mathrm{eq}} q_i q_j = 0 \qquad k=1,2,\ldots,3N \tag{2.21}$$

The second term of equation 2.21 can be simplified by noting that the partial derivative of all the terms in the summation for which neither i nor j are equal to k are zero and that when $i=k$ the summation runs over all j and when $j=k$ the summation runs over all i, that is

$$\begin{aligned}\frac{\partial}{\partial q_k}\sum_{i=1}^{3N}\sum_{j=1}^{3N}\left(\frac{\partial^2 V}{\partial q_i \partial q_j}\right)_{\mathrm{eq}} q_i q_j &= \sum_{j=1}^{3N}\left(\frac{\partial^2 V}{\partial q_k \partial q_j}\right)_{\mathrm{eq}} q_j + \sum_{i=1}^{3N}\left(\frac{\partial^2 V}{\partial q_i \partial q_k}\right)_{\mathrm{eq}} q_i \\ &= 2\sum_{i=i}^{3N}\left(\frac{\partial^2 V}{\partial q_i \partial q_k}\right)_{\mathrm{eq}} q_i \end{aligned} \tag{2.22}$$

Then equation 2.21 becomes

$$\frac{\mathrm{d}^2 q_k}{\mathrm{d}t^2}+\sum_{i=1}^{3N}\left(\frac{\partial^2 V}{\partial q_i \partial q_k}\right)_{\mathrm{eq}} q_i = 0 \qquad k=1,2,\ldots,3N \tag{2.23}$$

This is a system of $3N$ simultaneous linear homogeneous differential equations. The values of $(\partial^2 V/\partial q_i \partial q_k)_{\mathrm{eq}}$ need to be calculated using perturbation methods with the above discussed *ab initio* models. Using these values, the equations can be solved to give a set of $3N$ well defined solutions of the form[50]

$$q_i = \sum_{m=1}^{3N} A_{im}\sin(\sqrt{\lambda_m}t+b_m) \qquad i=1,2,\ldots,3N \tag{2.24}$$

where A_{im} is the displacement amplitude in one of the Cartesian dimensions for a particular nucleus in the molecule while vibrating in normal mode m, $\sqrt{\lambda_m}$ is the angular frequency of normal mode m and b_m is the phase of normal mode m. The A_{im} can only be calculated to within a multiplicative constant for a given mode m, but are independent for each m because the original equations are homogeneous. Normalizing the A_{im} for each mode defines unique values

$$l_{im} \equiv \frac{A_{im}}{\left(\sum_{i=1}^{3N} A_{im}^2\right)^{1/2}} \tag{2.25}$$

giving the normalized solutions

$$q_i = \sum_{m=1}^{3N} l_{im} \sin(\sqrt{\lambda_m} t + b_m) \qquad i = 1,2,\ldots,3N \tag{2.26}$$

The set of equations in equation (2.26) define the mass weighted Cartesian displacements in terms of the normal mode motions. A more useful solution is to invert this and define the normal mode motions in terms of their component mass weighted Cartesian displacements

$$Q_m = \sum_{i=1}^{3N} d_{mi} q_i \qquad i = 1,2,\ldots,3N \tag{2.27}$$

where the d_{mi} are chosen so that the kinetic and potential energies are given by

$$T = \frac{1}{2} \sum_{m=1}^{3N} \left(\frac{\mathrm{d}Q_m}{\mathrm{d}t} \right)^2 \qquad \text{and} \qquad V = V_{\mathrm{eq}} + \frac{1}{2} \sum_{m=1}^{3N} a_m Q_m^2 \tag{2.28}$$

where the a_m are constants. Such a solution exists, and the appropriate d_{mi} are simply[50]

$$d_{mi} = l_{im} \tag{2.29}$$

After performing the appropriate algebra[50] the equations of motion for the normal modes are given by

$$Q_m = B_m \sin(\sqrt{\lambda_m} t + b_m) \qquad m = 1,2,\ldots,3N \tag{2.30}$$

$$\text{where} \qquad B_m = \left(\sum_{i=1}^{3N} \frac{A_{im}}{l_{im}} \right)$$

These are the normal mode vibrations discussed in section 2.2.1. Although equation (2.30) suggests there are $3N$ normal modes, an actual calculation will find that 6 of the λ_m (5 in the case of a linear molecule) will actually be zero. As explained in section 2.2.1 these 6 zero-frequency modes are the three-dimensional translation and three-dimensional rotation of the molecule.

It is important to note that these solutions represent a logical coordinate system with which to describe molecular motion in terms of allowed vibrations. They do not directly describe the actual motions of the molecule. The actual molecular motions are represented by specifying the amplitude of each of the normal modes and the motion itself is a complex superposition of the various modes all occurring simultaneously.

In practice the vibrational frequencies calculated *ab initio* generally overestimate the values measured experimentally by 10-15%. This discrepancy arises because of approximations used to calculate $(\partial^2 V/\partial q_i \partial q_k)_{\text{eq}}$ and from the approximations used in finding the optimized geometry.

2.4.3 Molecular Orientation in SERS

Surface spectroscopy, used in conjunction with the results of *ab initio* calculations, can be used to determine molecular adsorption orientation. The basic reason for making such a determination is to compare the measured vibrational-band intensities to the values expected for randomly oriented molecules. The differences, along with the properties of the bands, can be used to determine the adsorption orientation. For surface infrared spectroscopy, which probes a vector quantity (the dipole moment) using a field that is essentially reduced to a single component at a metal surface, the process is simply a matter of comparing the projection of calculated transition dipole moment vectors to the measured spectra. For SERS, which probes the interaction with a tensor quantity (the polarizability) using multi-component fields, it requires an assessment of the enhancement mechanism involved and a detailed examination of the portions of the molecule that contribute to a particular vibrational mode. This entails briefly reviewing the enhancement theories discussed in section 2.3 and the vibrational modes calculated in section 2.4.2 as well as a cursory reexamination of the symmetry selection rules mentioned in section 2.2.3.

The intensity of a SERS band is a function of the intrinsic probability of Raman scattering from the band, the EM enhancement of the band and the CT enhancement of the band. The intrinsic probability can be calculated using the quantum mechanical model described in section 2.2.3 with the wavefunctions determined from the *ab initio* methods explained in section 2.4.2. Understanding the variation in enhancement for the different bands within a molecule requires a more detailed look at how the enhancement mechanisms work on an intramolecular scale.

The EM Mechanism and Molecular Orientation

There are three important aspects of the EM mechanism that require consideration when investigating how it can affect the SERS response of individual vibrational bands: how the surface affects the symmetry selection rules, how the field strength varies with distance from the surface, and how the geometry of the surface affects the relative orientation of the excitation field.

The Raman scattering selection rules mentioned in section 2.2.3 state that for a vibrational mode to be Raman-active it must belong to the same symmetry species as at least one non-zero component of the polarizability tensor. However, when a molecule is adsorbed on a surface its symmetry may be modified, affecting its selection rules. The matter is further complicated by the effect a metal surface has on the incident field, essentially doubling its normal component while decreasing its parallel component. Modified selection rules for a smooth metal surface have been derived rigorously[27] and have been modified and applied somewhat successfully to small spheres and other surfaces possessing sphere-like symmetry.[51,52] An additional difficulty in the case of larger molecules with complicated normal modes is that the modes do not typically possess any simple symmetry. However, by examining the relative motion of the individual atoms for a particular mode in conjunction with the effects of the surface, it is often possible to obtain qualitative information about the relative enhancement of the various bands. The rule of thumb is that the normal modes involving motions with dipole changes perpendicular to the surface generally experience the largest enhancement.

As was explained in section 2.3.1 the EM enhancement is the result of an amplification of the electromagnetic field at specific surface features. The sphere-based model used previously predicts that the enhanced field falls off as $(r/(r+d))^3$ where r is the radius of curvature of the feature and d is the distance from the surface.[52] This effect, coupled with the fact that the Raman intensity is proportional to the fourth power of the field enhancement (equation (2.10)), leads to $I_{\text{Raman}} \propto (r/(r+d))^{12}$. This implies that for surface features with small radii of curvature, the enhancement could noticeably vary over the length of a molecule causing a relative increase in enhancement of those modes

driven by the portion of a molecule adsorbed closer to the surface.

The rough surfaces required for SERS do not have a clearly defined surface normal, but rather a highly erratic and unpredictable orientation. It might be expected that such a configuration would eliminate any ability to collect information about the adsorption orientation although it turns out that this is not the case. Two important factors contribute to this situation: the fact that molecules absorb to the surface with the same relative orientation regardless of the orientation of the surface, and the fact that the Raman signal is dominated by those surface locations with maximum field enhancement, which will all have a similar orientation to the incident field. The measured Raman signal should therefore consist of the integrated signal from similarly oriented molecules adsorbed on similarly oriented surfaces preserving the information about the adsorption geometry.

The CT Mechanism and Molecular Orientation

As explained in section 2.3.2 the CT mechanism is the result of a resonance-like interaction between the incident field and a molecule-adatom complex. This interaction will only produce Raman scattering if the molecule undergoes a vibrational excitation (or relaxation) during the brief period that the transferred charge is out of place (see figure 2.5). Since the transferred charge is more likely to interact with (or be donated by) the portion of the molecule most strongly interacting with the adatom the vibrational modes involving that portion of the molecule are more likely to be enhanced. By using the normal coordinates calculated in section 2.4.2, which explicitly describe the nuclear motions involved in a particular vibrational mode, it is possible to find those modes which are most closely linked to a particular region of the molecule.

It is important to note that like the SERS effect itself, the EM and CT mechanisms both contribute and must be considered in combination with each other. The EM and CT differential enhancement are both rather qualitative, and are therefore only useful to distinguish between a limited set of possible logical adsorption geometries, and even then, depending on the specifics, may not be able to distinguish between certain options. Regardless of which mechanism might cause an enhancement difference between vibra-

tional modes, the SERS intensity is dominated by the signal from a limited number of special surface locations, and the SERS signal from these locations may not necessarily be representative of the entire surface.

2.5 Current Areas of Research

Surface-enhanced Raman scattering is an active research area with ongoing work in fields as diverse as biophysics, nanotechnology and environmental science. SERS research currently produces approximately 200 papers per year.[53] A brief introduction to three areas of ongoing work are included as examples of the interest in the field.

2.5.1 Excess Anti-Stokes Raman Scattering & Optical Pumping

In 1996 Kneipp *et al.* observed anti-Stokes SERS intensities for two common laser dyes, crystal violet and rhodamine 6G, significantly in excess of those expected.[54] They interpreted these results as an indication that the Raman cross section of these systems is sufficiently large so as to produce a non-thermal population of the first excited vibrational state, i.e. optical pumping. They argued that these systems had effective Raman cross sections 10 to 15 orders of magnitude larger than for typical Raman systems. Kneipp *et al.* published additional papers in 1998[55] and 1999[56] based on this interpretation.

In 2000 Haslett *el al.* pointed out that, as explained in section 2.3.1, the electromagnetic component of SERS enhancement acts on both the incident and Raman scattered fields, and therefore a Raman enhancement of 10^{15} would not indicate an equivalent increase in effective Raman cross section.[57] This effectively eliminates the possibility that Raman optical pumping is the cause of the unexpected anti-Stokes intensity. Furthermore, Haslett *el al.* were unable to reproduce certain non-linear behaviour[57] observed by Kneipp *et al.*[54] that supported the case for optical pumping. Haslett *el al.* suggested that the measured anti-Stokes excess is the result of resonance behaviour causing a significant difference between the Stokes and anti-Stokes cross sections,[57] something that was not considered by Kneipp *et al.* In 2004 Brolo *et al.* investigated the properties a resonance would require to produce the observed data and also explored the possibility that

the sample was not in thermal equilibrium with its surroundings.[58] Contemporaneously, Maher *et al.* were theoretically and experimentally examining the relationship between surface resonances, excitation wavelength and anti-Stokes intensity.[59] In 2006 Le Ru and Etchegoin examined the problem using techniques designed to separate the effects of general heating, vibrational pumping and variation in cross section, and found that variation in cross section plays a significant role in the anti-Stokes anomaly while general heating is also important. They found no evidence for vibrational pumping.[60] In contrast, Kneipp and Kneipp in 2006 confirmed a non-linear power dependence for both SERS anti-Stokes and surface-enhanced hyper Raman scattering[61] suggesting that pumping is occurring. In 2006 Maher *et al.*, taking a different tack, attempted to decouple the effects of possible optical pumping from thermal excitation by manipulating the temperature of the sample while using low laser power to avoid unexpected sample heating.[62–64] Their interpretation of the results is that optical pumping does occur, but in agreement with their previous results[59] it is only detectable at cryogenic temperatures and is insignificant in typical SERS experiments.

It is obvious that the debate over optical pumping is ongoing. This active area of research is the subject of chapter 4, where the SERS anti-Stokes to Stokes ratio is discussed in more detail.

2.5.2 SERS Single-Molecule Detection

In 1997 the field of SERS was rejuvinated when Kneipp *et al.*,[23] and nearly simultaneously Nie and Emory,[24] observed room temperature single-molecule SERS spectra for the first time. The advent of single-molecule SERS with its Raman-like molecular specificity and fluorescence-like sensitivity indicated the birth of an important new analytical tool. In addition to more accurately identifying molecular species, SERS has two other significant advantages over fluorescence. The relaxation time for an excited vibrational state is so much shorter than for an excited electronic state that, at saturation, 3 orders of magnitude more Raman photons than fluorescence photons would be produced. Also, since SERS does not typically produce excited electronic states the analyte is much less

susceptible to photodecomposition. The biggest disadvantage of SERS is the need for the analyte to be adsorbed onto an appropriate SERS-active surface. Progress in single-molecule SERS continues to open the field to new applications.

Nie and Emory's 1997 work used an excitation source (514.5 nm argon ion) within the absorption band of their laser-dye analyte (rhodamine 6G), and although they claim that such an absorption resonance is probably not required to achieve single-molecule sensitivity[24] their experimental setup does not enable them to state this conclusively. Kneipp *et al.*, however, used near-infrared excitation which is outside the absorption band of their analyte (crystal violet)[23] proving that single-molecule sensitivity does not require such a resonance. Both groups noted that the Raman signal "blinked" on and off, an expected result of the single analyte molecule drifting into and out of the scattering volume,[23,24] while Nie and Emory also noted fluctuations in the frequencies of the Raman bands over time.[24] Kneipp *et al.* carried out further analysis on the blinking behavior to show that it followed a Poisson distribution appropriate for their analyte concentration. In 1998 Kneipp *et al.* achieved single-molecule sensitivity for pseudoisocyanine,[65] another laser dye, and measured single-molecule anti-Stokes SERS for the first time. They again measured an appropriate Poisson distribution for the signal over time.

Later in 1998 Kneipp *et al.* applied their technique to the DNA base adenine and proved that SERS is capable of detecting single "colorless" molecules,[66] confirming that the technique is applicable to a broader range of molecules than just dyes. It is important to note that although fluorescence techniques are used extensively for biological samples, the samples typically need to be labeled with fluorescent markers before being detected. The prospect of being able to directly detect individual, biologically relevant molecules is extremely appealing.

In 1999 Michaels *et al.* attempted to determine the role of the CT mechanism in the enormous enhancement factors of single-molecule SERS by comparing the intensity of the Raman signal to the Rayleigh scatter which should only be affected by the EM enhancement, not the CT enhancement.[67] They found that there was little correlation between the two intensities suggesting that the CT mechanism plays an important role in

achieving single-molecule sensitivity. In 2002 Doering and Nie used silver nanoparticles immobilized in a micro-fluidic device to determine the importance of the CT mechanism in single-molecule SERS of rhodamine 6G.[68] They found that treatment with certain "activating" ions (chloride, bromide and iodide) increased the SERS intensity by factors of $\sim$100–1000 while others (citrate, sulfate and fluoride) had little effect, and still others (thiosulfate) eliminated the SERS signal completely. By using *in situ* surface plasmon resonance scattering they were able to prove that the chemical treatments were not affecting the EM enhancement of the nanoparticles confirming that CT enhancement is critically important to single-molecule SERS.

Another important aspect of single-molecule SERS is its ability to obtain information that would be lost if data is averaged over multiple molecules. Essentially all applications attempting to monitor an active process fall into this category because differences in rates and commencement times causes the data to be smeared out. One such application is the monitoring of biological processes. In 2002, Bjerneld *et al.* attempted to measure the enzymatic activity of horseradish peroxidase using single-molecule SERS.[69] Although they successfully measured single-molecule SERS, attaching the enzyme to a silver nanoparticle to achieve SERS interferes with the normal function of the protein, causing inaccurate results. Although not yet at the single-molecule level it is also possible to obtain SERS spectra from living cells.[70]

Theoretical research into the exact enhancement processes involved in single-molecule SERS is still ongoing. Otto continues to point out the importance of the CT mechanism and the size limitation imposed by the spacing between nanoparticles required to produce optimal enhancement.[71] In 2006 Futamata investigated the broad fluorescence background bands often associated with single-molecule SERS as well as the importance of the junctions between adjacent nanoparticles. Also in 2006 Zhao *et al.* developed models with dielectric-cored nanoshells that produce EM enhancement factors almost sufficient to produce single-molecule SERS without the need for any CT enhancement.

As our understanding of single-molecule SERS continues to grow, so too do its possible applications. With its fluorescence-rivalling intensity and explicit molecular identi-

fication, SERS shows great promise in fields requiring trace analysis, such as blood monitoring and environmental science, as well as those requiring non-aggregate rate information, such as biological processes and chemical interactions. Single-molecule SERS is currently one of the more active fields in spectroscopy with a great deal of cross-discipline involvement.

2.5.3 SERS-Active Surfaces

The perfect SERS-active surface would be precisely reproducible, completely stable, easy to fabricate and would produce extremely high enhancement. Unfortunately the perfect substrate does not exist and a trade-off between the various characteristics is often required. Due to the dielectric properties required for good SERS, as described in section 2.3.1, only gold, silver and copper are appropriate substrate materials. Research into producing better SERS substrates is a dynamic field with much work being done in the area of nanofabrication.

The earliest used activation procedures are, in general, the simplest: electrochemical roughening, colloidal aggregation and cold deposited island films. The seminal work in 1977[17,18] used oxidation-reduction cycling, a type of electrochemical roughening. This procedure, which was also applied for the work reported in chapters 3 and 4, uses an applied potential to temporarily dissolve a minute amount of the surface which is then redeposited, creating a randomly roughened surface. This procedure is extremely easy, especially if further electrochemistry is going to be carried out, produces moderate enhancement ($\sim 10^6$) with good stability, but, due to its random nature, is not very reproducible. Colloidal aggregation, which was used in the first single molecule SERS work,[23] is also a simple procedure which produces high enhancements ($\sim 10^8$, or higher if produced carefully), but is not completely stable nor reproducible. Cold deposited island films are the substrate of choice for working in vacuum systems because of their ease of preparation, although they only produce modest enhancements ($\sim 10^{4-5}$), are only stable while cold, and are not very reproducible. These random-deposition methods lack the consistency required of a top-notch SERS substrate.

One approach to improve uniformity has been to try and control the colloid aggregation process. The single molecule SERS work by Nie and Emory in 1997 attempted this by pre-screening and immobilizing their colloids.[24] Although somewhat successful it appears that what they thought were single colloids were likely aggregates, suggesting their reproducibility was the same as for standard colloid aggregation. In 2005 Addison and Brolo attempted to use stacked, self-assembled monolayers to create reproducible colloid structures, but produced samples with regularity similar to typical colloid aggregates.[72,73]

It is hoped that the use of nanofabrication techniques to produce SERS substrates will improve both the reproducibility and the enhancement. A number of techniques have been employed with varying degrees of success. One of the known advantages of nanofabrication techniques is that a substrate can be customized for a particular analyte and excitation source to try to maximize the sensitivity. For example, in 2004 Brolo *et al.* used focussed ion beam milling to produce nanohole arrays and showed that the SERS enhancement is a function of the spacing between the holes.[74] In 2001 Gennarsson *et al.* used electron-beam lithography to produce arrays of silver particles on silicon and found that enhancement increased rapidly as the spacing between the particles decreased.[75] In 2004 Félidj *et al.* produced arrays of gold nanoparticles on smooth gold with electron-beam lithography and produced tunable enhancements up to $\sim 10^8$ but found that the thickness of the smooth gold layer also affected the results.[76] In 2001, Litorja *et al.*,[77] and in 2002, Dick *et al.*,[78] investigated and characterized substrates of metal film over nanospheres and found them to be stable under variations in temperature and applied potential with reasonably reproducible enhancements. In 2003 Haynes and Van Duyne performed a systematic study of silver nanoparticle substrates produced by nanosphere lithography and achieved enhancements of $\sim 10^8$ and $\sim 10^{10}$ under resonance conditions.[79] Cintra *et al.* used nanosphere lithography to fabricate an array of gold hemispherical nanovoids with an enhancement of $\sim 10^7$ which was consistent within 10% across the entire surface, compared to a 1000% variation in enhancement over a typical electrochemically roughened surface.[80] It is clear that nanofabrication has produced some very promising SERS-active substrates although high costs keep it from being widely used.

The biggest impediment to producing perfect substrates is still a lack of reproducibility. Even with seemingly identical fabrication techniques, individual samples can differ by as much as an order of magnitude in enhancement[53] suggesting that a better understanding of the fabrication process itself may be required in addition to a more complete understanding of the SERS mechanisms. However, recent years have produced substantial improvements in SERS substrates and the field is still advancing.

Chapter 3

Spectroelectrochemistry of Oxazine 720

This chapter describes spectroelectrochemical results collected for oxazine 720. It begins with a brief introduction to oxazine 720 and a description of the experimental equipment and methods used. Results given include the electrochemically determined surface coverage, the normal and surface-enhanced Raman spectra, the assignment of certain well-enhanced SERS bands, a qualitative determination of molecular orientation, the verification of resonant behavior for a particular SERS band and the spectroscopic confirmation of the quasi-reversible electrochemistry of oxazine 720. The bulk of the material in this chapter has been previously published as "Surface-enhanced Raman scattering (SERS) from a silver electrode modified with oxazine 720" in the Canadian Journal of Chemistry, volume 82, number 10, pages 1474–1480, 2004.

3.1 Introduction

Oxazine 720 is a typical laser dye with a strong emission band in the 660–730 nm range and a strong photoabsorption band in the visible with a maximum at ~620 nm. Oxazine 720 is one of a number of laser dyes based on a phenoxazine ring, which is the structure responsible for its strong photoabsorption. Oxazine 720 is shown schematically in figure 3.1 along with phenoxazine and two other common phenoxazine dyes.

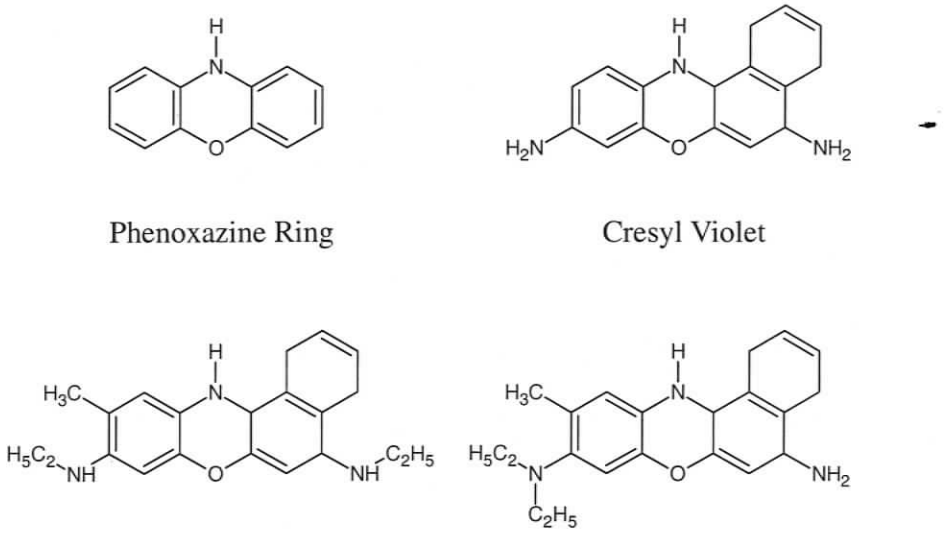

Figure 3.1: Molecular schematic of phenoxazine ring, oxazine 720 and two other common phenoxazine based laser dyes.

In addition to strong photoabsorption, phenoxazine based compounds typically possess reversible electrochemistry at metallic[81] and semi-conducting surfaces.[82] These physical properties make phenoxazine compounds suitable for applications in several industrial fields including electrocatalysis[83] and energy conversion.[84] The phenoxazine ring is hydrophobic which promotes molecular aggregation in aqueous solutions.[85] The resulting dye aggregates are important for several photo-conversion applications such as photography,[86] solar energy collection,[84] and photocatalytic remediation of ground water.[87] Phenoxazines can also be used as a charge transfer mediator in systems involving biological molecules such as NADH.[81,88] Furthermore, electrodes modified by polymeric phe-

noxazine compounds show electrocatalytic activity and have been used for such projects as the voltammetric determination of dissolved molecular oxygen in water at the μmol/L level.[89]

The electrochemistry of electrodes modified by phenoxazines is regularly reported in the contexts mentioned above, but there are few reports in the literature on the application of spectroelectrochemical methods to elucidate the electrochemical behaviour. This is particularly true for oxazine 720, where the utilization of *in situ* electronic spectroscopy to evaluate the reduction/oxidation (redox) potential of a metalloprotein[90] is among the few examples available. SERS is an ideal tool to investigate this class of compounds adsorbed on gold, silver or copper electrodes because adsorbed phenoxazines yield very large Raman enhancements, especially when excited with radiation within their electronic resonance, a condition termed surface-enhanced resonance Raman scattering (SERRS).[91] As discussed in section 2.5.2 the SERRS signal from dyes adsorbed on aggregated silver nano particles are capable of producing Raman enhancements up to 10^{15}. This high sensitivity has recently led to the exploration of the use of dyes as SERS (and SERRS) labels for the detection of minute amounts of biological species.[92]

Although there are no reports in the literature related to the SERS of oxazine 720 adsorbed on electrode surfaces under potential control (*in situ* SERS), the SERS spectrum of oxazine 720 adsorbed on silver colloids was reported by Schneider *et al.*[93] It was noted that the relative SERS intensities of several dyes (including oxazine 720) adsorbed on silver colloids are dependent on the nature of the anion present in the aqueous environment.[93] This phenomenon can be explained in terms of a tunable CT enhancement or in terms of anion-induced reorientation.[93] As discussed in section 2.3.2, the CT enhancement depends on the interaction between the adsorbate and the metallic adatom at the surface. If this coupling is affected by the interaction with the co-adsorbed anion it is possible that the anions can tune the CT resonance, producing variations in the SERS intensity for different anions. On the other hand, it is possible that interaction with the co-adsorbed anion could cause reorientation of the adsorbed dye, which would also produce variations in the SERS intensity. As shown in figure 2.5 it is possible to adjust the contri-

bution of the CT enhancement in an electrochemical environment by modifying the Fermi level via an applied potential.[94] *In situ* spectroelectrochemical SERS is an ideal tool to help clarify which of these possibilities is responsible for the anion-induced variation in enhancement measured by Schneider *et al.*[93]

Both electrochemical and SERS results from a silver surface modified with oxazine 720 in a 0.2 M KCl solution are presented in this chapter. The electrochemical and SERS data show that oxazine 720 undergoes reduction at ~ -500 mV versus a silver/silver-chloride reference electrode. The dependence of the SERS band intensities on the applied potential provides insights into the molecular orientation and the role of the CT mechanism. It will also be demonstrated that the reduced form of oxazine 720 remains adsorbed at the SERS active sites on the silver surface even at potentials as negative as -1000 mV.

3.2 Experimental

3.2.1 Solutions

Solutions for electrochemical and spectroelectrochemical measurements were prepared using 99% KCl from ACP and ultra-pure water (18.2 MΩ cm) from a Barnstead NANOpure Diamond water purification system. Analyte solutions were prepared with oxazine 720 from Lambdachrome and HPLC (high performance liquid chromatography) grade methanol from Aldrich.

3.2.2 Cell, Electrodes and Electrochemical Equipment

The working electrode was fabricated using a 99.99% silver rod from Alfa Aesar, machined into a silver disk $\sim$6.35 mm in diameter and mounted in a Teflon holder. Electrical contact with the silver is made through a stainless-steel rod threaded into a hole in the back surface of the electrode . Before each experiment, the silver electrode was polished with emery paper, followed by progressively finer grades of alumina powder down to 0.05 μm. After the surface polishing treatment, the silver electrode was rinsed thoroughly with ultra-pure water. The reference electrode was a 99.99% silver wire coated with an elec-

trochemically deposited silver chloride layer in a saturated potassium chloride solution. All potentials are given with respect to this saturated silver/silver chloride electrode. The counter electrode was a 0.3 mm platinum wire from Alfa Aesar. The potential at the silver surface was controlled with a model HAB-151 Hokuto Denko potentiostat/galvanostat.

The custom built spectroelectrochemical cell used for the SERS measurements was made entirely of glass and teflon. It contains a replaceable optics grade window for high quality spectroscopy and allowed all three electrodes to be independently positioned for optimal electrochemistry. This cell has been described in detail in a previous publication[95] and is shown schematically in figure 3.2. The solution-filled cell was purged with pre-purified nitrogen for 30 minutes prior to taking measurements and a gentle stream of nitrogen was maintained to blanket the solution during data acquisition to prevent oxygen exposure.

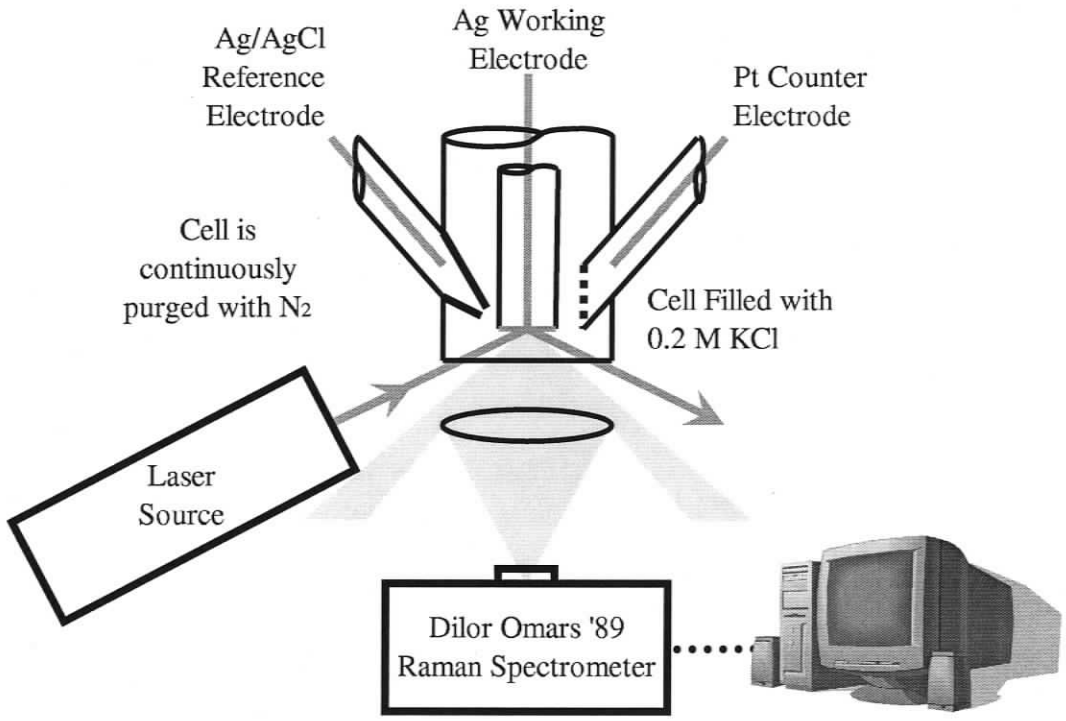

Figure 3.2: Sketch of the setup used to collect Raman spectra. The collection angle and the angle of incidence are not shown accurately here. See the text for the correct angles.

3.2.3 Activation Procedure

To create a SERS-active silver surface a sequence of oxidation-reduction cycles (ORCs) was performed on the polished silver electrode immersed in a 0.2 M KCl aqueous solution. A triangular potential sweep was applied, changing the surface potential from -700 mV to $+250$ mV and back to -700 mV at a scan rate of 5 mV/s. Typically three such cycles were performed to produce the desired roughness. The metallic silver oxidizes in this medium at potentials more positive than $+50$ mV, producing an insoluble AgCl film which is reduced back to metallic silver at ~ -100 mV during the reverse scan. The freshly formed silver surface obtained during the reduction is naturally rough, with features ranging in size from 50-400 nm.[96,97] This type of surface facilitates significant enhancement of the Raman signal for adsorbed molecules.[95,97]

The modified electrode was prepared using a droplet evaporation procedure. After the activation procedure, the rough silver electrode was removed from the cell and a drop of a $\sim 10\ \mu$mol/L solution of oxazine 720 in methanol was deposited on the electrode surface. The solvent was allowed to evaporate after which the surface was rinsed with ultra pure water and the modified electrode was returned to the cell. Electrochemical control was resumed and the desired potential was applied. The objective of this procedure was to adsorb a single monolayer of the dye on the surface. The quality of the SERS spectra obtained confirms that an extremely large Raman enhancement is produced with this procedure.

The silver electrode was not oxidized in the presence of oxazine 720. This ensured that the dye molecules were neither trapped nor electrochemically degraded by the activation ORC.[98]

3.2.4 Raman Instrumentation

SERS spectra were collected using a Dilor OMARS89 spectrometer coupled to an optical multichannel analyzer. The detector was a thermoelectrically cooled (~ -15°C) intensified diode array (512 diodes) interfaced to a computer for data collection. Excitation at 514.5 nm was provided by a Spectra Physics Model 2020 argon ion laser with the power

set to less than 40 mW at the laser head. Excitation at 632.8 nm was provided by a Melles Griot He-Ne laser at similar power levels. The Raman signal was collected at $\sim 90^{\circ}$ to the incident beam with the spectroelectrochemical cell aligned to optimize the intensity. The acquisition time for each measurement was 1 s and a minimum of 10 measurements were summed for each spectrum. Each measurement was background corrected with an independent 1 s measurement with the laser shuttered. The resulting spectra were baseline corrected during analysis.

The normal Raman spectrum of solid oxazine 720 was collected with a Renishaw inVia microscope Raman spectrometer system utilizing a Spectra-Physics 514.5 nm argon ion laser .

3.3 Results

Figure 3.3 shows cyclic voltammograms (a graph of current flow versus an applied triangular-waveform potential) at different scan rates for a silver electrode modified with oxazine 720 immersed in a 0.2 M KCl solution. The cathodic peak (produced while the voltage is being made more negative, in this case the negative current peak) and the anodic peak (produced while the voltage is being made more positive) are related to the reduction and oxidation (redox) of the phenoxazine ring as proposed elsewhere.[99] At neutral pH the electrochemical process, depicted in figure 3.4, involves the transfer of two electrons and one proton. The process is pH-dependent and in acidic medium two protons should be exchanged.[99] The electrochemical mechanism may involve the formation of a radical cation intermediate.[100] Both the cathodic and the anodic peaks presented in figure 3.3 shift with the scan rate, but this effect is more pronounced for the reductive process. The cathodic peak moves from ~ -525 mV at 20 mV/s to ~ -590 mV at 200 mV/s (not shown) and the anodic peak shifts from -460 mV at 20 mV/s to -430 mV at 200 mV/s (not shown) with all potentials reported against a saturated silver/silver chloride reference electrode. The redox potential observed here is more negative than the formal redox potential of -325 mV reported for the reduction of oxazine 720,[90] although the redox potential of surface confined phenoxazines may differ significantly from that observed for

the molecule in solution.[88] The peak current presents a linear relationship with the square root of the scan rate, v. A direct relationship with the scan rate is expected for strongly bound species,[101] and the dependence with $\sqrt{v}$ indicates that diffusion from solution is playing a significant role in the electrochemical mechanism. This is to be expected since protons are involved in the electrochemical reaction (see figure 3.4).

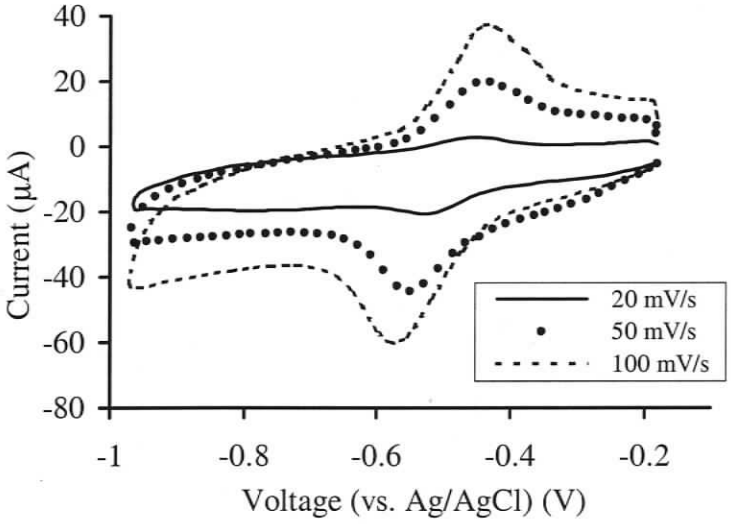

Figure 3.3: Cyclic voltammograms of oxazine 720 on a silver electrode in a 0.2 M KCl solution.

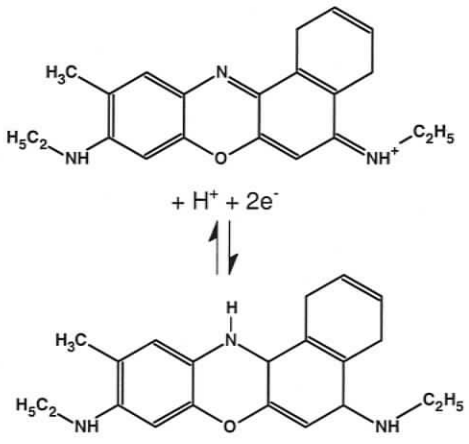

Figure 3.4: Molecular schematic of oxazine 720 showing the redox process involving the transfer of two electrons and a proton

The cathodic charge (Q_c) is ~40% higher than the anodic charge (Q_a) at slow scan rates. This difference decreases as the scan rate increases and a Q_c/Q_a ratio equal to one is observed for scan rates faster than 100 mV/s. After correcting for the surface roughness[99] the electrochemical charges were used to estimate the amount of oxazine 720 at the solid-liquid interface. The calculated values depend on the scan rate and on the nature of the process (cathodic or anodic) with the amount ranging between 3 and 8×10^{-10} mol/cm^2. The expected coverage for a monolayer of a phenoxazine species adsorbed flat on the metallic surface is estimated to be between 1 and 2×10^{-10} mol/cm^2.[102] Therefore, if oxazine 720 is flat-adsorbed on the modified surface multilayers must be present. On the other hand, the higher surface coverage reported here may also indicate that the molecule is adsorbed edge-on, probably attached by the nitrogens from the amino groups. Oxazine 720 is known to form dimers in aqueous solution[85] and measurements using second-harmonic generation have demonstrated that oxazine 720 dimers are the main species present at a liquid-air interface,[103] thus another possible explanation for the higher than expected surface coverage may be related to the preferential adsorption of the dimer.

Figure 3.5 compares the normal Raman spectrum of solid oxazine 720 to the SERS signal from the modified electrode. These spectra were obtained using 514.5 nm laser excitation which is not in resonance with the ~620 nm absorption maximum for oxazine 720. Figure 3.5 shows that there are two regions that contain a wealth of vibrational information in both the solid and the adsorbed molecule spectra: the region between 500 and 700 cm^{-1} and the region between 1100 and 1700 cm^{-1}. Six notable bands are significantly enhanced under adsorption and appear in the SERS spectrum at 546, 585, 675, 1339, 1395 and 1644 cm^{-1}. The assignment of these six oxazine 720 vibrational modes was performed using a DFT calculation produced with Gaussian 98W®,[104] carried out at the B3LYP level (3-parameter Becke, Lee, Yang, Parr exchange functional) using the 6 31G(d) basis set (6 gaussians to represent the inner shells, 3 gaussians for the first valence band, 1 gaussian for the second valence band plus diffuse polarization functions) and previous work for other dyes that also contain the phenoxazine ring.[99,105] The results are presented in table 3.1 and graphical representations of the normal modes of these

six surface-enhanced bands are given in figure 3.6. The vibrational frequencies from the adsorbed molecule are similar to the ones observed for the solid, suggesting a relatively weak adsorption.

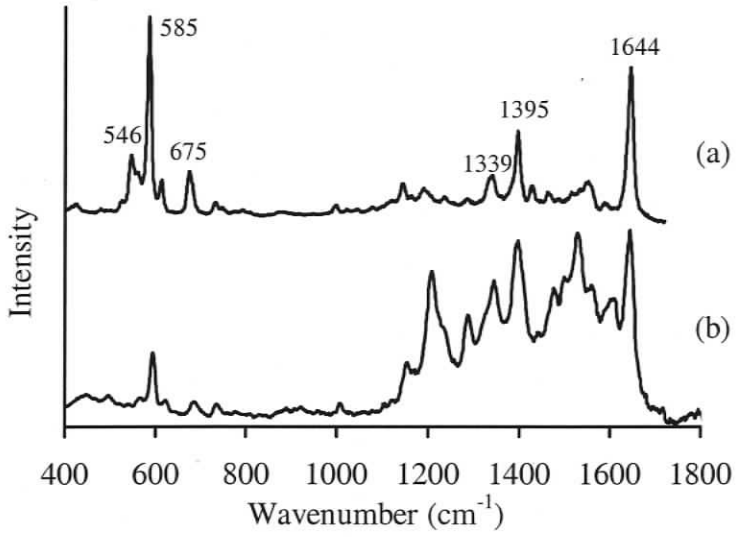

Figure 3.5: The SERS spectra of oxazine 720 on a rough silver electrode (a) compared to the Raman spectra of solid oxazine 720 (b). Six vibration bands with significant SERS enhancement are labelled.

ν_{cal} (cm^{-1})	ν_{SERS} (cm^{-1})	ν_{solid} (cm^{-1})	ν_{cresyl} (cm^{-1})*
547.3	546		548
607.5	585	594	589
701.6	675	687	673
1386.0	1339	1343	1330
1452.3	1395	1395	1401
1696.7	1644	1642	1641

* Cresyl violet is a phenoxazine dye similar to oxazine 720. Data from Ref. [105]

Table 3.1: Calculated vibrational wavenumbers (B3LYP/6 31G(d)), along with the measured SERS and Raman band positions for oxazine 720. The last column contains measured SERS bands of cresyl violet, a similar phenoxazine containing dye.

Although not evident from the single point of view shown in figure 3.6 these 6 vibrational modes are dominated by motions within the plane of the rings. Further analysis of the SERS spectrum shows little enhancement of the modes dominated by out-of-plane

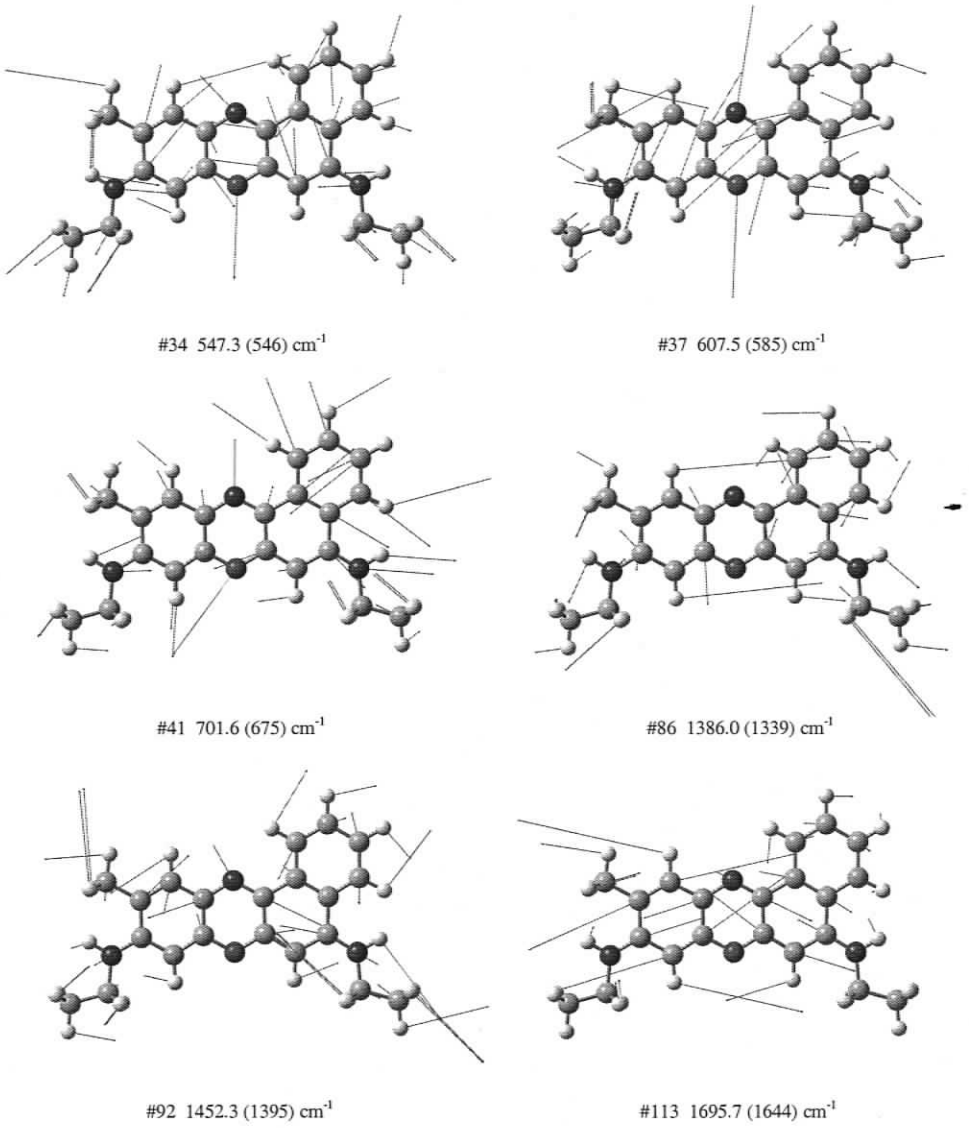

Figure 3.6: Normal coordinate diagrams of the six oxazine 720 bands labelled in figure 3.5. The mode number and calculated wavenumber from Guassian 98W®[104] as well as the measured SERS wavenumber (in brackets) are given for each mode. The lines represent the direction and relative magnitude of nuclear motion for the given mode.

motions which, according to the SERS selection rules, are expected to show significant intensity if the ring is adsorbed flat on the surface.[98] SERS from the breathing mode of benzene shifts to lower frequency when the molecule is adsorbed flat on the surface,[106] and although the multi-ring oxazine 720 system is more complex than benzene, if the

molecule is adsorbed flat on the surface some shift to lower frequency should be observed for vibrations that are dominated by ring modes . All these pieces of evidence indicate that the oxazine 720 ring is not flat-adsorbed, but is interacting with the surface through the aliphatic amino groups. The tilt angle between the molecule and the surface normal cannot be evaluated solely from the data presented in figure 3.5, but it suggests that the oxygen-nitrogen axis is in an upright position with the ring in a position perpendicular to the surface. Since such an orientation allows more molecules to be packed on the silver surface the spectroscopic data is in agreement with the high surface coverage obtained from the electrochemical data presented in figure 3.3 where cyclic voltammetry suggested coverage in excess of a monolayer of flat-adsorbed oxazine 720. This upright orientation was also suggested by Schneider *et al.*[93] for high coverage of oxazine 720 adsorbed on silver colloidal particles. The edge-on orientation is also consistent with the tendency of oxazine 720 to form H-aggregates in aqueous environments.[85] Spectroelectrochemical SERS studies involving other phenoxazine rings, such as nile blue, also suggest the edge-on orientation for the adsorption from acidic solutions.[99]

SERS spectra from a silver electrode modified with oxazine 720 obtained at different applied potentials are shown in figure 3.7. These spectra were collected using 514.5 nm excitation. Data collected using 632.8 nm excitation, which is within the absorption band of the free oxazine 720 molecule, showed similar relative intensities of the modes indicated in figure 3.6 and table 3.1. A plot of the intensity of selected peaks from figure 3.7 versus the applied potential is shown in figure 3.8. The intensity of most of the SERS bands did not change significantly when the applied potential was more positive than $-500\,\text{mV}$. This can be seen in the potential profile for the 1545 and $1644\,\text{cm}^{-1}$ bands shown in figure 3.8. On the other hand the band at $1475\,\text{cm}^{-1}$ was nearly absent in the SERS spectrum with applied potential more positive than $-250\,\text{mV}$, but increased as the potential was scanned more negative, reaching a maximum at $\sim -450\,\text{mV}$. As with the bands shown in figure 3.8 the SERS intensity for all of the modes of adsorbed oxazine 720 decreased sharply as the potential was made more negative than $-500\,\text{mV}$. This behaviour can be correlated to the electrochemical curves presented in figure 3.3 demonstrating that

the SERS intensity decreases as the onset of oxazine 720 reduction is reached. Two possible explanations for the transient nature of the 1475 cm^{-1} band are that it is the result of some sort of molecular rearrangement that occurs with changing potential, or that it is the result of a tunable CT enhancement. As discussed in section 2.3.2 the CT enhancement is the result of a charge-transfer resonance between the metal and the molecular orbitals of the adsorbed species.[94,95] This resonance can be controlled to some extent by altering the energy of the Fermi level via the applied potential. The CT enhancement contribution can then be probed with electrochemical SERS by obtaining the potential profile at different excitation wavelengths and observing the changes in the potential required to maximize the SERS intensity.[95] The SERS spectra from a silver electrode modified with oxazine 720 using 632.8 nm excitation produced potential profiles for most bands similar to those observed for the 1545 and 1644 cm^{-1} bands in figure 3.8. In these cases the SERS intensity remained almost constant for an applied potential between -200 and -500 mV and then decreased as the applied voltage became more negative than -500 mV. The potential-transient 1475 cm^{-1} band was not observed at any applied potential when using 632.8 nm excitation. This behaviour confirms that the measured variation is not related to reorientation. The intensity of the 1475 cm^{-1} mode for oxazine 720 adsorbed on colloidal silver has been reported to be sensitive to the nature of the anion in solution which was interpreted as an indication that this vibration could be tuned in and out of resonance by the anion-induced modification of the electronic properties of the silver particles.[93] The results reported here suggest a similar but more readily controlled resonance behaviour and confirms the importance of the CT mechanism for this specific mode.

As discussed above the decrease in intensity of the SERS bands as the potential is made more negative than -500 mV is clearly related to the reduction of oxazine 720. Interestingly, the SERS signal is recovered when the potential is returned to values more positive than -500 mV. This process is illustrated in figure 3.9. The initial SERS spectrum was collected with an applied potential of -200 mV (figure 3.9(a)) after which the potential was gradually swept to -1000 mV where the SERS signal completely vanished due to the reduction of oxazine 720 (figure 3.9(b)). The potential was then returned to

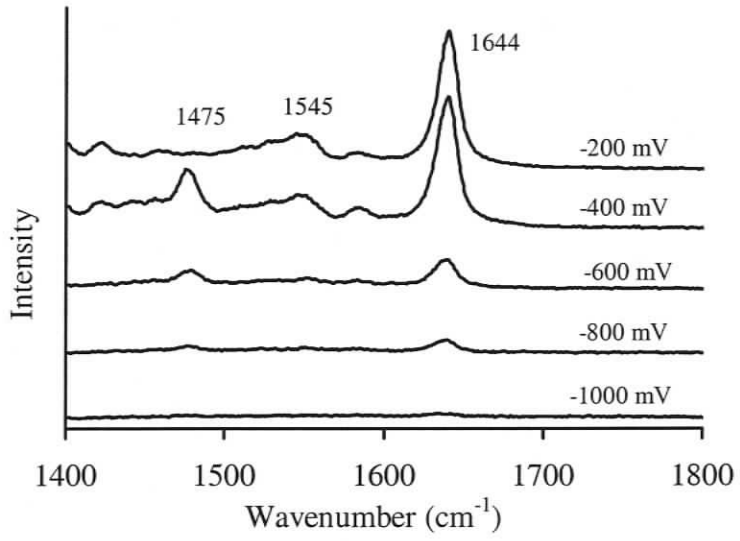

Figure 3.7: SERS spectra of oxazine 720 on a rough silver electrode at various applied potentials.

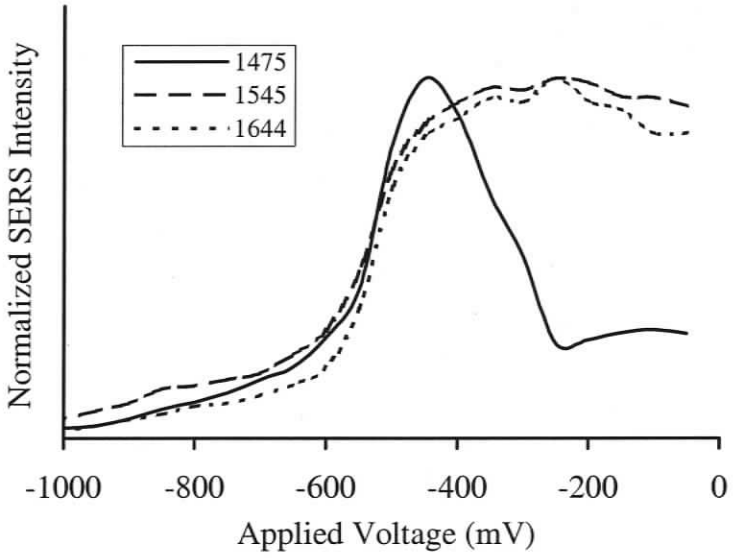

Figure 3.8: Potential profiles of the three oxazine 720 bands labelled in figure 3.7.

−200 mV where a good quality SERS signal was recovered (figure 3.9(c)). Figure 3.3 indicates that the electrochemical behaviour of oxazine 720 adsorbed on silver is quasi-reversible in agreement with the observations from figure 3.9. It is well established in the SERS literature that the active sites that support major enhancement are lost during

incursions to highly negative potential[99] due to potential-induced morphological changes related to molecular (or anionic) desorption followed by surface-diffusive smoothing of the roughness features.[107] The fact that the SERS signal is recovered in figure 3.9(c) suggests that the molecule remains adsorbed at the SERS active site in its reduced form protecting the enhancement sites from being lost. This is in agreement with the observed SERS bands of the reduced form of other phenoxazine dyes adsorbed on silver surfaces at negative potentials.[99] It is important to stress that SERS signals are dominated by a small number of active sites, and the observation that the molecule stays adsorbed at highly negative potentials may not represent a typical behaviour that would be observed from a smooth surface. The weak SERS signal from the reduced form of oxazine 720 reported here is not caused by molecular desorption: the reduction populates the lowest unoccupied molecular orbital (LUMO) shifting the CT resonance to higher energies not accessible with the laser excitations used in this work.

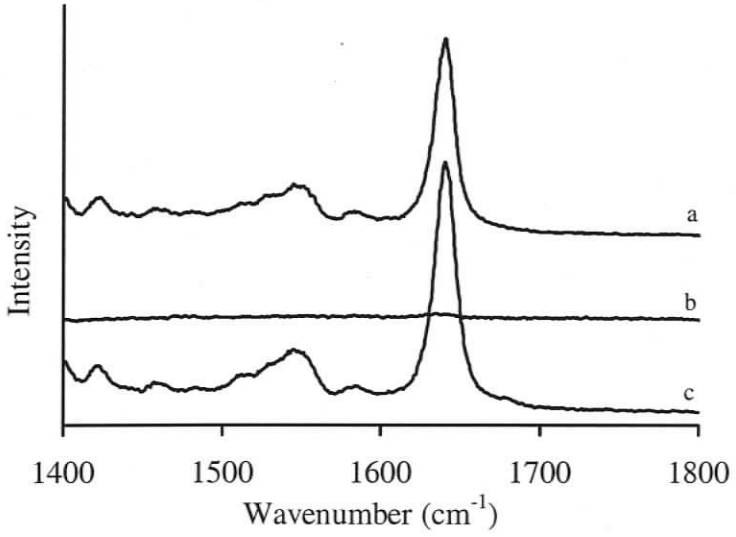

Figure 3.9: SERS spectra of oxazine 720 showing the recoverability of the SERS signal. The initial spectrum (a) was collected with an applied potential of −200 mV. The potential was then changed to −1000 mV, where the SERS signal is no longer visible (b). The applied potential was then returned to −200 mV, and the SERS signal was recovered (c).

3.4 Conclusions

The redox behaviour of a silver electrode modified with oxazine 720 was investigated by SERS and cyclic voltammetry. The combination of electrochemical and spectroelectrochemical data indicate that oxazine 720 adsorbs in an edge-on position, interacting with the surface via the nitrogens from the amino side chains. A quasi-reversible redox was observed around $-500\,\text{mV}$ and the reduced molecule was shown to remain adsorbed at the surface down to an applied potential of $-1000\,\text{mV}$. The role of the CT mechanism on the overall SERS intensity was explored and specific SERS bands were found to be significantly enhanced at specific applied potentials indicating a resonant behaviour. This resonant characteristic was confirmed by the collection of SERS spectra at different excitation energies. The observation of resonant SERS bands confirms that the CT mechanism plays a role in SERS enhancement while the observation of non-resonant bands verifies the existence of other enhancement mechanisms such as the EM mechanism.

Chapter 4

Anti-Stokes to Stokes Ratios: An Analysis of Raman Optical Pumping

THIS CHAPTER BEGINS WITH AN INTRODUCTION TO THE SERS ANTI-STOKES ASYMMETRY ISSUE FOLLOWED BY RESULTS THAT CONFIRM THAT THE ASYMMETRY EXISTS EVEN IN SYSTEMS INCAPABLE OF OPTICAL PUMPING. IT THEN PRESENTS A RESONANCE MODEL THAT REPRODUCES THE RESULTS PRESENTED HERE AS WELL AS DATA PREVIOUSLY PUBLISHED BY OTHERS. THE EFFECT OF LASER INDUCED HEATING IS CONSIDERED AND MODELED AFTER WHICH SHORTCOMINGS OF THE OPTICAL PUMPING MODEL ARE DISCUSSED. MUCH OF THE MATERIAL IN THIS CHAPTER HAS BEEN PREVIOUSLY PUBLISHED AS "RATIO OF THE SURFACE-ENHANCED ANTI-STOKES SCATTERING TO THE SURFACE-ENHANCED STOKES-RAMAN SCATTERING FOR MOLECULES ADSORBED ON A SILVER ELECTRODE" IN PHYSICAL REVIEW B, VOLUME 69, PAGES 045424-1 THROUGH 9, 2004. THIS CHAPTER CONCLUDES WITH A SUMMARY OF RECENT RESEARCH IN THE FIELD.

4.1 Introduction

As was discussed in section 2.5.1 one of the more controversial topics in current SERS research is the interpretation of the preferential enhancement of the anti-Stokes Raman signal observed for dyes adsorbed on silver colloids.[54,57] Kneipp *et al.*, who first reported the excess anti-Stokes intensity,[54] posit that the increase in anti-Stokes intensity is due to optical pumping. They suggest that, under appropriate conditions, the surface-enhanced Raman cross section is so large that Stokes Raman scattering leads to an overpopulated excited vibrational state leading to an excess of anti-Stokes scattering. Such an effect would represent a previously undetected SERS mechanism. However, Haslett *et al.*[57] reproduced similar results but argue that the cause is simply the manifestation of a resonance in the SERS enhancement producing a disparity between the Stokes and anti-Stokes Raman scattering cross sections. The research reported in this chapter is intended to contribute to an understanding of the process.

In their pioneering work on the topic Kneipp *et al.*[54] defined a normalized ratio, $K(\nu_m)$, to express the excess anti-Stokes intensity for a Raman band with Raman shift ν_m. This K-ratio is the ratio between the surface-enhanced anti-Stokes and surface-enhanced Stokes intensities $((I_{AS}(\nu_m)/I_S(\nu_m))_{SERS})$ normalized by a similar ratio for an unenhanced Raman (UR) scatterer with a similar Raman shift $((I_{AS}(\nu_m)/I_S(\nu_m))_{UR})$. This normalization helps eliminate systematic errors and corrects for variations in the response of the equipment. The anti-Stokes Raman excess, or K-ratio, is then:[54]

$$K(\nu_m) = \frac{\left(\frac{I_{AS}(\nu_m)}{I_S(\nu_m)}\right)_{SERS}}{\left(\frac{I_{AS}(\nu_m)}{I_S(\nu_m)}\right)_{UR}} \tag{4.1}$$

Kneipp *et al.* measured the K-ratio for a number of SERS bands of crystal violet and rhodamine 6G adsorbed on colloidal silver using a high intensity 830 nm excitation. They found that K was significantly higher than 1 for all the bands investigated, indicating a preferential increase in the intensity of the anti-Stokes scattering.[54] The K-ratio was found to increase significantly with the Raman shift.[54] They also measured a quadratic dependence of anti-Stokes intensity on the incident laser power.[54] As mentioned ear-

lier Kneipp *et al.* attribute these features to strong optical pumping of vibrationally excited states induced by the large SERS enhancement experienced by a small number of molecules.[54] According to Kneipp *et al.* an intense excitation source combined with an exceptional surface-enhanced Raman cross section should significantly populate the first vibrationally excited state of a given vibrational mode, assuming vibrational relaxation on the order of 10 ps.[54] This effect would lead to a non-thermal overpopulation of higher vibrational states and an increase in the intensity of the anti-Stokes scattering compared to what would be expected from a system with a Boltzmann-distributed population.

In 2000 Haslett *et al.*, using multiple excitation sources (514.5 nm, 780 nm, 830 nm), reproduced the above-unity K-ratios for rhodamine 6G and crystal violet adsorbed on colloidal silver, and observed K-ratios close to unity for a number of colorless molecules such as pyridine and phthalazine adsorbed on the same type of substrate.[57] However Haslett *et al.* reported a linear dependence of the anti-Stokes intensity on the incident laser power[57] rather than the quadratic one reported by Kneipp *et al.*[54] Even though Haslett *et al.* produced results very similar to those reported by Kneipp *et al.*, Haslett *et al.* challenged the optical pumping model used to explain the non-unity K-ratios.[57] As explained in section 2.3.1 the EM mechanism enhances both the incident and Raman scattered fields.[19] Since the enhancement of the Raman scattered field yields photons from the metal substrate, not the molecule, it does not produce vibrationally excited molecules and should not be involved in optical pumping. This implies that the non-equilibrium situation required for SERS-induced optical pumping must be driven solely by the enhanced incident field. Consequently, it was easily shown by Haslett *et al.* that the field intensity required to produce optical pumping via the mechanism proposed by Kneipp *et al.* would be prohibitively high ($\sim 10^{15}\,\mathrm{W\,cm^{-2}}$).[57] Such tremendous fields would provoke significant ionization and molecular decomposition. Since Haslett *et al.* found no support for optical pumping they attributed the measured K-ratios to differences in cross section between the surface-enhanced Stokes and anti-Stokes scattering caused by a resonant silver-adsorbate charge-transfer complex.[57]

Due to its ability to independently affect the CT component of enhancement, electro-

chemical SERS is an excellent experimental method to help resolve this controversy. As explained in section 2.3.2 a potential applied to a SERS surface influences the Fermi level of the metal which plays a significant role in the CT mechanism.[95] This chapter presents electrochemical SERS spectra of rhodamine 6G, oxazine 720 and pyridine adsorbed on a roughened silver electrode. Calculated K-ratios for various applied potentials, using two different electrolyte solutions and two excitation energies, are included. It is important to note that the power densities used here are orders of magnitude lower than those used by Kneipp *et al.*[54] and are not expected to produce any measurable optical pumping, so any non-unity K-ratios must have an alternative explanation.

4.2 Experimental

The experimental apparatus and methods used to collect the data presented in this chapter are identical to the equipment and methods described in section 3.2. In addition to the chemicals disclosed in section 3.2.1, $NaClO_4$ from ACP, pyridine and liquid benzene from Aldrich, CCl_4 from Fisher Scientific and rhodamine 6G from Lambdachrome were also used. Oxazine 720 and rhodamine 6G were applied to the electrode using the evaporative technique described in section 3.2.3 whereas pyridine was simply added to the cell solution after the activation procedure was completed. In all cases the silver electrode was never oxidized in the presence of the molecule of interest. The power supplied by the lasers was less than 20 mW at the sample.

SERS spectra were collected using both 0.1 M $NaClO_4$ and 0.2 M KCl electrolyte solutions. Although changing the solution yields different SERS enhancement factors, it did not significantly affect the ratio between the Stokes and anti-Stokes scattering intensities and therefore only the spectra collected with 0.2 M KCl solution are presented below.

Unenhanced Raman spectra were collected from benzene and carbontetrachloride using the same equipment and under the same experimental conditions as the SERS data. The ratio between the Stokes and anti-Stokes Raman intensity was calculated for all the substantial bands. These ratios, and the interpolated values between them, were used for the unenhanced Raman normalization in equation 4.1.

4.3 Results and Discussion

Prominent peaks at 546, 585, 675, 1339, 1395 and 1644 cm^{-1} were observed for oxazine 720 adsorbed on a silver electrode, as shown in figures 3.5 and 4.1. When this data was collected there were no published results dealing with electrochemical SERS of oxazine 720. However the spectra are very similar to published SERS spectra of oxazine 720 adsorbed on silver colloids reported by Schneider *et al.*[93] although some discrepancies were noted between the relative intensities of the SERS bands. These differences can be ascribed to variations in the morphology of the SERS substrates and the effects of the applied potential.

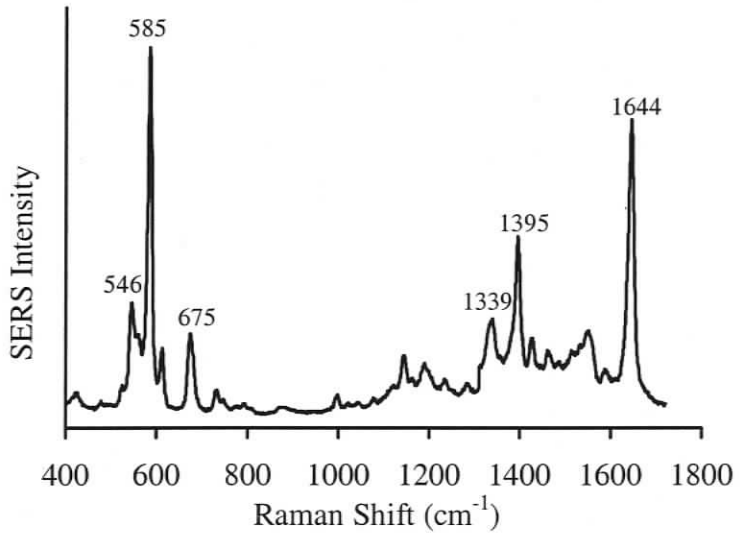

Figure 4.1: SERS spectrum of oxazine 720 adsorbed on a roughened silver electrode excited with the 514.5 nm Ar^+ line.

The normalized intensity of the vibrational SERS bands from oxazine 720 adsorbed on silver was plotted against the applied potential bias. This type of curve is referred to as a potential profile. Figure 4.2 shows potential profiles for the surface-enhanced Stokes bands at 585 and 675 cm^{-1} for oxazine 720 adsorbed on a roughened silver electrode obtained using 514.5 nm (19436 cm^{-1} or 2.41 eV) laser excitation. The SERS bands of oxazine 720 adsorbed on silver present maximum intensities when the potential applied to

the surface is between -50 and -450 mV. The SERS signal drops sharply between -450 and -600 mV and decreases further as the potential is made more negative. This is the same behaviour as shown in figure 3.8 for bands at 1545 and 1644 cm^{-1}. This behavior suggests that an electron is transferred to the molecule between -450 and -600 mV. The SERS signal reaches a minimum at the extreme negative limit in figure 4.2 but, as described in section 3.3, it is fully recovered when the applied potential is returned to more positive values. This indicates that the suggested electron-transfer process is reversible. The value of the potential where this charge-transfer occurs (~ -500 mV) is consistent with a low-lying lowest unoccupied molecular orbital (LUMO) for this molecule. The main characteristics of the potential profile presented in figure 4.2 were reproduced in experiments using 632.8 nm (15803 cm^{-1} or 1.96 eV) laser excitation.

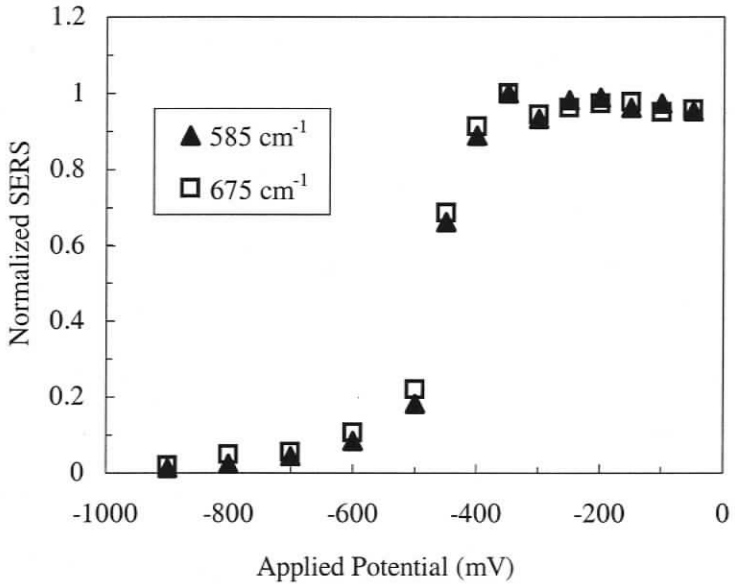

Figure 4.2: Potential profiles of the 585 cm^{-1} and 675 cm^{-1} vibration bands of oxazine 720 adsorbed on a roughened silver electrode. Excitation is provided by the 514.5 nm Ar^{+} line.

The characteristic SERS vibrational bands for rhodamine 6G adsorbed on a silver electrode observed at 620, 770 and 1180 cm^{-1}, as shown in figure 4.3, agree well with results available in the literature.[54,57,108–110] The potential profiles for the 620 and 770 cm^{-1}

surface-enhanced Stokes bands of rhodamine 6G, obtained using 632.8 nm excitation, are presented in figure 4.4. The maximum SERS intensity is observed at the most positive potential for both bands and the SERS signal decreases as the potential bias is made more negative. The decrease in SERS intensity with potential is less dramatic for rhodamine 6G than for oxazine 720. There is no clear indication of electron transfer for rhodamine 6G and no reversible recovery of the SERS signal is observed when the potential is returned from the negative limit to a more positive potential.

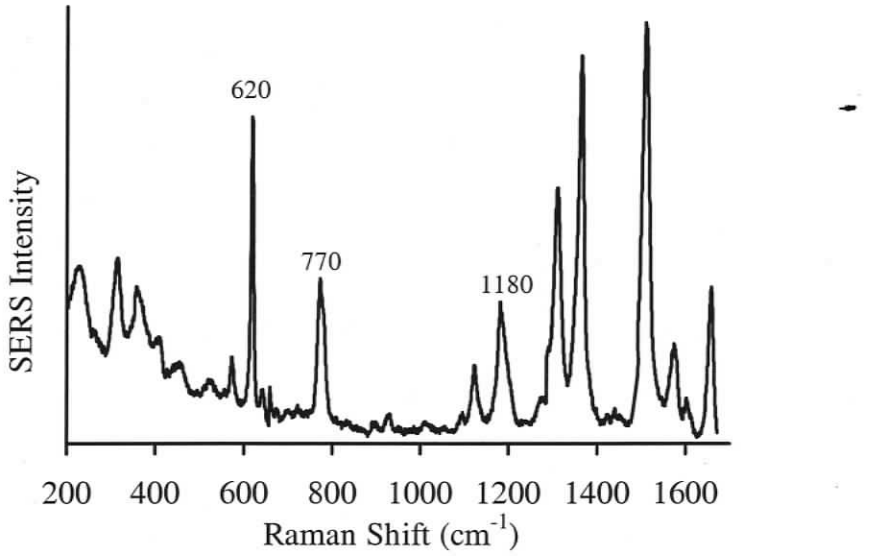

Figure 4.3: SERS spectrum of rhodamine 6G adsorbed on a roughened silver electrode excited with the 632.8 nm He-Ne line.

The SERS of pyridine adsorbed on a silver surface under electrochemical control, shown in figure 4.5, presents strong vibrational bands at 620, 1003, 1032, 1220, and 1596 cm^{-1}. These general features agree well with available literature for pyridine adsorbed on silver,[111–113] gold,[114] and copper[115] electrodes. Figure 4.6 shows the potential profile for the 1003 cm^{-1} ring breathing mode of pyridine for excitations of 514.5 nm and 632.8 nm. Both excitation energies yields a bell shaped curve with maximum intensity at a specific applied potential (Φ_{max}). This curve is in contrast with those of the dyes presented in figures 4.2 and 4.4 which show a monotonic decrease in intensity. The Φ_{max} for pyridine varies with excitation energy due to a CT resonance,[40] as described in

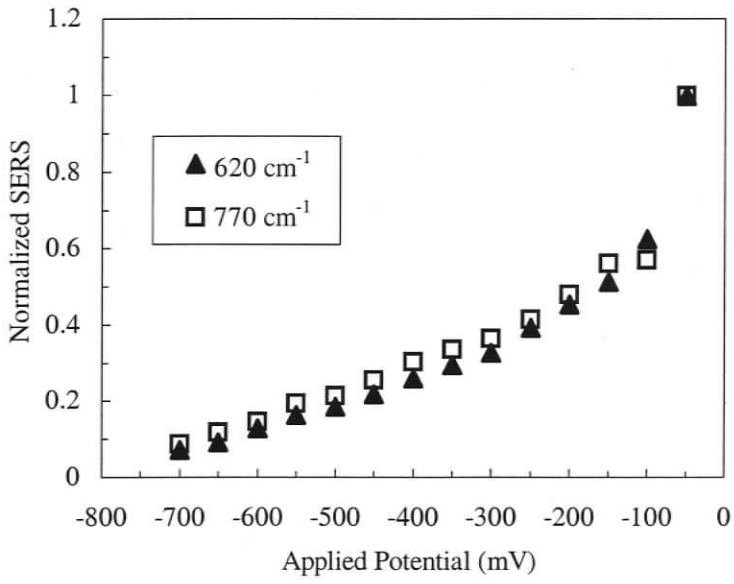

Figure 4.4: Potential profiles of the 620 cm^{-1} and 770 cm^{-1} vibration bands of rhodamine 6G adsorbed on a roughened silver electrode. Excitation is provided by the 632.8 nm He-Ne line.

section 2.3.2, and is about -600 mV with 514.5 nm excitation, and about -850 mV for 632.8 nm excitation.

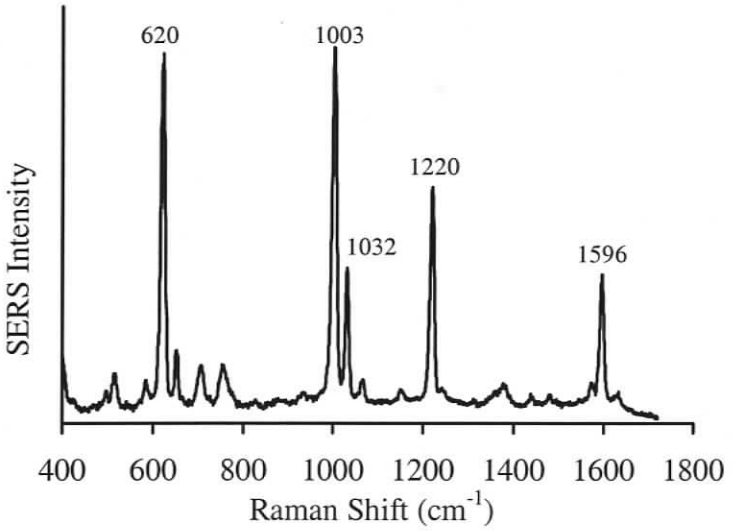

Figure 4.5: SERS spectrum of pyridine adsorbed on a roughened silver electrode excited with the 514.5 nm Ar^+ line.

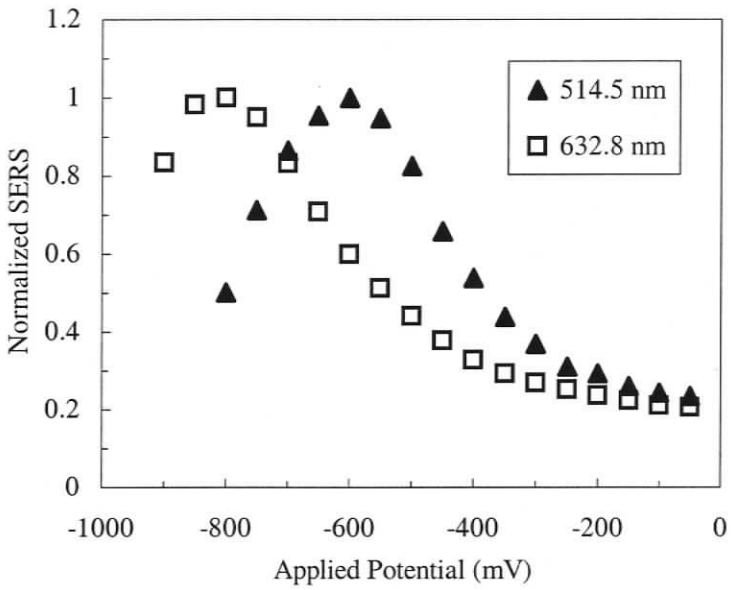

Figure 4.6: Potential profile of the 1003 cm^{-1} vibration band of pyridine adsorbed on a roughened silver electrode excited by the 514.5 nm Ar^+ and 632.8 nm He-Ne lines.

Using data like that shown in figures 4.2–4.6 for both the Stokes and anti-Stokes Raman intensities, K-ratios were calculated for oxazine 720, rhodamine 6G and pyridine, adsorbed on a roughened silver electrode, as a function of applied potential. The unenhanced Raman spectra of pure liquid benzene and carbontetrachloride were used to normalize the ratios as prescribed by equation (4.1). Figure 4.7 shows K^{-1}-ratios for oxazine 720 as a function of the applied potential for both 514.5 nm and 632.8 nm excitation energies. Figure 4.8 shows a similar plot using the SERS data obtained from pyridine. Since these systems show an excess Stokes intensity, rather than anti-Stokes, it is more meaningful to plot K^{-1} instead of K. Although a slight slope is present in a number of the data sets, the maximum variation in K^{-1} over the range of applied potentials is less than 1.5 in all eight data sets, and less than 0.5 in all but two. It is important to note that since the absolute anti-Stokes Raman intensity decreases with increasing Raman shift, the uncertainty on the experimentally calculated K-ratios increases with the energy of the vibrational mode. Also, since the SERS bands of oxazine 720 and rhodamine 6G decrease in intensity as the applied potential is made more negative, additional uncertainty

in the calculated K-ratios occurs in this situation. This explains some of the fluctuations observed in figures 4.7 and 4.8.

For oxazine 720 the K^{-1}-ratios for the bands at 585 and 675 cm^{-1} are between 1.2 and 1.5 with the 514.5 nm excitation and between 1.8 and 2.2 with the 632.8 nm excitation. For a given excitation energy the K^{-1}-ratios for the two bands are very similar. The results for pyridine adsorbed on a silver electrode indicate K^{-1}-ratios of ~ 1 for the 620 cm^{-1} band for both the 514.5 and 632.8 nm excitations. The K^{-1}-ratios for the 1003 cm^{-1} mode are around 1.8 for the 514.5 nm excitation and around 3.0 for the 632.8 nm excitation. The K^{-1}-ratios higher than unity observed in figures 4.7 and 4.8 indicate a preferential increase of the surface-enhanced Stokes scattering relative to the surface-enhanced anti-Stokes scattering.

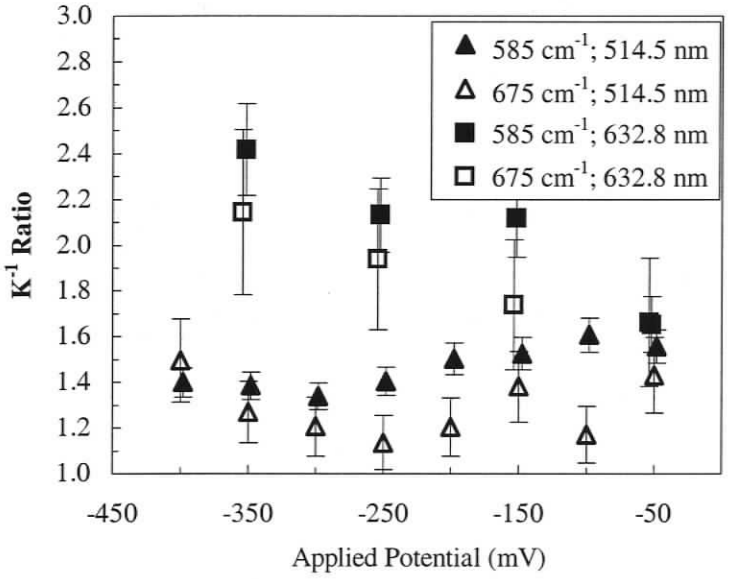

Figure 4.7: K^{-1}-ratios of the 585 cm^{-1} and 675 cm^{-1} vibration bands of oxazine 720 adsorbed on a roughened silver electrode excited by the 514.5 nm Ar^{+} and 632.8 nm He-Ne lines. The error bars represent the statistical uncertainty in the values.

SERS K^{-1}-ratios for pyridine adsorbed on Cu, Ag and Au have been obtained by others using several excitation wavelengths.[116] Marinyuk *et al.* reported K^{-1}-ratios higher than one for all excitation energies[116] in good agreement with the results for pyridine

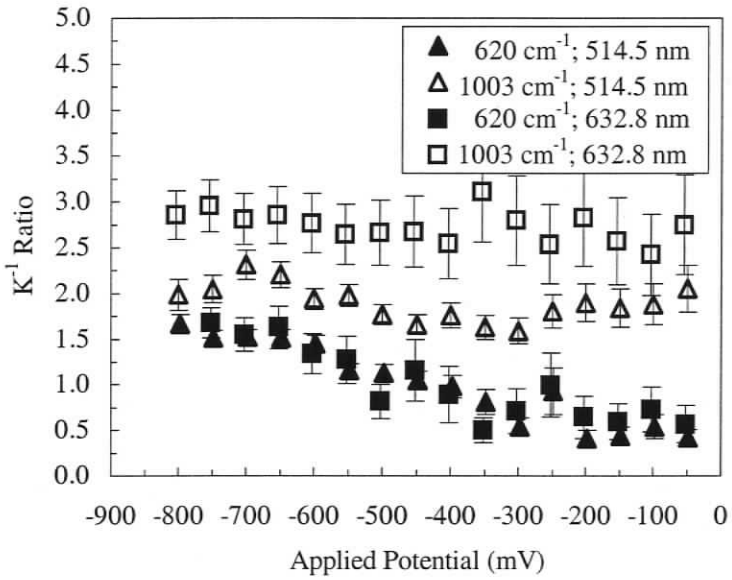

Figure 4.8: K^{-1}-ratios of the 620 cm^{-1} and 1003 cm^{-1} vibration bands of pyridine adsorbed on a roughened silver electrode excited by the 514.5 nm Ar^{+} and 632.8 nm He-Ne lines. The error bars represent the statistical uncertainty in the values.

presented in figure 4.8. However, in contrast to the results presented here, they observed higher K^{-1}-ratios for 514.5 nm excitation than for 632.8 nm, and their ratios were potential independent.

Figure 4.9 shows a plot of the K-ratios for the 620 cm^{-1} and 770 cm^{-1} modes of rhodamine 6G at several applied potentials using 632.8 nm excitation. Attempts to measure the SERS of rhodamine 6G using 514.5 nm were unsuccessful due to fluorescence and photodecomposition. K-ratios between 2.5 and 3.0 and between 3.5 and 5.5 were obtained for the bands at 620 and 770 cm^{-1} respectively, showing that the K-ratios of rhodamine 6G increase with Raman shift for a given applied potential. The observed K-ratios were higher than unity for all vibrational bands of rhodamine 6G adsorbed on a silver electrode. The higher than one K-ratios indicate that a relative enhancement of the anti-Stokes scattering occurred, as observed by Kneipp *et al*[54] and Haslett *et al*.[57]

Several factors can cause the SERS intensity to vary with the applied potential. Such factors include molecular reorientation, changes in surface coverage, electrochemical re-

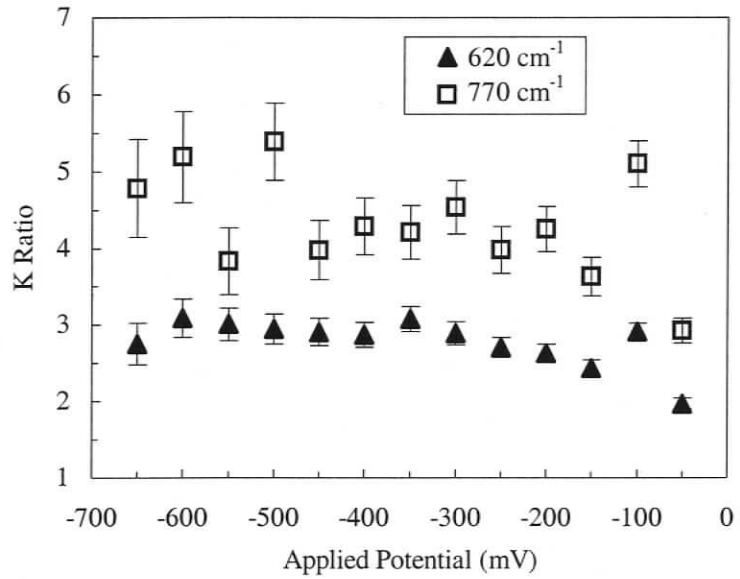

Figure 4.9: K-ratios of the $620\,\mathrm{cm}^{-1}$ and $770\,\mathrm{cm}^{-1}$ vibration bands of rhodamine 6G adsorbed on a roughened silver electrode excited by the 632.8 nm He-Ne line. The error bars represent the statistical uncertainty in the values.

actions such as the reduction observed for oxazine 720 in figure 4.2, and CT resonance tuning. All but the last of these should affect the Stokes and anti-Stokes signal equally. Thus, any potential dependence of the K-ratios can best be interpreted as a manifestation of the CT contribution to the overall enhancement.[94,117]

Resonance arguments can be invoked to explain the results presented in figures 4.7–4.9. If formation of a metal-adsorbate charge-transfer complex is assumed for each of the molecules investigated then the preferential enhancement of either the Stokes (figures 4.7 and 4.8) or anti-Stokes (figure 4.9) scattering can be the result of the relative position of the absolute energy of the Raman-shifted photon with respect to the electronic transition of the complex. This type of situation is common in the resonance Raman literature and the K-ratios can be readily calculated using[116,118]

$$K(\nu_{\text{vib}}) = \left(\frac{(\bar{\nu}_{\text{exc}} + \bar{\nu}_{\text{vib}})_{\text{SERS}} (\bar{\nu}_{\text{exc}} - \bar{\nu}'_{\text{vib}})_{\text{UR}}}{(\bar{\nu}_{\text{exc}} - \bar{\nu}_{\text{vib}})_{\text{SERS}} (\bar{\nu}_{\text{exc}} + \bar{\nu}'_{\text{vib}})_{\text{UR}}} \right)^4 \exp\left(-\frac{\bar{\nu}_{\text{vib}}}{kT_{\text{SERS}}} \right) \times \exp\left(\frac{\bar{\nu}'_{\text{vib}}}{kT_{\text{UR}}} \right) \left(\frac{(\bar{\nu}_{\text{exc}} - \bar{\nu}_{\text{elect}} - \bar{\nu}_{\text{vib}})^2 + \Gamma^2}{(\bar{\nu}_{\text{exc}} - \bar{\nu}_{\text{elect}} + \bar{\nu}_{\text{vib}})^2 + \Gamma^2} \right) \quad (4.2)$$

The subscripts SERS and UR correspond to the adsorbed molecule and the pure liquid used as a reference respectively, as in equation (4.1). The energies for the excitation laser, Raman shift of the SERS band, Raman shift of the UR band and electronic transition of the complex are $\bar{\nu}_{\text{exc}}$, $\bar{\nu}_{\text{vib}}$, $\bar{\nu}'_{\text{vib}}$, and $\bar{\nu}_{\text{elect}}$ respectively. Temperatures are designated by T, and k is the Boltzmann constant. The half-width of the electronic band of the complex is given by Γ.

It should be noted that equation (4.2) was formulated under the assumption that the non-resonant part of the Raman tensor responsible for a given Stokes scattering is equal to its anti-Stokes counterpart, allowing their ratio to be eliminated from the equation. Equation (4.2) can be further simplified with two additional assumptions. The same vibrational energy can be assumed for both the SERS and the unenhanced Raman, $\bar{\nu}_{\text{vib}} = \bar{\nu}'_{\text{vib}}$, which can be achieved by careful selection of the reference material or by interpolating between bands for the reference material. If the same temperature is assumed for both the SERS surface and the the reference liquid, $T_{\text{SERS}} = T_{\text{UR}}$, the exponential terms drop out. Applying both assumptions gives

$$K(\nu_{\text{vib}}) = \left(\frac{(\bar{\nu}_{\text{exc}} - \bar{\nu}_{\text{elect}} - \bar{\nu}_{\text{vib}})^2 + \Gamma^2}{(\bar{\nu}_{\text{exc}} - \bar{\nu}_{\text{elect}} + \bar{\nu}_{\text{vib}})^2 + \Gamma^2} \right) \quad (4.3)$$

Figure 4.10 shows a plot of K^{-1} versus excitation energy based on equation (4.3) for a vibrational mode at $1000\,\text{cm}^{-1}$ with $\bar{\nu}_{\text{elec}} = 13300\,\text{cm}^{-1}$ and $\Gamma = 1600\,\text{cm}^{-1}$. This vibrational energy is similar to the observed ring breathing mode of adsorbed pyridine. The energy of the electronic transition and the value for the half-width of the electronic band were adjusted to match the K^{-1}-ratios observed in figure 4.8 for the ring breathing mode ($1003\,\text{cm}^{-1}$) of pyridine adsorbed on silver. It is important to note that the objective here is not to extract the electronic transition parameters by fitting the equation to the experimental data. Such a procedure would not yield a satisfactory result since more than

one combination of $\bar{\nu}_{\text{elec}}$ and Γ would produce a fit to the limited number of data points. The goal is to demonstrate that the experimental results presented in figures 4.7–4.9 can be explained using resonance Raman concepts. The arrows in figure 4.10 represent the energies of laser excitation lines at 800 nm (Ti:Sapphire), 632.8 nm (He-Ne) and 514.5 nm (Ar^+). Figure 4.10 indicates that it is possible to be in resonance in the anti-Stokes ($K^{-1} < 1$) when 800 nm excitation is used and to be in resonance in the Stokes ($K^{-1} > 1$) when the experiment is performed using 632.8 nm or 514.5 nm excitation, as is observed in figure 4.8. Figure 4.11 shows how the same parameters used in figure 4.10 reproduce the observed dependence of the K^{-1}-ratio on the energy of the vibrational mode as shown in figure 4.8 for pyridine.

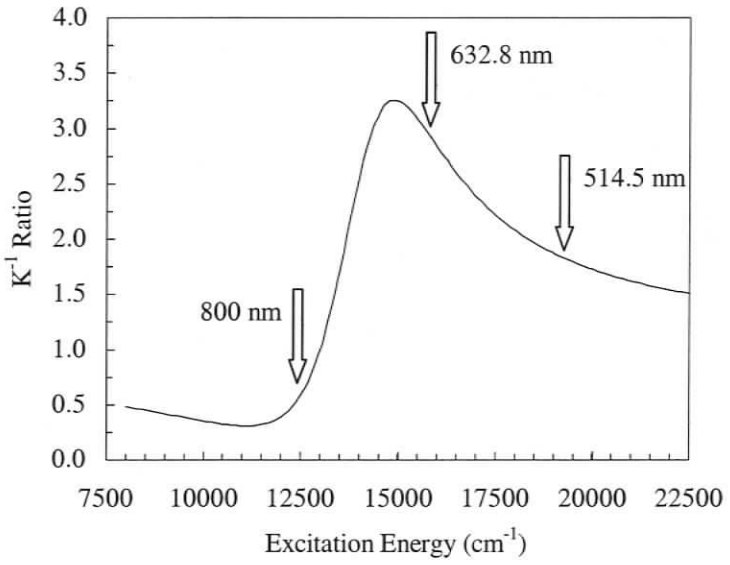

Figure 4.10: Dependence of K^{-1} on excitation energy in a resonance Raman model with $\bar{\nu}_{\text{elec}} = 13300\,\text{cm}^{-1}$, $\Gamma = 1600\,\text{cm}^{-1}$ and $\bar{\nu}_{\text{vib}} = 1000\,\text{cm}^{-1}$. The arrows are at typical laser excitations: Ti-sapphire at 800 nm, He-Ne at 632.8 nm, and Ar^+ at 514.5 nm.

The resonance Raman model described here can also be used to explain the results presented by Kneipp *et al*[54] and Haslett *et al*.[57] Experimental data for crystal violet adsorbed on silver colloids from both groups[54,57] is plotted in figure 4.12. Theoretical fits calculated using equation (4.3) are also plotted in the figure. Again, the objective is not to obtain a quantitative description of the phenomenon, but simply to determine if the

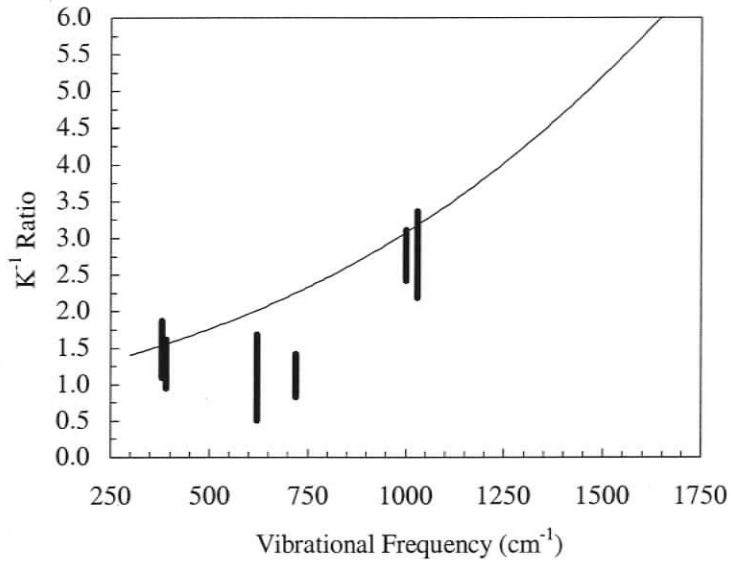

Figure 4.11: Dependence of K^{-1} on the Raman shift of the vibrational band being measured, calculated with $\bar{\nu}_{\text{elec}} = 13300\,\text{cm}^{-1}$, $\Gamma = 1600\,\text{cm}^{-1}$ and excitation at 632.8 nm. The bars represent the measured K^{-1}-ratios for 6 vibration bands of pyridine with applied potentials between -50 and -800 mV. The $620\,\text{cm}^{-1}$ and $1003\,\text{cm}^{-1}$ vibration-band data is also plotted in figure 4.8.

resonance model is sufficient to qualitatively explain the trends in the experimental data. The results presented by Kneipp *et al*[54] are shown in figure 4.12(a), and are satisfactorily described by the model with $\bar{\nu}_{\text{elec}}$=14400 cm^{-1} and Γ=600 cm^{-1} for all reported Raman shifts except the highest energy mode. Results reported by Haslett *et al*[57] for the same system with two different excitation energies are plotted in figure 4.12(b). These are also adequately described by the resonance model, with $\bar{\nu}_{\text{elec}}$=14800 cm^{-1} and Γ=600 cm^{-1}. According to this model the K-ratios reported by Kneipp *et al*[54] and Haslett *et al*[57] can be interpreted as a localized electronic-band resonance in the anti-Stokes region.

The K-ratio for the vibrational mode at $1600\,\text{cm}^{-1}$ in figure 4.12(a) is much higher than expected from the proposed resonance model. Haslett *et al.* have demonstrated an increase in K-ratio with increasing laser power density and have suggested that the effect of the laser power on K could be related to photobleaching of the sample.[57] However, photobleaching of individual crystal violet molecules is much more efficient when the

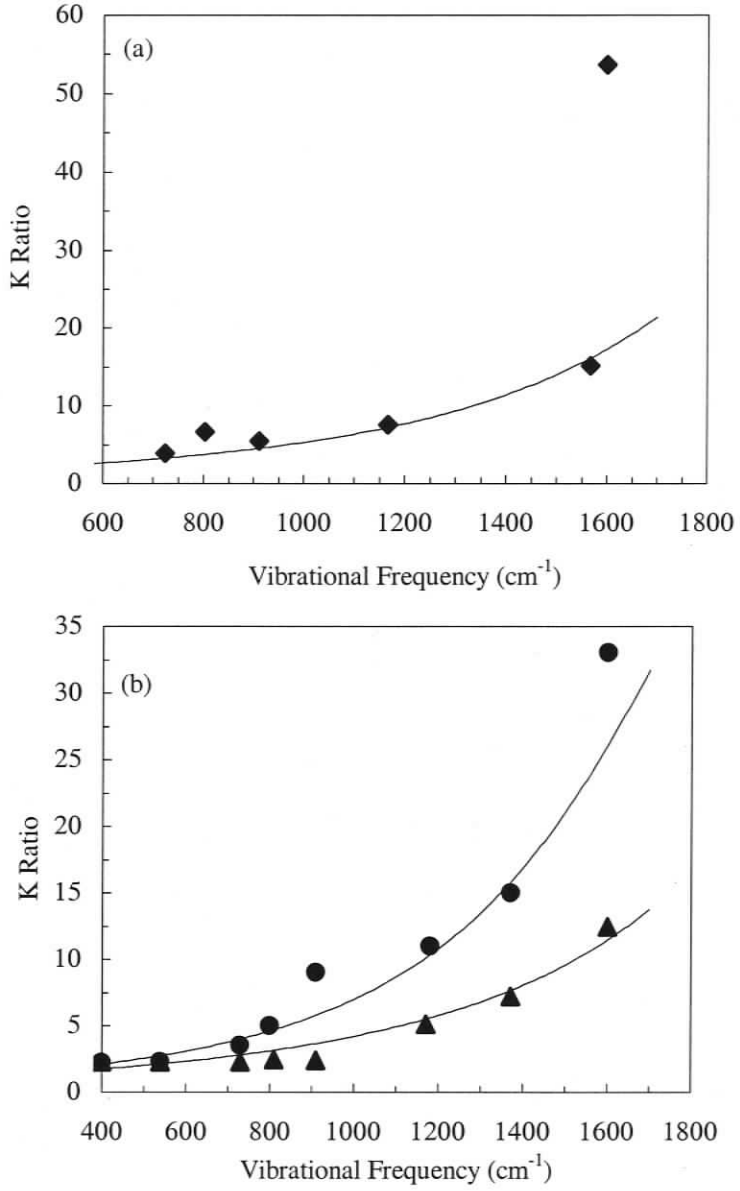

Figure 4.12: Data points from Kneipp *et al.*[54] (a), and Haslett *et al.*[57] (b), for crystal violet showing the dependence of K on the Raman shift of the vibrational band being measured. Data points in (a) collected with 830 nm excitation. Circle data points in (b) collected with 780 nm excitation while triangle data points collected with 830 nm excitation. The solid lines are resonance Raman model fits using (a) $\bar{\nu}_{elec}$=14400 cm^{-1} and Γ=600 cm^{-1}, and (b) $\bar{\nu}_{elec}$=14800 cm^{-1} and Γ=600 cm^{-1}.

laser excitation energy is within the free molecule resonance,[119] implying that photodecomposition of crystal violet is unlikely for the near IR excitation used by Kneipp *et al.*[54] It is also well established that at high laser power densities the incident radiation has a direct effect on the SERS intensity independent of the wavelength of the laser or the nature or chemical composition of the substrate.[120] No mechanism that would explain the increase in K-ratio at these decomposing laser powers was suggested by Haslett *et al.*[57] Perhaps the increase in K-ratio with laser power, and the excessively large K observed for high Raman shift vibrational modes, can be attributed to the fact that the approximations used to derive equation (4.3) are not appropriate under these extreme conditions.

One of the assumptions used to derive equation (4.3) is that the temperature at the SERS surface is the same as the temperature of the liquid used as a reference. However, the photodecomposition observed, even with non-resonant laser excitation, suggests that the temperature of the metal substrate may have changed significantly. A temperature increase is more probable in Raman microscopy experiments, as performed by Kneipp *et al*[54] and Haslett *et al*,[57] due to the tight focus conditions that create high power densities. The temperature is related to the absorption of the substrate-molecule system, the reflectivity of the metal and the rate of energy dissipation. Water is not a very efficient heat conductor, but metals are well known to dissipate heat relatively quickly although this process may be more limited in a nanometric-sized colloidal substrate.

In order to estimate any possible temperature change caused by laser-induced heating, simple models of an electrode and a colloid were constructed based on standard heat transfer calculations.[121,122] In the case of an electrode the area illuminated by the laser is only a small fraction of the total area, implying that it is reasonable to approximate the electrode by a semi-infinite slab. Since silver is a much better conductor of heat than the surrounding water, heat loss through the water is ignored. In the case of the colloid cluster, the model consists of a 100 nm silver sphere suspended in non-convective water with the assumption of a constant temperature over the surface of the sphere. In both models, the heat source is an 830 nm laser with a 2 μm-radius, Gaussian beam and an intensity of 5×10^{24} photons $\mathrm{cm}^{-2}\,\mathrm{s}^{-1}$ as used by Kneipp *et al.*[54] An absorption coefficient of 15%

is used. Under these conditions the models predict an increase in surface temperature of $\sim$70 K for the colloid cluster and $\sim$10 K for the electrode. The colloid result is similar to the temperature of a silver colloidal particle considered, and deemed insignificant, by Kneipp *et al.*[54] For details of these calculation see appendix A.

The expected bias on the experimentally determined K-ratio due to a temperature difference between the substrate and the reference liquid can be evaluated using equation (4.2). Figure 4.13 shows theoretical plots of equation (4.2) with a fixed $T_{UR} = 298$ K and varying values of T_{SERS}. The curves in figure 4.13 were calculated using an 800 nm excitation and an electronic band at 14400 cm^{-1} with a half width of 1000 cm^{-1}. The plots show the multiplicative effect of the temperature factor on the K-ratios obtained under resonant conditions. Since the ratio between the Boltzmann factors is exponential with Raman shift, the difference between T_{UR} and T_{SERS} provokes a significant increase in the K-ratios of the high energy modes. This may explain why a half-width of only 600 cm^{-1}, which is unusually narrow for an electronic transition, is required to fit the data in figure 4.12. Consequently this effect causes a positive bias for the measured K-ratios above that caused by the resonance itself. Considering a band at 1600 cm^{-1}, figure 4.13 shows that this additional bias ranges from a factor of $\sim$2 for a 10 K temperature difference to a factor of $\sim$5 for T_{SERS} 75 K higher than the reference temperature.

According to these estimates the laser-induced temperature changes are not as significant for molecules adsorbed on electrode surfaces as for species adsorbed on colloidal particles due to differences in heat dissipation to the bulk metal. Moreover, the temperature increase for a silver electrode illuminated under the conditions used in this research (power densities $\sim 10^{22}$ photons cm^{-2} s^{-1}) would be very small. Therefore this effect cannot significantly contribute to the results presented in figures 4.7 – 4.9. It is possible that the temperature increase depends on the resonances present in the SERS system, and could therefore be a molecule and excitation-energy dependent effect.

The resonance Raman model presented here can explain the dependence of K on both the excitation energy and the Raman shift of the vibrational bands. However this resonance model is independent of the origin of the resonance and does not require the

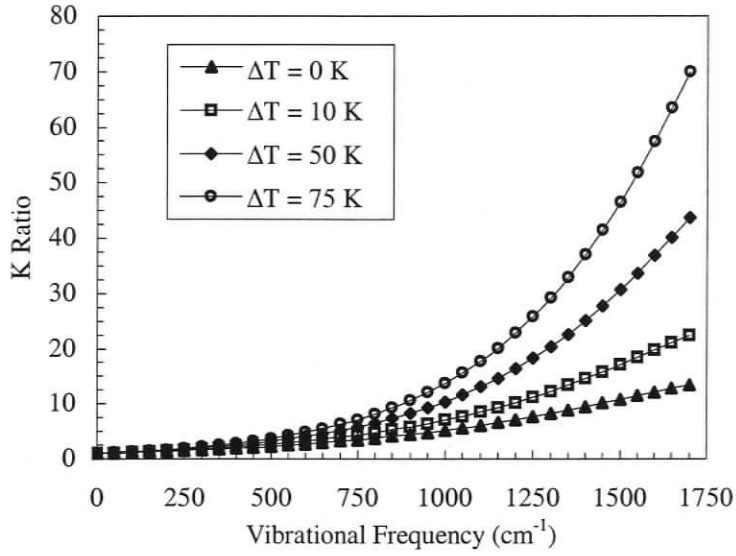

Figure 4.13: Theoretical plots of equation (4.2) for $T_{UR} = 298$ K and $T_{SERS} = T_{UR} + 0$, 10, 50 and 75 K assuming an 800 nm excitation source and an electronic band at 14400 cm^{-1} with a half width of 1000 cm^{-1}.

resonance to be the result of a dominant mechanism. A methodology for the theoretical evaluation of the EM enhancement factor from molecules adsorbed on metal particle aggregates has been suggested by Corni and Tomasi.[123] The model predicts molecule-specific resonant behavior with a relatively narrow bandwidth and suggests a resonance in the near IR for pyridine adsorbed on silver colloids. This resonance would lead to a preferential enhancement of the anti-Stokes for experiments using near IR excitation ($K > 1$) and an enhancement of the Stokes signal for experiments using visible excitation ($K^{-1} > 1$). A simple calculation using this model yields K-ratios of 0.92, 0.89, 4.2 and 5.0 for experiments using laser excitations at 514.5, 632.8, 780, and 830 nm, respectively.[124] These values are in good agreement with figures 4.8 and 4.10.

The work presented here shows that a preferential enhancement of Stokes or anti-Stokes scattering can be explained using a resonance model without the need to invoke optical pumping, and that this model can be applied regardless of the origin of the resonance. The data presented was obtained under experimental conditions significantly different than those used by Kneipp *et al*[54] and Haslett *et al*[57] although differential en-

hancement of the Stokes and anti-Stokes intensities was still observed for a number of different systems. This indicates that this phenomenon is not specific to a given substrate (silver colloids) nor limited to high power density excitation. Moreover, the power densities used were of the order of 10^{22} photons $cm^{-2}\,s^{-1}$, which is 2–3 orders of magnitude lower than used in the experiments reported by Kneipp *et al*[54] and Haslett *et al*.[57] This implies that an interpretation of the rhodamine 6G results presented here, based on the optical pumping mechanism, would yield SERS cross sections 100 times bigger than the ones reported by Kneipp *et al*,[54] which were already astonishingly large. Kneipp *et al* also measured a quadratic relationship between the anti-Stokes intensity and the incident laser power[54] which would support the concept of SERS-induced optical pumping, but other authors have been unable to reproduce this result and have measured a simple linear relationship.[57] Changes in laser power can affect the anti-Stokes/Stokes ratio, without invoking optical pumping, through well accepted processes such as temperature variation, changes in the structure of the substrate, thermal-induced desorption/adsorption and photodecomposition.[120]

A mechanism to explain SERS-induced optical pumping not only requires processes beyond the currently accepted standard SERS model[57] but also appears to contradict some well known results regarding the dynamics of vibrationally excited states. The vibrational relaxation of molecules in solution is known to occur in several steps.[118,125,126] Immediately after photoexcitation, the excess vibrational energy is localized in a specific vibrational mode which is then redistributed to other internal modes through intramolecular vibrational redistribution: this occurs in sub-picosecond time for large molecules and leads to an uniform vibrational temperature among all vibrational modes.[118,126] Vibrational cooling through the dissipation of the excess energy to the solvent molecules then occurs over $\sim$10 ps.[118,126] The presence of the SERS surface provides several additional channels for vibrational relaxation.[127,128] Vibrational relaxation through phonon modes is the main relaxation channel for molecules adsorbed on dielectric material,[127] whereas for metals, quanta of vibrational energy can be transferred from the adsorbate to the conduction electrons via electron-hole pairs,[128] a mechanism that dominates for

high-frequency modes. Low frequency molecular vibrations can couple directly with the surface modes. Considering all of these possible relaxation pathways it is unlikely that the vibrational energy in a molecule like rhodamine 6G or crystal violet would remain localized for an appreciable length of time, eliminating the possibility of any significant optical pumping.

4.4 Conclusions

SERS K-ratios for oxazine 720, rhodamine 6G and pyridine adsorbed on a silver electrode were obtained and the dependence of the K-ratios on the applied potential, excitation wavelength and Raman shift were explained using established SERS theories. Ratios different from unity were observed for all of the investigated molecules indicating that a CT complex between the SERS substrate and the molecule was likely formed in all cases. The position of the CT band of the complex, relative to the energy of the Raman shifted photon, determines if a resonance occurs in the Stokes or the anti-Stokes region for a given excitation energy. A resonance Raman model was used to calculate the expected dependence on excitation wavelength and Raman shift, showing good qualitative agreement with the experimental data presented here and previously reported in the literature.[54,57] Resonances based on an EM model were discussed and shown to also be capable of reproducing the measured K-ratios. Laser induced heating of the surface during a SERS experiment was modeled and shown to be potentially significant when using high incident power densities. Such heating can yield unusually high K-ratios, especially for modes with large Raman shifts.

Although the concept of SERS-induced vibrational optical pumping is intriguing, it is both unnecessary and physically improbable. If such a process does exist, it is unlikely to produce any observable effect except possibly at very low temperature. Since such an optical pumping process would require significant changes to the existing SERS model, its use demands substantial justification. As has been shown, optical pumping is not needed to explain any of the results observed here or reported in the literature, indicating that such justification does not exist. As was discussed above, the EM mechanism enhances both

the incident and scattered fields so an increase in SERS intensity is not linearly related to the number of scattering molecules,[129] implying that an extremely large incident field, or an unphysically large cross section, is required to produce sufficient pumping to produce the measured K-ratios. This is especially apparent in low laser power experiments like those described here. Also, the expected relaxation lifetime for a molecule adsorbed on a metal surface is too short to allow any significant pumping to occur. It appears that there is neither the need nor the supporting evidence to accept optical pumping as a viable explanation for the experimentally measured K-ratios.

4.5 Post Publication Optical Pumping Research

The results given in the preceding portion of this chapter were published in 2004.[58] Since that time various groups have published research with connections to SERS optical pumping. This section gives a brief overview of some of this work.

At approximately the same time as the publication of the results given above,[58] Maher *et al* published a paper[59] exploring the importance of excitation wavelength and Raman shift on the measured K-ratio. This paper considered the problem from both a theoretical and experimental point of view. They argue that it is imperative to take into account the internal resonances of the system under study and the possibility that cross sections for the Stokes and anti-Stokes scattering are not equal. They conclude, as here, that resonances within a system can produce K-ratios above or below unity depending on the excitation wavelength. They point out that absorption effects and the detailed behaviour of hot spots can play an important role in the measured K-ratio. Experimentally, they found evidence of non-linear power dependence for a specific combination of excitation wavelength and Raman shift, suggesting that optical pumping may be involved. Their main conclusion is that interpretation of K-ratios requires careful consideration of the specific details of the system, something that had been overlooked in previous publications.

Later in 2004, Maher *et al* published a second paper[130] that explores the reproducibility and reliability of K-ratios calculated from SERS at single, or near-single, molecule sensitivity using both experimental and computational results. They argue that K-ratios

measured at single molecule sensitivity are fundamentally inaccurate because each hot spot has unique EM resonances leading to a unique K-ratio for each Raman band. Such a result is confirmed by their experimental data and supported by their computational model which also shows that such measurements tend to favour, through purely EM mechanisms, an above unity K-ratio for loosely modeled colloid systems. Notwithstanding this result, the paper introduces a technique to help distinguish between the effects of optical pumping and sample heating in a single-molecule sensitivity experiment. Due to small differences in energy between the $0 \leftrightarrow 1$ and the $1 \leftrightarrow 2$ vibrational transitions, if excited-state transitions are involved for a particular mode, the resulting peak will be the sum of two slightly offset peaks, resulting in broadening. If the broadening is a result of heating, it should be more pronounced at bands with lower Raman shifts than bands with higher Raman shifts, but if the excited state is the result of pumping, it should be uncorrelated to the broadening of non-pumped states. By examining the correlation between parameters of individual Stokes scattering events for multiple bands it should be possible to distinguish between a pumped and an unpumped band. Analysis of their data suggests that pumping plays a significant role for at least one band under their experimental conditions.

In 2005, Peyser-Capadona *et al* produced single molecule sensitivity SERS using substrates that should be incapable of producing plasmon resonances within the standard EM model.[131] The SERS substrate consisted of nanoclusters of 2–8 silver atoms encapsulated within large biomolecules. The dimensions of such nanoclusters are too small to support EM resonances at the energy of the incident field. In addition to observing single-molecule SERS, they also observed a higher than expected anti-Stokes signal. Since the work was carried out under conditions insufficient to produce optical pumping (low power densities and low EM enhancement) they suggest that the result may be caused by an enhancement of the anti-Stokes cross section due to a CT resonance. This is another example of an above-unity K-ratio that cannot be the result of optical pumping.

To help clarify the role resonances play in K-ratios Maher *et al* conducted a comprehensive study of resonances in 2005 that involved four excitation wavelengths, three different substrate geometries, and five different analyte molecules.[132] The study began by

enumerating the various possible resonances: plasmon resonance within a single nanoparticle, resonance between interacting nanoparticles, resonance of the free analyte molecule, and resonances within the molecule-adatom complex (CT). By appropriate choice of excitation, substrate and analyte the effect of the various resonances could be explored. The entire study was conducted at low laser intensities to eliminate the effects of optical pumping and laser induced heating yet K-ratios above and below unity were common, confirming that a K-ratio above one does not necessarily indicate optical pumping. Maher *et al* conclude that the CT resonance and the interacting nanoparticle resonance were the dominant processes.

In their 2006 paper, Le Ru and Etchegoin suggest that the difference between heating and optical pumping is partly a matter of semantics since optical pumping is essentially heating a single localized mode of a molecule.[60] To further clarify the issue at hand, they define five regimes to describe different heating/pumping processes and explore the time scales of the various excitation and relaxation processes in relation to these different heating regimes. Rather than analyzing their data using K-ratios, which have been shown to produce anomalous results regarding the population of a given vibrational mode, they used a method similar to that used by Maher *et al*[130] that involves measuring the width and shift of a particular band to determine the population of the excited states. To calibrate this method, they collected SERS spectra using a low intensity source and a temperature controlled sample. Their analysis shows that optical pumping does not play a significant role in producing the anti-Stokes excess which is predominantly driven by differences in cross section with a small contribution from local heating.

In two papers published in 2006, Kneipp *et al*[61,70] reconfirm their confidence in their previous finding[54] of a quadratic dependence of anti-Stokes intensity on incident power density. They also insist that to properly extract information about the optical pumping process the experiments need to be performed "under nonresonant Raman conditions".[70] Unfortunately, this is essentially an impossible condition to achieve since the SERS process relies heavily on various resonance mechanisms which are often indistinguishable from any additional resonances. No new data appears to have been included to

support their proposition that the anti-Stokes excess is the result of optical pumping.

In a sequence of four papers published in 2006, Maher *et al* develop and exploit a technique that allows the K-ratio contributions from heating, pumping and cross section asymmetry to be separated from each other.[62–64,133] The results can be used to estimate the cross section of the Raman Stokes and anti-Stokes scattering without needing to know the number of molecules being probed. The technique uses a low power laser and a temperature controlled sample. By calculating the K-ratio over a range of temperatures, it is possible to deconvolute the effect of temperature, pumping, and the effect caused by differences in Stokes and anti-Stokes cross section. By using sufficiently low temperatures Maher *et al* directly observe the transition from a pumping dominated regime to a thermally dominated regime. After collecting and analyzing data for a number of analytes they conclude that optical pumping does play a part in SERS, but is only observable at temperatures low enough to damp thermal excitations (typically between 50 and 200 K). They also find that significant differences exist between the Stokes and anti-Stokes cross section and that their calculated absolute cross sections are in reasonable agreement with those calculated from single molecule SERS and those calculated from computational models. Ironically, while their results convincingly support the existence of optical pumping they clearly confirm that its effects are not measurable at normal temperatures.

It is apparent that optical pumping is still an active and controversial subject. Some groups claim that optical pumping plays an important role in the anti-Stokes asymmetry issue, some claim it is a physical impossibility, while others claim it exists but is not observable under typical SERS conditions. As the field continues to develop it should continue to produce exciting results.

Chapter 5

Summary and Conclusions

THIS CHAPTER CONTAINS A SUMMARY OF THE RESULTS PRESENTED IN THE EARLIER CHAPTERS. THIS INCLUDES RESULTS RELATED TO THE SPECTROELECTROCHEMISTRY OF OXAZINE 720 AND THOSE RELATED TO THE ANTI-STOKES ASYMMETRY ISSUE. THE CHAPTER ENDS WITH A BRIEF DISCOURSE ON THE CURRENT STATE AND FUTURE DIRECTION OF SERS RESEARCH.

Spectroelectrochemistry of Oxazine 720

Electrochemistry and spectroscopy are often complementary techniques with results from one frequently being supported or extended by the other. In some cases, used together, the combination of techniques can produce results unobtainable by either technique alone.

A silver electrode modified with oxazine 720 was studied using a combination of cyclic voltammetry and SERS under an applied bias. The electrochemistry indicates that the oxazine 720 does not adsorb with its ring structure flat on the surface. This is supported by the SERS data which suggests that oxazine 720 adsorbs edge-on, most likely via the nitrogen side chains. The cyclic voltammetry shows that oxazine 720 has a quasi-reversible reduction-oxidation at ~ -500 mV. This was confirmed by the SERS data which shows a distinct change in intensity at the same applied potential. The recoverability of the SERS signal after oxazine 720 reduction indicates that the reduced molecules remain adsorbed on the surface down to an applied potential of at least -1000 mV. The spectroelectrochemistry data shows that a band at 1475 cm^{-1} has a resonance-like behaviour versus the applied potential indicating that the CT mechanism plays a role in the SERS enhancement of this band. The lack of such behaviour by other bands proves that the CT mechanism is not a requirement of SERS.

Anti-Stokes/Stokes Ratios

In 1996 it was discovered that certain SERS systems produce anti-Stokes intensities above those expected,[54] an effect referred to here as the anti-Stokes asymmetry issue. Electrochemical SERS can often elucidate the contribution of resonances to the SERS cross section, making it an ideal tool with which to study this effect.

The ratio of anti-Stokes to Stokes SERS intensity, or K-ratio, for oxazine 720, rhodamine 6G and pyridine, adsorbed on a roughened silver electrode, were collected as a function of applied potential. Non-unity K-ratios that varied with applied potential and excitation wavelength were observed for all of the molecules investigated with values both above and below unity. Such behaviour indicates that a CT complex is likely formed between the molecule and the silver surface creating a SERS cross section resonance. A

resonance Raman model was constructed and is able to reproduce all of the observed K-ratio variation, both here and previously reported.[54,57] Thus, all of the available data is accounted for using established SERS theories, implying that an optical pumping[54] mechanism is unnecessary. Analysis using such a mechanism under conditions like those used here leads to implausibly large Raman cross sections. Laser induced heating was modeled for two typical SERS set-ups and is found to be a potentially significant contributor to above-unity K-ratios, especially when high power densities are used with colloid based substrates.

Overall

SERS is a vigorous and growing discipline with researchers actively working on both the fundamental and applied aspects of the field. Single-molecule sensitivity, substrate construction, and biomedical application are just a few of the current topics helping keep SERS a vibrant field. The technique of collecting SERS spectra from the electrode of an electrochemical cell is a powerful analytical technique capable of independently probing the CT contribution to SERS. This technique has been used to good effect here to explore the properties of a specific analyte, as well as to investigate the more general consequence of resonances. The field of SERS is not without its controversies as investigators still debate the exact role of the CT mechanism in the enhancement, the cause of the anti-Stokes asymmetry, the possibility of optical pumping, and the exact nature of hot spots. But it is controversies like these that keep the field fresh and interesting, and more generally, it is controversies like these that make up the dialogue of science, allowing us to advance our collective understanding and move forward in the pursuit of knowledge.

References

[1] C. V. Raman and K. S. Krishnan, "A new type of secondary radiation," *Nature*, vol. 121, p. 501, 1928.

[2] A. Smekal, "Zur quantentheorie der dispersion," *Naturwiss.*, vol. 11, no. 43, p. 873, 1923.

[3] D. A. Long, *The Raman Effect: A Unified Treatment of the Theory of Raman Scattering by Molecules*. England: John Wiley and Sons, 2002.

[4] Lord Rayleigh, "On the transmission of light through an atmosphere containing small particles in suspension," *Phil. Mag.*, vol. 41, p. 447, 1871.

[5] J. R. Ferraro and K. Nakamoto, *Introductory Raman Spectroscopy*. San Diego: Academic Press, 1994.

[6] A. G. Brolo, *Surface-Enhanced Raman Scattering (SERS) Studies of Pyazine Adsorbed on Polycrystalline and Single Crystal Electrodes*. PhD thesis, University of Waterloo, 1998.

[7] R. L. McCreery, *Raman Spectroscopy for Chemical Analysis*. John Wiley and Sons, 2000.

[8] N. B. Colthup, L. H. Daly, and S. E. Wiberley, *Introduction to Infrared and Raman Spectroscopy*. Academic Press, 4 ed., 1990.

[9] W. J. Hehre, L. Radom, P. V. R. Scleyer, and J. A. Pope, *Ab Initio Molecular Orbital Theory*. New York: John Wiley and Sons, 1985.

[10] J. D. Jackson, *Classical Electrodynamics*. John Wiley and Sons, 2 ed., 1975.

[11] M. Born and E. Wolf, *Electromagnetic Theory of Propogation, Interference and Diffraction of Light*. Cambridge University Press, 7 ed., 1999.

[12] J. Tang and A. C. Albrecht, "Developements in the theories of vibrational Raman intensities," in *Raman Spectroscopy Theory and Practice* (H. A. Szymanski, ed.), vol. 2, ch. 2, pp. 33–68, Plenum Press, 1970.

[13] H. Eyring, J. Walter, and G. Kimball, *Quantum Chemistry*. John Wiley and Sons, 1944.

[14] M. Born and J. R. Oppenheimer, "Zur quantentheorie der molekeln," *Ann. Phys. (Leipzig)*, vol. 389, no. 20, pp. 457–484, 1927.

[15] D. A. Long, *Raman Spectroscopy*. McGraw-Hill, 1977.

[16] P. W. Atkins, *Physical Chemistry*. Oxford University Press, 3 ed., 1986.

[17] D. L. Jeanmaire and R. P. Van Duyne, "Surface raman spectroelectrochemistry: Part I. Heterocyclic, aromatic, and aliphatic amines adsorbed on the anodized silver electrode," *J. Electroanal. Chem.*, vol. 84, no. 1, pp. 1–20, 1977.

[18] M. Albrecht and J. A. Creighton, "Anomalously intense Raman spectra of pyridine at a silver electrode," *J. Am. Chem. Soc.*, vol. 99, p. 5215, 1977.

[19] M. Moskovits, "Surface-enhanced spectroscopy," *Rev. Mod. Phys.*, vol. 57, pp. 783 – 826, 1985.

[20] A. Otto, I. Mrozek, H. Grabhorn, and W. Akemann, "Surface-enhanced Raman scattering," *J. Phys.: Condens. Matter*, vol. 4, pp. 1143–1212, 1992.

[21] B. Pettinger, "In situ raman spectroscopy at metal electrodes," in *Adsorption of Molecules at Metal Electrodes* (J. Lipkowski and P. N. Ross, eds.), ch. 6, p. 285, Berlin: VCH, 1992.

[22] K. Kneipp, H. Kneipp, I. Itzkan, R. R. Dasari, and M. S. Feld, "Surface-enhanced Raman scattering and biophysics," *J. Phys. Condens. Matter*, vol. 14, pp. R597 – R624, 2002.

[23] K. Kneipp, Y. Wang, H. Kneipp, L. T. Perelman, I. Itzkan, R. R. Dasari, and M. S. Feld, "Single molecule detection using SERS," *Phys. Rev. Lett.*, vol. 78, pp. 1667 – 1670, 1997.

[24] S. Nie and S. R. Emory, "Probing single molecule and single nanoparticles by SERS," *Science*, vol. 275, pp. 1102 – 1105, 1997.

[25] E. J. Zeman and G. C. Schatz, "An accurate electromagnetic theory study of surface enhancement factors for Ag, Au, Cu, Na, Al, Ga, In, Zn, and Cd," *J. Phys. Chem.*, vol. 91, pp. 634–643, 1987.

[26] M. Kerker, "Electromagnetic model for surface-enhanced Raman scattering (SERS) on metal colloids," *Acc. Chem. Res.*, vol. 17, pp. 271–277, 1984.

[27] M. Moskovits, "Surface selection rules," *J. Chem. Phys.*, vol. 77, no. 9, pp. 4408–4416, 1982.

[28] M. Kerker, D.-S. Wang, and H. Chew, "Surface enhanced raman scattering (sers) by molecules adsorbed at spherical particles: errata," *Appl. Opt.*, vol. 19, no. 24, pp. 4159–4174, 1980.

[29] J. Gersten and A. Nitzan, "Electromagnetic theory of enhanced Raman scattering by molecules adsorbed on rough surfaces," *J. Chem. Phys.*, vol. 73, no. 7, pp. 3023–3037, 1980.

[30] D.-S. Wang and M. Kerker, "Enhanced Raman scattering by molecules adsorbed at the surface of colloidal spheroids," *Phys. Rev. B.*, vol. 24, no. 4, pp. 1777–1790, 1981.

[31] M. Xu and M. J. Dignam, "Raman scattering by high-density dispersions. I. Formulation of theory and application to a pair of coated particles," *J. Chem. Phys.*, vol. 96, no. 10, pp. 7758–7770, 1992.

[32] E. V. Albano, S. Daiser, G. Ertl, R. Miranda, K. Wandelt, and N. Garcia, "Nature of surface-enhanced-Raman-scattering active sites on coldly condensed Ag films," *Phys. Rev. Lett.*, vol. 51, no. 25, pp. 2314–2317, 1983.

[33] F. J. Garcia-Vidal and J. B. Pendry, "Collective theory for surface enhanced Raman scattering," *Phys. Rev. Lett.*, vol. 77, pp. 1163 – 1166, 1996.

[34] M. I. Stockman, V. M. Shalaev, M. Moskovits, R. Botet, and T. F. George, "Enhanced raman scattering by fractal clusters: Scale-invariant theory," *Phys. Rev. B*, vol. 46, no. 5, pp. 2821–2830, 1992.

[35] H. Xu, J. Aizpurua, M. Kall, and P. Apell, "Electromagnetic contributions to single-molecule sensitivity in SERS," *Phys. Rev. E*, vol. 62, pp. 4318 – 4324, 2000.

[36] A. Otto, J. Timper, J. Billmann, G. Kovacs, and I. Pockrand, "Surface roughness induced electronic Raman scattering," *Surf. Sci.*, vol. 92, no. 1, pp. L55–L57, 1980.

[37] J. Billmann, G. Kovacs, and A. Otto, "Surface roughness induced electronic Raman scattering," *Surf. Sci.*, vol. 92, pp. 153–173, 1980.

[38] M. Moskovits and D. P. DiLella, "Vibrational spectroscopy of molecules adsorbed on vapor-deposited metals," in *Surface Enhance Raman Scattering* (R. K. Chang and T. E. Furtak, eds.), pp. 243–274, New York: Plenum Press, 1982.

[39] S. L. McCall and P. M. Platzman, "Raman scattering from chemisorbed molecules at surfaces," *Phys. Rev. B*, vol. 22, no. 4, pp. 1660–1662, 1980.

[40] J. Billmann and A. Otto, "Electronic surface state contribution to surface enhanced Raman scattering," *Solid State Commun.*, vol. 44, no. 2, pp. 105–107, 1982.

[41] J. M. Seminario, "An introduction to density functional theory in chemistry," in *Modern Density Functional Theory: A Tool for Chemistry* (J. M. Seminario and P. Pokitzer, eds.), vol. 2 of *Theoretical and Computational Chemistry*, ch. 1, pp. 1–27, Elsevier Science, 1995.

[42] W. Koh and M. C. Holthausen, *A Chemist's Guide to Density Functional Theory*. Germany: Wiley-VCH Verlag, 2000.

[43] D. R. Hartree, "The wave mechanics of an atom with a non-Coulomb central field. part I-theory and methods," *Proc. Cambridge Phil. Soc.*, vol. 24, pp. 89–110, 1928.

[44] V. Fock, "Näherungsmethode zur lösung des quantenmechanischen mehrkörper-problems," *Z. Physik*, vol. 61, pp. 126–148, 1930.

[45] C. C. J. Roothaan, "New developments in molecular orbital theory," *Rev. Mod. Phys.*, vol. 23, no. 2, pp. 69–89, 951.

[46] J. C. Slater, "Atomic shielding constants," *Phys. Rev.*, vol. 36, no. 1, pp. 57–64, 1930.

[47] S. F. Boys, "Electronic wave functions. i. a general method of calculation for the stationary states of any molecular system," *Proc. R. Soc. London A*, vol. 200, no. 1063, pp. 542–554, 1950.

[48] P. Hohenberg and W. Kohn, "Inhomogeneous electron gas," *Phys. Rev.*, vol. 136, no. 3B, pp. B864–B871, 1964.

[49] W. Kohn and L. J. Sham, "Self-consistent equations including exchange and correlation effects," *Phys. Rev.*, vol. 140, no. 4A, pp. A1133–A1138, 1965.

[50] I. N. Levine, *Quantum Chemistry - Volume II: Molecular Spectroscopy*. Boston: Allyn and Bacon, 1970.

[51] M. Moskovits and J. S. Suh, "Surface selection rules for surface-enhanced Raman spectroscopy: calculations and application to the surface-enhanced Raman spectrum of phthalazine on silver," *J. Phys. Chem.*, vol. 88, no. 23, pp. 5526 – 5530, 1984.

[52] J. A. Creighton, "The selection rules for surface-enhanced Raman spectroscopy," in *Spectroscopy of Surfaces* (R. J. H. Clark and R. E. Hester, eds.), ch. 2, p. 37, New York: John Wiley & Sons, 1988.

[53] C. L. Haynes, A. D. McFarland, and R. P. V. Duyne, "Surface-enhanced Raman spectroscopy," *Anal. Chem.*, vol. 77, pp. 338A – 346A, 2005.

[54] K. Kneipp, Y. Wang, H. Kneipp, I. Itzkan, R. R. Dasari, and M. S. Feld, "Population pumping of excited vibrational states by spontaneous SERS," *Phys. Rev. Lett.*, vol. 76, no. 14, pp. 2444 – 2447, 1996.

[55] K. Kneipp, H. Kneipp, R. Manoharan, and e. al, "Near-infrared surface-enhanced Raman scattering can detect single molecule and observe hot vibrational transitions," *J. Raman Spectrosc.*, vol. 29, no. 8, pp. 743 – 747, 1998.

[56] K. Kneipp, H. Kneipp, I. Itzkan, R. R. Dasari, and M. S. Feld, "Surface-enhanced non-linear Raman scattering at the single-molecule level," *Chem. Phys.*, vol. 247, no. 1, pp. 155–162, 1999.

[57] T. L. Haslett, L. Tay, and M. Moskovits, "Can SERS serve as a channel for strong optical pumping?," *J. Chem. Phys.*, vol. 113, pp. 1641 – 1646, 2000.

[58] A. G. Brolo, A. C. Sanderson, and A. P. Smith, "Ratio of the surface-enhanced anti-Stokes scattering to the surface-enhanced Stokes-Raman scattering for molecules adsorbed on a silver electrode," *Phys. Rev. B.*, vol. 69, p. 045424, 2004.

[59] R. C. Maher, L. F. Cohen, P. Etchegoin, H. J. N. Hartigan, R. J. C. Brown, and M. J. T. Milton, "Stokes/anti-Stokes anomalies under surface enhanced Raman scattering conditions," *J. Chem. Phys.*, vol. 120, no. 24, pp. 11746–11753, 2004.

[60] E. C. Le Ru and P. G. Etchegoin, "Vibrational pumping and heating under SERS conditions: fact or myth?," *Faraday Discuss.*, vol. 132, pp. 63–75, 2006.

[61] K. Kneipp and H. Kneipp, "SERS signals at the anti stokes side of the excitation laser in extremely high local optical fields of silver and gold nanoclusters," *Faraday Discuss.*, vol. 132, pp. 27–33, 2006.

[62] R. C. Maher, L. F. Cohen, E. C. L. Ru, and P. G. Etchegoin, "A study of local heating of molecules under surface enhanced Raman scattering (SERS) conditions using the anti-Stokes/Stokes ratio," *Faraday Discuss.*, vol. 132, pp. 77–83, 2006.

[63] R. C. Maher, L. F. Cohen, J. C. Gallop, E. C. L. Ru, and P. G. Etchegoin, "Temperature-dependent anti-Stokes/Stokes ratios under surface-enhanced Raman scattering conditions," *J. Phys. Chem. B*, vol. 110, no. 13, pp. 6797–6803, 2006.

[64] R. C. Maher, P. G. Etchegoin, E. C. L. Ru, and L. F. Cohen, "A conclusive demonstration of vibrational pumping under surface enhanced Raman scattering conditions," *J. Phys. Chem. B*, vol. 110, no. 24, pp. 11757–11760, 2006.

[65] K. Kneipp, H. Kneipp, V. B. Kartha, R. Manoharan, G. Deinum, I. Itzkan, R. R. Dasari, and M. S. Feld, "Single-molecule detection of a cyanine dye in silver colloidal solution using near-infrared surface-enhanced Raman scattering," *Appl. Spectrosc*, vol. 52, no. 2, pp. 175–178, 1998.

[66] K. Kneipp, H. Kneipp, V. B. Kartha, R. Manoharan, G. Deinum, I. Itzkan, R. R. Dasari, and M. S. Feld, "Detection and identification of a single DNA base molecule using surface-enhanced Raman scattering (SERS)," *Phys. Rev. E*, vol. 57, no. 6, pp. R6281–R6284, 1998.

[67] A. M. Michaels, M. Nirmal, and L. E. Brus, "SERS of individual rhodamine 6G molecules on large Ag nanocrystals," *J. Am. Chem. Soc.*, vol. 121, pp. 9932 – 9939, 1999.

[68] W. E. Doering and S. Nie, "Single molecule and single nanoparticle SERS: Examing the role of surface active sites and chemical enhancement," *J. Phys. Chem. B*, vol. 106, pp. 311 – 317, 2002.

[69] E. J. Bjerneld, Z. Földes-Papp, M. Käll, and R. Rigler, "Single-molecule surface-enhanced Raman and fluorescence correlation spectroscopy of horseradish peroxidase," *J. Phys. Chem. B.*, vol. 106, no. 6, pp. 1213 – 1218, 2002.

[70] K. Kneipp, H. Kneipp, and J. Kneipp, "Surface-enhanced Raman scattering in local optical fields of silver and gold nanoaggregates - from single-molecule Raman spectroscopy to ultrasensitive probing in live cells," *Acc. Chem. Res.*, vol. 39, no. 7, pp. 443–450, 2006.

[71] A. Otto, "What is observed in single molecule SERS, and why?," *J. Raman Spectrosc.*, vol. 33, no. 8, pp. 593–598, 2002.

[72] C. J. Addison and A. G. Brolo, "Nanoparticle-containing structures as a substrate for surface-enhanced Raman scattering," *Langmuir*, vol. 22, no. 21, pp. 8696–8702, 2006.

[73] C. J. Addison, *Fabrication, characterization and optical properties of three-dimensional colloidal gold nanostructures*. PhD thesis, University of Victoria, 2005.

[74] A. G. Brolo, E. Arctander, R. Gordon, B. Leathem, and K. L. Kavanagh, "Nanohole-enhanced Raman scattering," *Nano Lett.*, vol. 4, no. 10, pp. 2015 – 2018, 2004.

[75] L. Gunnarsson, E. J. Bjerneld, H. Xu, S. Petronis, B. Kasemo, and M. Käll, "Interparticle coupling effects in nanofabricated substrates for surface-enhanced Raman scattering," *Appl. Phys. Lett.*, vol. 78, no. 6, pp. 802–804, 2001.

[76] N. Félidj, S. L. Truong, J. Aubard, G. Lévi, J. R. Krenn, A. Hohenau, A. Leitner, and F. R. Aussenegg, "Gold particle interaction in regular arrays probed by surface enhanced Raman scattering," *J. Chem. Phys.*, vol. 120, no. 15, pp. 7141–7146, 2004.

[77] M. Litorja, C. L. Haynes, A. J. Haes, T. R. Jensen, and R. P. V. Duyne, "Surface-enhanced Raman scattering detected temperature programmed desorption: Optical properties, nanostructure, and stability of silver film over SiO_2 nanosphere surfaces," *J. Phys. Chem. B*, vol. 105, no. 29, pp. 6907 – 6915, 2001.

[78] L. A. Dick, A. D. McFarland, C. L. Haynes, and R. P. V. Duyne, "Metal film over nanosphere (MFON) electrodes for surface-enhanced Raman spectroscopy (SERS): Improvements in surface nanostructure stability and suppression of irreversible loss," *J. Phys. Chem. B*, vol. 106, no. 4, pp. 853 – 860, 2002.

[79] C. L. Haynes and R. P. V. Duyne, "Plasmon-sampled surface-enhanced Raman excitation spectroscopy," *J. Phys. Chem. B*, vol. 107, no. 30, pp. 7426 – 7433, 2003.

[80] S. Cintra, M. E. Abdelsalam, P. N. Bartlett, J. J. Baumberg, T. A. Kelf, Y. Sugawara, and A. E. Russell, "Sculpted substrates for SERS," *Faraday Discuss.*, vol. 132, pp. 191–199, 2006.

[81] A. de S. Santos, L. Gorton, and L. T. Kubota, "Nile blue adsorbed onto silica gel modified with niobium oxide for electrocatalytic oxidation of NADH," *Electrochim. Acta*, vol. 47, no. 20, pp. 3351–3360, 2002.

[82] I. Bedja, S. Hotchandani, and P. V. Kamat, "Photoelectrochemistry of quantized WO_3 colloids. Electron storage, electrochromic, and photoelectrochromic effects," *J. Phys. Chem.*, vol. 97, pp. 11064–11070, 1993.

[83] L. Gorton, "Chemically modified electrodes for the electrocatalytic oxidation of nicotinamide coenzymes," *J. Chem. Soc. Faraday Trans. 1*, vol. 82, p. 1245, 1986.

[84] A. Hagfeldt and M. Graetzel, "Light-induced redox reactions in nanocrystalline systems," *Chem. Rev.*, vol. 95, pp. 49–68, 1995.

[85] D. A. Steinhurst and J. C. Owrutsky, "Second harmonic generation from oxazine dyes at the air/water interface," *J. Phys. Chem. B*, vol. 105, no. 15, pp. 3062–3072, 2001.

[86] J. Bourdon, "Spectral sensitization of chemical effects in solids," *J. Phys. Chem.*, vol. 69, pp. 705–713, 1965.

[87] P. V. Kamat, "Photochemistry on nonreactive and reactive (semiconductor) surfaces," *Chem. Rev.*, vol. 93, pp. 267–300, 1993.

[88] A. Malinauskas, T. Ruzgas, and L. Gorton, "Electrochemical study of the redox dyes nile blue and toluidine blue adsorbed on graphite and zirconium phosphate modified graphite," *J. Electroanal. Chem.*, vol. 484, no. 1, pp. 55–63, 2000.

[89] H. Ju and C. Shen, "Electrocatalytic reduction and determination of dissolved oxygen at a poly(nile blue) modified electrode," *Electroanalysis*, vol. 13, no. 8-9, p. 789793, 2001.

[90] I. Taniguchi, C. zhong Li, M. Ishida, and Q. Yao, "Electrochemical and spectroelectrochemical properties of manganese reconstituted myoglobin," *J. Eletroanal. Chem.*, vol. 460, pp. 245–250, 1999.

[91] K. Kneipp, H. Kneipp, I. Itzkan, R. R. Dasari, and M. S. Feld, "Ultrasensitive chemical analysis by Raman spectroscopy," *Chem. Rev.*, vol. 99, pp. 2957 – 2975, 1999.

[92] Y. C. Cao, R. Jin, and C. A. Mirkin, "Nanoparticles with Raman spectroscopic fingerprints for DNA and RNA detection," *Science*, vol. 297, no. 5586, pp. 1536–1540, 2002.

[93] S. Schneider, H. Grau, P. Halbig, P. Freunscht, and U. Nikel, "Stabilization of silver colloids by various types of anions and their effect on the SERS of organic dyes," *J. Raman Spectrosc.*, vol. 27, pp. 57 – 68, 1996.

[94] J. R. Lombardi, R. L. Birke, T. Lu, and J. Xu, "Charge transfer theory of SERS: Herzberg - Teller contributions," *J. Chem. Phys.*, vol. 84, pp. 4174 – 4180, 1986.

[95] A. G. Brolo, D. E. Irish, and B. D. Smith, "Applications of SERS to the study of metal-adsorbate interactions," *J. Mol. Spectrosc.*, vol. 405, pp. 29 – 44, 1997.

[96] J. Pemberton and M. M. Girand, "Electrochemical and SEM characterization of Ag electrodes roughened by potential steps," *J. Electroanal. Chem.*, vol. 217, pp. 79 – 92, 1987.

[97] D. D. Tuschel, J. E. Pemberton, and J. E. Cook, "SERS and SEM of roughened Ag electrode formed by controlled ORC in aqueous Cl solution," *Langmuir*, vol. 2, pp. 380 – 388, 1986.

[98] A. G. Brolo and D. E. Irish, "The adsorption and orientation of pyrazine on Ag electrodes: a SERS study," *J. Electroanal. Chem.*, vol. 414, pp. 183 – 196, 1996.

[99] F. Ni, H. Feng, L. Gorton, and T. M. Cotton, "Electrochemical and SERS studies of chemically modified electrodes: Nile blue A, a mediator for NADH oxidation," *Langmuir*, vol. 6, no. 1, pp. 66–73, 1990.

[100] S. H. de Araujo Nicolai, P. R. P. Rodrigues, S. M. L. Agostinho, and J. C. Rubim, "Electrochemical and spectroelectrochemical (SERS) studies of the reduction of methylene blue on a silver electrode," *J. Electroanal. Chem.*, vol. 527, pp. 103–111, 2002.

[101] A. Bard and L. R. Faulkner, *Electrochemical Methods - Fundamentals and Applications*. Toronto: Wiley, 2 ed., 2001.

[102] L. Gortona, A. Torstenssona, H. Jaegfeldt, and G. Johanssona, "Electrocatalytic oxidation of reduced nicotinamide coenzymes by graphite electrodes modified with an adsorbed phenoxazinium salt, meldola blue," *J. Electroanal. Chem.*, vol. 161, no. 1, pp. 103–120, 1984.

[103] D. A. Steinhurst, A. P. Baronavski, and J. C. Owrutsky, "Transient second harmonic generation from oxazine dyes at the air/water interface," *J. Phys. Chem. B*, vol. 106, no. 12, pp. 3160–3165, 2002.

[104] M. J. Frisch, G. W. Trucks, H. B. Schlegel, G. E. Scuseria, M. A. Robb, J. R. Cheeseman, V. G. Zakrzewski, J. A. Montgomery, Jr., R. E. Stratmann, J. C. Burant, S. Dapprich, J. M. Millam, A. D. Daniels, K. N. Kudin, M. C. Strain, O. Farkas, J. Tomasi, V. Barone, M. Cossi, R. Cammi, B. Mennucci, C. Pomelli, C. Adamo, S. Clifford, J. Ochterski, G. A. Petersson, P. Y. Ayala, Q. Cui, K. Morokuma, D. K. Malick, A. D. Rabuck, K. Raghavachari, J. B. Foresman, J. Cioslowski, J. V. Ortiz, A. G. Baboul, B. B. Stefanov, G. Liu, A. Liashenko, P. Piskorz, I. Komaromi, R. Gomperts, R. L. Martin, D. J. Fox, T. Keith, M. A. Al-Laham, C. Y. Peng, A. Nanayakkara, C. Gonzalez, M. Challacombe, P. M. W. Gill, B. G. Johnson, W. Chen, M. W. Wong, J. L. Andres, M. Head-Gordon, E. S. Replogle, and J. A. Pople, "Gaussian 98, Revision A.9." Gaussian, Inc., Pittsburgh PA, 1998.

[105] E. Vogel, A. Gbureck, and W. Kiefer, "Vibrational spectroscopic studies on the dyes cresyl violet and coumarin 152," *J. Mol. Struct*, vol. 550-551, pp. 177–190, 2000.

[106] M. Moskovits and D. P. DiLella, "Surface-enhanced Raman spectroscopy of benzene and benzene-d_6 adsorbed on silver," *J. Chem. Phys.*, vol. 73, no. 12, pp. 6068–6075, 1980.

[107] R. L. Sobocinski and J. E. Pemberton, "Laser-induced thermal decay of pyridine and chloride. Surface-enhanced Raman scattering as a probe of silver surface-active sites," *Langmuir*, vol. 4, no. 4, pp. 836–845, 1988.

[108] P. Hildebrandt and M. Stockburger, "Surface-enhanced resonance Raman spectroscopy of rhodamine 6G adsorbed on colloidal silver," *J. Phys. Chem.*, vol. 88, no. 24, pp. 5935 – 5944, 1984.

[109] G. Li, H. Li, Y. Mo, X. Huang, and L. Chen, "SERRS of R6G adsorbed on Ag electrode in Li batteries," *Chem. Phys. Lett.*, vol. 330, pp. 249 – 254, 2000.

[110] B. Pettinger, K. Krischer, and G. Ertl, "Giant Raman scattering cross section for an adsorbed dye at Ag colloids associated with low EM field enhancement," *Chem. Phys. Lett.*, vol. 151, pp. 151 – 155, 1988.

[111] A. Kudelski, J. Bukowska, and K. Jackowska, "Relative SERS enhancement factors for pyridine adsorbed on a silver electrode," *J. Raman Spectrosc.*, vol. 25, pp. 153 – 158, 1994.

[112] D. J. Rogers, S. D. Luck, D. E. Irish, D. A. Guzonas, and G. F. Atkinson, "SERS of pyridine, pyridinium ions and chloride ions adsorbed on the silver electrode," *J. Electroanal. Chem.*, vol. 167, pp. 237 – 249, 1984.

[113] J. C. Rubin, P. Corio, M. C. C. Ribeiro, and M. Matz, "Contribution of resonance Raman scattering to the SERS effect on electrode surfaces. description using the time dependent formalism," *J. Phys. Chem.*, vol. 99, pp. 15765 – 15774, 1995.

[114] A. G. Brolo, D. E. Irish, and J. Lipkowski, "SERS of pyridine and pyrazine adsorbed on Au(210) electrode," *J. Phys. Chem. B*, vol. 101, pp. 3906 – 3909, 1997.

[115] J. S. Gao and Z. Q. Tian, "SERS of pyridine at copper electrodes excited with a 514.5 nm line," *Chem. Phys. Lett.*, vol. 262, pp. 151 – 154, 1996.

[116] V. V. Marinyuk, R. M. Lazorenko-Manevich, and Y. M. Kolotyrkin, "Nature of the interaction of adsorbate molecules with metal ad-atoms," *J. Electroanal. Chem.*, vol. 110, pp. 111 – 118, 1980.

[117] J. Thietke, J. Billmann, and A. Otto, "CT excitations in SERS: a comparative study of benzene, pyridine and pyrazine," in *Dynamics on Surfaces* (B. Pullman, ed.), pp. 345 – 364, New York: Reidel, 1984.

[118] H. Okamoto, T. Nakabayashi, and M. Tasumi, "Transient vibrational temperature estimated from anti Stokes and Stokes Raman intensities," *J. Raman Spectrosc.*, vol. 31, pp. 305 – 309, 2000.

[119] R. C. Maher, L. F. Cohen, and P. Etchegoin, "Single molecule photo-bleaching observed by surface enhanced resonant Raman scattering (SERRS)," *Chem. Phys. Lett.*, vol. 352, no. 5-6, pp. 378–384, 2002.

[120] C. Viets and W. Hill, "Laser power effects in SERS spectroscopy at thin metal films," *J. Phys. Chem. B*, vol. 105, pp. 6330 – 6336, 2001.

[121] K. C. Rolle, *Heat and Mass Transfer*. Prentice-Hall, 2000.

[122] J. F. Ready, *Effects of High-Power Laser Radiation*. Academic Press, 1971.

[123] S. Corni and J. Tomasi, "Surface enhanced Raman scattering from a single molecule adsorbed on a metal particle aggregate: A theoretical study," *J. Chem. Phys.*, vol. 116, no. 3, pp. 1156–1164, 2002.

[124] S. Corni. (private communication), 2002.

[125] T. Nakabayashi, H. Okamoto, and M. Tasumi, "Probe-wavelength dependence of ps anti-Stokes Raman spectra of trans-stibene," *J. Phys. Chem. B*, vol. 101, pp. 7189 – 7193, 1997.

[126] T. Nakabayashi, H. Okamoto, and M. Tasumi, "Vibration relaxation dynamics of trans stibene in lowest excited singlet state," *J. Phys. Chem. A*, vol. 102, pp. 9686 – 9695, 1998.

[127] C. T. Rettner, D. J. Auerbach, J. C. Tully, and A. W. Kleyn, "Chemical dynamics at gas-surface interface," *J. Phys. Chem.*, vol. 100, pp. 13021 – 13033, 1996.

[128] J. C. Tully, "Chemical dynamics at metal surfaces," *Annu. Rev. Phys. Chem.*, vol. 51, pp. 153 – 178, 2000.

[129] M. Moskovits, "Surface-enhanced Raman spectroscopy: a brief retrospective," *J. Raman Spec.*, vol. 36, pp. 485–496, 2005.

[130] R. Maher, M. Dalley, E. Le Ru, L. Cohen, P. Etchegoin, H. Hartigan, R. Brown, and M. Milton, "Physics of single molecule fluctuations in surface enhanced Raman spectroscopy active liquids," *J. Chem. Phys.*, vol. 121, no. 18, pp. 8901–8910, 2004.

[131] L. Peyser-Capadona, J. Zheng, J. Gonzalez, T. Lee, S. Patel, and R. Dickson, "Nanoparticle-free single molecule anti-Stokes Raman spectroscopy," *Phys. Rev. Lett.*, vol. 94, no. 5, p. 058301, 2005.

[132] R. C. Maher, J. Hou, L. F. Cohen, E. C. L. Ru, J. M. Hadfield, J. E. Harvey, P. G. Etchegoin, F. M. Liu, M. G. R. J. C. Brown, and M. J. T. Milton, "Resonance contributions to anti-Stokes/stokes ratios under surface enhanced Raman scattering conditions," *J. Chem. Phys.*, vol. 123, p. 084702, 2005.

[133] R. C. Maher, L. F. Cohen, E. C. L. Ru, and P. G. Etchegoin, "On the experimental estimation of surface enhanced Raman scattering (SERS) cross sections by vibrational pumping," *J. Phys. Chem. B*, vol. 110, no. 39, pp. 19469 –19478, 2006.

[134] P. C. Lee and D. Meisel, "Adsorption and surface-enhanced Raman of dyes on silver and gold sols," *J. Phys. Chem*, vol. 86, no. 17, pp. 3391–3395, 1982.

[135] T. López-Ríos, Y. Borensztein, and G. Vuye, "Roughening of Ag surfaces by Ag deposits studied by differential reflectivity," *Phys. Rev. B*, vol. 30, no. 2, pp. 659–671, 1984.

[136] M. A. Bryant and J. E. Pemberton, "Differential reflectance spectroscopy and SERS of mildly roughened silver electrodes," *Langmuir*, vol. 6, no. 4, pp. 751–758, 1990.

Appendix A

Surface Temperature Estimates

The calculations given here are used to produce credible estimates of the surface temperature via reasonably simple models. They are not expected to precisely model the systems or to provide exact temperatures. Two systems are modeled: the colloidal-silver SERS system used by Kneipp *et al* when they first discovered the anti-Stokes excess in 1996,[54] and a roughened silver electrode illuminated by the same laser. The laser used by Kneipp *et al* has significantly more power than the laser used in the current work, and is focussed more tightly, making the result for the roughened electrode model an upper limit for the actual system used here. The same laser was used for both models to allow a more direct comparison of the results.

Laser Parameters

In their 1996 work Kneipp *et al* used a Ti:sapphire laser operating in continuous-wave mode at 830 nm.[54] Most of their data was collected with 150 mW of laser power which they equate to an intensity of $5\times10^{24}\,\text{photons}\cdot\text{cm}^{-2}\,\text{s}^{-1}$. In units of power density this intensity is

$$I=\left(5\times10^{24}\,\frac{\text{photons}}{\text{cm}^2\cdot\text{s}}\right)\left(\frac{6.62\times10^{-34}\,\text{J}\cdot\text{s}}{830\times10^{-7}\,\text{cm}}\right)\left(2.998\times10^{10}\,\frac{\text{cm}}{\text{s}}\right)=1.20\times10^{6}\,\frac{\text{W}}{\text{cm}^2} \quad \text{(A.1)}$$

Assuming this intensity (I) was calculated by dividing the total power density (P) by the observed spot size the observed beam radius (r) was

$$r = \sqrt{\frac{\pi I}{P}} = \sqrt{\frac{\pi\left(1.2\times10^{6}\,\frac{\mathrm{W}}{\mathrm{cm}^2}\right)}{150\,\mathrm{mW}}} = 2\times10^{-4}\,\mathrm{cm} = 2\,\mu\mathrm{m} \tag{A.2}$$

Kneipp *et al* give no indication as to what criteria they might have used to determine their beam radius. A reasonable estimate is to assume the above calculated radius corresponds to the Gaussian radius, w_0, which is the radius at which the intensity falls to $1/e^2$ of its peak value and is the typical parameter used when dealing with Gaussian beams. This assignment, which is not based on any evidence supplied by Kneipp *et al*, may not accurately represent their estimated beam spot, but a radius 50% smaller would include less than 40% of the laser power and a radius 50% larger would contain more than 98% of the laser power. Therefore any rational definition of the beam radius is roughly approximated by the Gaussian radius.

Using equations given by Ready[122] and assuming the radius calculated in equation A.2 is the Gaussian radius, the intensity at the center of the beam is

$$I_{\mathrm{peak}} = \frac{2P}{\pi w_0^2} = \frac{2(150\,\mathrm{mW})}{\pi(2\,\mu\mathrm{m})^2} = 2.40\times10^{6}\,\frac{\mathrm{W}}{\mathrm{cm}^2} \tag{A.3}$$

Therefore the parameters for the modeled laser system are

$$\begin{aligned} w_0 &= 2\,\mu\mathrm{m} \\ I_{\mathrm{peak}} &= 2.40\times10^{6}\,\frac{\mathrm{W}}{\mathrm{cm}^2} \end{aligned} \tag{A.4}$$

Colloid Calculation

The colloidal preparation technique used by Kneipp *et al*[54] produces 10–20 nm diameter colloids[57,134] which, when activated for SERS, aggregate into clusters 100–150 nm in diameter.[23] A rigorous thermodynamic model of such clusters would be excessively complicated considering the desired precision of the overall model. Instead, since the system is in a steady state, the cluster can be approximated by simply considering the

energy transferred to the cluster from the laser and the heat transferred from the cluster to the surrounding water.

The laser energy transferred to the cluster is simply the portion of the laser incident on the cluster multiplied by the absorptivity. Using the laser parameters calculated above (equation A.4), and assuming the cluster is centered in the laser and its extent is roughly spherical with a radius of 50 nm, the laser power incident on the cluster is

$$\begin{aligned} P|_0^R &= \int_0^R I_{\text{peak}} \left(e^{-2(r/w_0)^2}\right) 2\pi r\, dr \\ &= I_{\text{peak}} \left(\frac{\pi {w_0}^2}{2}\right) \left(-e^{-2(r/w_0)^2}\right) \Big|_{r=0}^{R} \\ &= I_{\text{peak}} \left(\frac{\pi {w_0}^2}{2}\right) \left(1 - e^{-2(R/w_0)^2}\right) \\ &= \left(2.40 \times 10^6 \frac{\text{W}}{\text{cm}^2}\right) \left(\frac{\pi (2\,\mu\text{m})^2}{2}\right) \left(1 - e^{-2((50\,\text{nm})/(2\,\mu\text{m}))^2}\right) \\ &= 188\,\mu\text{W} \end{aligned} \tag{A.5}$$

Published values of the absorptivity of roughened silver at 800 nm vary between ~10%[135] and ~20%.[136] Using an average of these values of 15% gives the power absorption as

$$\dot{Q}_{\text{absorbed}} = 15\% \times 188\,\mu\text{W} = 28\,\mu\text{W} \tag{A.6}$$

In order to model the heat transfer from the cluster to the water it is important to note that the limiting factor for heat dissipation is not the contact area between the silver and the water but rather the heat conduction through the water itself. This means that the thermodynamic surface of interest is the smallest surface that fully contains the cluster, not the surface area of the cluster itself. This implies that the appropriate model is again a sphere with a radius of 50 nm. Convection at these length scales is inefficient[121] and can safely be ignored. The change in temperature at the surface of a sphere of radius r is given by[121]

$$\Delta T_{\text{surface}} = \frac{\dot{Q}_{\text{conduction}}}{4\pi r \kappa} \tag{A.7}$$

In a steady state situation $\dot{Q}_{\text{absorbed}}$ in equation A.6 must equal $\dot{Q}_{\text{conduction}}$ in equation A.7. Noting that the thermal conductivity of water is 0.608 $\frac{\text{W}}{\text{m}\cdot\text{K}}$,[121] the increase in

surface temperature of the colloid cluster is

$$\Delta T_{\text{colloid}} = \frac{(28\,\mu\text{W})}{4\pi(50\,\text{nm})0.608\,\frac{\text{W}}{\text{m}\cdot\text{K}}} = 73\,\text{K} \tag{A.8}$$

Electrode Surface Calculation

As explained in chapter 3, the area of the electrode illuminated by the laser is such a small fraction of the total area that the electrode can be reasonably approximated by a semi-infinite slab. Also, since the thermal conductivity of silver ($418\,\frac{\text{W}}{\text{m}\cdot\text{K}}$)[122] is almost three orders of magnitude larger than the thermal conductivity of water ($0.608\,\frac{\text{W}}{\text{m}\cdot\text{K}}$),[121] the conductive heat loss through the water can be ignored, as can convective heat loss. According to Ready,[122] the steady state maximum increase in temperature of a laser illuminated semi-infinite slab is given by

$$\Delta T_{\text{peak}} = \sqrt{\pi/2}\cdot\dot{Q}_{\text{peak}}\cdot\frac{w_0}{2\kappa} \tag{A.9}$$

Using the laser parameters given above (equation A.4), the maximum increase in surface temperature of the electrode is

$$\Delta T_{\text{electrode}} = \sqrt{\pi/2}\cdot(15\%\cdot 2.40\times 10^6\,\frac{\text{W}}{\text{cm}^2})\cdot\frac{(2\,\mu\text{m})}{2(418\,\frac{\text{W}}{\text{m}\cdot\text{K}})} = 11\,\text{K} \tag{A.10}$$